INTERACTING FERMIONS IN TWO DIMENSIONS: EFFECTIVE MASS, SPECIFIC HEAT, AND SINGULARITIES IN THE PERTURBATION THEORY

By

SUHAS GANGADHARAIAH

A DISSERTATION PRESENTED TO THE GRADUATE SCHOOL
OF THE UNIVERSITY OF FLORIDA IN PARTIAL FULFILLMENT
OF THE REQUIREMENTS FOR THE DEGREE OF
DOCTOR OF PHILOSOPHY

UNIVERSITY OF FLORIDA

2005

To my parents.

ACKNOWLEDGMENTS

First and foremost I would like to thank my research advisor Professor Dmitrii Maslov, for his constant encouragement and guidance throughout the entire course of my research work. His enthusiasm, dedication, and optimism toward physics research has been extremely infectious. The countless hours I spent discussing research problems with him were highly productive scientifically and intellectually.

I would also like to thank Professor Kevin Ingersent, Professor Pradeep Kumar, and Professor Richard Woodard who were always willing and open to discuss any research-related issues. I am honored and grateful to Professor Russell Bowers, Professor Alan Dorsey, Professor Kevin Ingersent, and Professor Khandker Muttalib for serving on my supervisory commitee.

My thanks go to the Physics Department secretaries, Ms. Balkcom and Ms. Lattimer; and to my friends Aditi, Gregg, Hyunchang, Lingyin, Tamara, Sudarshan, and Yongke for their valuable help and support. My special thanks go to Aparna, Evren, and Ronojoy for their support, friendship and encouragement.

I would like to thank my parents for the unconditional love, support, and encouragement they provide through the years.

TABLE OF CONTENTS

LIST OF FIGURES

Abstract of Dissertation Presented to the Graduate School
of the University of Florida in Partial Fulfillment of the
Requirements for the Degree of Doctor of Philosophy

INTERACTING FERMIONS IN TWO DIMENSIONS:
EFFECTIVE MASS, SPECIFIC HEAT, AND SINGULARITIES IN THE
PERTURBATION THEORY

By

Suhas Gangadharaiah

May 2005

Chair: Dmitrii Maslov
Major Department: Physics

In this work, we analyzed the anomalous behavior of a two dimensional interacting Fermi system. The first anomaly that has been investigated is related to the low-energy property of Fermi liquids in two dimensions. The forward scattering processes, in the second order, lead to a log divergence in the imaginary part of the self-energy on the mass shell. We found that this divergence becomes even more singular at higher orders and takes the form of a power-law, potentially leading to the breakdown of Fermi-liquid theory. We deal with the divergence by re-summing the maximally divergent terms at each order of interaction, with the result that the renormalized imaginary part of self-energy is well defined on the mass shell. We also investigated in detail the contribution of the collective modes: zero-sound mode (for a contact potential) and the plasmon mode (for a Coulomb potential) to the nonanalytic temperature (T^2) dependent term in the specific heat. We found that the zero-sound mode does not make any contribution to the nonanalytic T^2-dependent term in the specific heat, whereas the plasmons do make a nonanalytic contribution.

The second anomaly is the lack of experimental observation of a polarization-dependent effective mass as a function of the applied parallel magnetic field in a Si-MOSFET sample. We investigated this experimental observation in the framework of an

N-component model, where N is an additional degree of freedom (which in our case is the valley degree of freedom). This model gives the change in the effective mass between an unpolarized and a fully polarized state to be not more than 1 to 3%, a result consistent with the experiment.

CHAPTER 1
INTRODUCTION

1.1 Survey

The physics of two-dimensional (2D) systems has been the subject of intense research both experimentally and theoretically, over the last few decades. Exciting physics such as Wigner crystallization of electrons at low electron densities [1] and the scaling theory of localization [2], were first predicted and later confirmed by experiments. On the other hand, novel phenomena such as the existence of a metal-to-insulator (MIT) transition [3], the quantum hall effect [4], the fractional-quantum hall effect [5], and radiation-induced zero-resistance states [6, 7] were discovered first and later given theoretical explanation. Many 2D systems have been described successfully in the framework of Fermi-liquid theory. However, the validity of Fermi-liquid theory in 2D has been a contentious issue. Fermi-liquid theory is known to break down in 1D. Anderson conjectured that even in 2D, Fermi liquid is destroyed for arbitrarily weak interactions [8].

The basic postulates of the Landau Fermi-liquid theory state that, low energy properties of a interacting fermionic system can be described similar to a non-interacting Fermi system [9]. This phenomenological theory makes specific predictions for the low-energy dependence of thermodynamic and transport properties on temperature, frequency and other small energy or momentum scales. In particular, the predictions for specific heat and spin susceptibility are as follows. Specific heat, $C(T)$ scales linearly with temperature T, for $T \to 0$, whereas the spin susceptibility approaches a constant as $T \to 0$. Over the past five decades, this theory has been enormously successful in describing the low-energy properties of many fermionic systems, particularly ^{3}He and also a large number of metals. The common features of a metallic Fermi-liquid system include, the existence of a Fermi surface, a specific heat proportional to temperature, a constant spin susceptibility, a finite density of low-energy single particle excitations and a conductivity which increases with decrease in temperature. This theory, though, has failed to account for the behavior of

quite a few heavy fermion systems and high-T_c superconductors. The deviation from the simple Fermi-liquid picture for the electrical conductivity and other features such as the thermal conductivity, the nuclear relaxation rate *etc.*, in the normal state of high-T_c superconductors is quite perplexing given the fact that many of these materials have large Fermi surfaces [10, 11].

Issues related with the validity of Fermi-Liquid theory in systems which exhibit metal-insulator-transition have also come under intense scrutiny. Two-dimensional systems can exhibit insulating and metallic behavior depending on the concentration of impurities and the density of charged carriers. Among the many different theoretical approaches to understand 2D systems in either the metallic or the insulating regime, those based on the framework of Fermi-liquid theory have been more successful, compared to other theories, in describing the transport and thermodynamic properties. Nevertheless, deviations from the Fermi-liquid universality have been observed, such as the absence of spin-split mass in a spin-polarized system and nonanalytic terms in the thermodynamic and transport quantities. Section 1.2 discusses nonanalyticities in the thermodynamic and transport properties, and addresses the important question regarding the validity of Fermi-liquid theory in 2D. Section 1.3 discusses the metal-insulator-transition in 2D. The issues related to anomalous effective mass behavior have been taken up in Section 1.4.2.

1.2 Deviation from Fermi-Liquid Universality

Recent studies on the low energy behavior of Fermi-liquid systems away from the critical point, reveal deviations from the Fermi-liquid universality due to the presence of soft-modes which are responsible for the nonanalytic terms in thermodynamic quantities like specific heat and spin susceptibility. These nonanalytic terms survive near the quantum critical point and are responsible for the breakdown of the Hertz-Millis-Moriya (HMM) theory [12], leading to either a first-order or incommensurate ordering (or both) [13]. Thus a study of the low-energy physics of Fermi systems, which has its own inherent merit, acquires extra significance due to its implications near the quantum critical point [13, 14, 15].

Approaches to understand a system of weakly interacting fermions in 3D through perturbative techniques on a tractable microscopic model of short-range interacting

fermions have added to a regular T term in the leading specific heat term and a constant term for the spin susceptibility as $T \to 0$, in agreement with the results of a Fermi gas [16, 17]. These results, when extended to arbitrary dimensionality $D > 1$, yield similar results provided the interaction falls off rapidly. The similarity in behavior of the Fermi-gas result and the Fermi-liquid result obtained via perturbative calculations, stop at the leading order corrections. Perturbative calculations beyond the leading term in $3D$ obtain a nonanalytic $T^3 \ln T$ term [18, 19, 20] and in $2D$ a T^2 term [21, 22, 23] for the specific heat, different from the regular T^3 term as obtained for the Fermi gas. The non-uniform susceptibility, in terms of the momentum Q, gets a nonanalytic $Q^2 \ln Q$ term for 3D [15] and for 2D $max(Q, T)$ [13, 15, 22, 24] instead of a analytic $max(Q^2, T^2)$ as the next-to-leading term. Some of these predictions, especially on the specific heat behavior, have been confirmed by experiments. Specific-heat measurements on bulk ^{3}He have revealed beyond the linear-in-T term an additional $T^3 \log T$ term [25], a similar $T^3 \log T$ behavior was also observed in heavy-fermion UPt_3 [26]. The origin of the nonanalytic terms were attributed to nonperturbative spin-fluctuation processes. Heat capacity measurements on monolayers of ^{3}He adsorbed on atomically flat graphite yield a T^2 correction to the specific heat in agreement with theoretical predictions [27].

For $D = 1$ the perturbation theory is singular and Fermi-liquid theory is destroyed. This break-down shows up already at second order in the interaction [28]. Apart from the low dimensionality there are other sources which can lead to the breakdown of Fermi-liquid theory. Using weak coupling analysis one can show that for certain special shapes of the Fermi surface, for example, a Fermi surface satisfying the 'nesting' property (*i.e.*, $\xi_{\vec{p}} = -\xi_{\vec{p}+\vec{Q}}$), the Fermi liquid is unstable. A 'nesting' Fermi surface can lead to the breakdown of translational invariance by the formation of a charge/spin density wave with a typical ordering vector $\vec{Q}$. There have been suggestions that the non-Fermi liquid behavior of high-T_C materials is due to the shape of the Fermi surface [29]. A dispersion relation in momentum space which has saddle points on the Fermi surface can also affect the low energy properties of fermions (the velocity is zero at the Fermi surface). A second-order perturbation analysis reveals that the quasi-particle decay rate depends

linearly on energy or, in other words, is of the same order as the real part of the self-energy [29], signaling a non-Fermi liquid behavior. The validity of Fermi-liquid theory in two dimensions has been a source of intense research since Anderson suggested that in two dimensions the Fermi liquid is unstable even for weak coupling [8]. His argument was that scattering of two interacting particles at the same point of the Fermi surface will cause a finite phase shift. This means that even in the limit of the lowest energies, two particles with opposite spin cannot occupy the same quantum-mechanical state, as is assumed in the quasi-particle picture of Landau's Fermi-liquid theory. A second argument was that the presence of an anti-bound state (pole in the particle-particle channel) will lead to an instability of the Fermi liquid. The effect of phase-space shifts and the anti-bound state has been analyzed in detail with the conclusion that one cannot infer the breakdown of the Fermi liquid from these effects [30].

In this work we have considered a 2D fermion with a weak short-range interaction potential. A perturbative analysis of such a system with a linearized single-particle spectrum reveals a singularity in the imaginary part of the self-energy at second order in the interaction [22, 31, 32, 33]. This singularity is present on the mass shell ($\varepsilon = \xi_p$) and is logarithmic in nature. The divergence is even more singular at higher orders and starting from the third order onward goes as a power law. An important point is that these divergences are present even for an arbitrarily weak interaction. A similar divergence on the mass shell is observed in 1D. This divergence is due to what is known as the infra-red catastrophe, where an on-shell fermion can emit an infinite number of soft bosons consisting of spin and charge fluctuations, leading to a power-law divergence on the mass shell [28]. At each order in the interaction, the divergences can be cutoff by invoking the finite curvature of the single-particle spectrum, yet the series itself remain non-convergent at low energies [34]. These result seem to justify Anderson's conjecture about the invalidity of the Fermi-liquid picture in 2D. This, however, is not the complete analysis.

The divergence in the self-energy which at each order in the interaction is due to the interaction of fermions with the upper edge of the particle-hole continuum, when summed to all orders corresponds to the interaction of fermions with the zero-sound mode. A

careful selection of diagrams that at each order are the most divergent, and re-summing to all orders in the interaction removes these divergences, thus restoring the Fermi-liquid picture. The resulting renormalized self-energy with the divergences removed acquire features which indicate a deviation from the standard Fermi-liquid behavior. Of these the most prominent is a non-Lorentzian shape of the spectral function, The spectral function acquires a shoulder at the threshold for the emission of zero-sound bosons and a nonanalytic $\omega|\omega|$ term in the real part of the self-energy. In addition to the contribution to the $\omega|\omega|$ term from the nonperturbative processes, the second order term in perturbation also contributes to the $\omega|\omega|$ nonanalytic term to the real part of the self-energy. A nonanalytic $\omega|\omega|$ term in the real part of the self-energy, in principle, translates into a nonanalytic T^2 term in the specific heat.

The nonanalyticities in the thermodynamic and transport (for a disordered system) properties are due to what are known in a general sense as the Generic Scale Invariance (GSI) of the system [14]. Correlation functions away from the critical point generally decay exponentially and are short-ranged with a characteristic length or time scale. On the other hand, near the critical point the correlations become long ranged and the decay is only power-law. Correlation functions with long-range order exhibit scale invariance: a change of scale, *e.g.,* in length, represents a change in the correlation function by an overall factor. For cases where long-range order is obeyed, even for regions away from the critical point, the system is said to exhibit "generic scale invariance" (GSI). In simple terms, correlation function that are long ranged and belong to the class of GSI (also called soft modes) have their Fourier components $\propto 1/k^{\alpha}$ (where α is some positive exponent and k is the momentum) for regions even away from the critical point. Correlation functions which are short-ranged have the form $\propto 1/(k^{\alpha}+m)$, where m is a constant mass term. One such example is an $O(N)-$symmetric Heisenberg ferromagnet which exhibits, in the ordered phase, nonanalyticity in the magnetization as a function of the magnetic field. The ordered phase contains gapless Goldstone modes and the corresponding correlation functions are long-ranged and belong to the class of GSI. These are responsible for the nonanalyticity in the magnetization. Other examples include the nonanalytic behavior of conductivity as a function of frequency. In a disordered system the leading term in the

conductivity is $\sigma_0 = ne^2\tau/m_e$ (Drude result, where n, e, τ and m_e are the density, charge, scattering time of electrons with impurities and the mass of electrons respectively) and the leading-order weak-localization correction is given by [36]

$$\delta\sigma = -\frac{\sigma_0}{\pi N_F}\int d^D q \frac{1}{\bar{D}q^2 - i\Omega}, \tag{1.1}$$

where $\bar{D}, q, \Omega$ and N_F are the diffusion constant, momentum, frequency and density of state respectively. For $D = 2$ this leads to a logarithmic correction and for $2 < d < 4$, this results in a nonanalytic frequency dependence

$$\frac{\sigma(\Omega \to 0)}{\sigma(0)} = 1 + \beta\Omega^{(d-2)/2} \tag{1.2}$$

with $\beta > 0$.

The thermodynamic properties acquire nonanalytic corrections even for disorder-free, point-like interacting fermions. Although the bare interaction is short-ranged, the effective interaction at finite frequencies is long-ranged. At second-order in the interaction U the effective potential is $\overline{U} = U^2\Pi(\Omega, q)$, where $\Pi(\Omega, q)$ is the dynamical polarization bubble, which for the momentum range

$$|\Omega|/v_F \ll q \ll k_F \text{ is given by } \overline{U} = U^2 a_D \frac{|\Omega|}{v_F q} + \cdots,$$

where a_D is a constant and $1/q$ is the generic scale invariant term [22]. The long range interaction forces, prevent a regular expansion of the self-energy in powers of ω leading to a nonanalytic expansion in frequency. The nonanalyticity that arises in the self-energy is transferred to the observable quantities thus resulting in non-regular subleading terms (Section 3.2.1). In a system with disorder, fermions interact with Friedel oscillations (these oscillations are due to the presence of a static local perturbation). This interaction falls off as r^{-D} with the distance from the impurity and are the source for nonanalyticities in transport properties(these are the interaction corrections, unlike the earlier example of weak localization correction).

Chubukov and Maslov [22] identified the nonanalyticities in the self-energy for $D = 2$ with the three scattering processes, which are essentially one-dimensional in character. These are the forward-scattering process with the incoming momenta nearly

the same, undergoing small transfer of momentum and two back-scattering processes involving scattering of near-opposite-momentum quasi-particles, undergoing either a small momentum transfer or large "$2k_F$" transfer. Second-order perturbative analysis reveals a nonanalytic T^2 behavior of $C(T)$ arising from the back-scattering processes , whereas the forward-scattering process, for a linearized spectrum, contributes an unexpected log singularity at the mass shell in the imaginary part of the self-energy. As discussed earlier this divergence is the analog of a stronger power-law-singularity in 1D and is dealt with by re-summing the perturbative series by including the maximally divergent diagrams. An offshoot of this re-summation is a collective mode. In the past, the role of collective modes in the nonanalyticity in the thermodynamic potential had been treated by assuming that the collective modes are free. Indeed, by invoking power counting arguments [21], it can be shown that the collective mode contributes to a T^D term in the nonanalyticity. However, collective modes are not free excitations. The contribution of the collective mode to $C(T)$ has been analyzed in detail in this work (Secs. 3.2.1 and 3.2.2). We show that the collective modes do not contribute to the T^2 term in the specific heat in 2D.

In the next Section, we will discuss the validity of Fermi-liquid theory in 2D systems which exhibit a metal-to-insulator transition.

1.3 Metal-Insulator-Transition (MIT) in 2D

In the late 1970s, an interesting theoretical viewpoint emerged on the conductance of a 2D system. Following the concepts of Thouless [35], Abrahams *et al.* [2], developed a single-parameter scaling theory of localization (electron-electron interactions were not taken into account). The scaling equation being

$$\frac{d\ln g(L)}{d\ln L} = \beta(g(L)), \tag{1.3}$$

where $g = G(L)/(e^2/2\hbar)$ is the dimensionless conductance and is the scaling parameter, and L is the typical length along each of the directions. The asymptotic values of $\beta(g(L))$ obtained via physical arguments can qualitatively describe the flow equation. That is, starting from a given conductance $G(L)$ for a system of size L (volume L^D, where D is the system dimensionality), the flow equation can in principle predict the conductance (for example, when the linear dimension L is doubled). (Of course it is implicit that the

material property, the density of disorder and the electron density, do not change). In the large-conductance ($G \gg e^2/\hbar$) regime, the conductance shows Ohm's-law behavior with $G \propto L^{D-2}$, thus $\beta = D - 2$. In the other extreme with the electrons localized, the conductance gets exponentially suppressed with increasing length and $\beta = -L/\xi$, where ξ is the localization length. It is assumed that β varies monotonically between these two asymptotic limits.

The consequence of this theory is that a 2D system with $L \to \infty$ is an insulator at zero magnetic field and zero temperature. For a finite-sized sample, the scaling relation implies that an insulating behavior will be observed. If the 2D sample were dirty to begin with, the system would show exponential localization as a function of system size. If the sample were relatively clean to begin with, then the system on further increase in size would show logarithmic localization (in 3D, there is a critical disorder separating localized and metallic behavior). The form of the 2D conductivity showing logarithmic behavior is given by

$$\sigma(L) = \sigma(L_0) - \frac{\alpha e^2 \ln(L/L_0)}{\pi^2 \hbar}. \tag{1.4}$$

The above result obtained for zero temperatures can describe the conductivity at nonzero temperatures with a slight modification. According to Gorkov *et al.* [36] and Thouless [37], at finite temperatures, inelastic scattering introduces random fluctuations in the time evolution of an electronic state thus limiting the quantum interference necessary for localization. Typical lengths (cut-off lengths) beyond which the phase is not conserved are given by $L_{Th} = (D\tau_{in})^{1/2}$, where D is the diffusion constant and τ_{in} is the inelastic lifetime. (Altshuler *et al.* [38, 39] argued that for a collision event with small energy change $\Delta E \ll \tau_{in}^{-1}$, τ_{in} cannot be taken as the dephasing time; the dephasing time will be $\tau_\phi \sim (\Delta E \tau_{in})^{-2/3} \tau_{in}$.) The inelastic lifetime itself is temperature-dependent: $\tau_{in}^{-1} \propto T^p$, with the lifetime decreasing with increasing temperatures. This temperature dependence of the inelastic lifetime is responsible for the temperature dependence of the conductivity. Thus Eqn. (1.5) the conductivity equation (in 2D)

$$\sigma(L) = \sigma(L_0) + \frac{\alpha p e^2 \ln(T/T_0)}{2\pi^2 \hbar}, \tag{1.5}$$

acquires a nonanalytic $\log T$ temperature dependence. This result was almost immediately confirmed by experiments performed on thin metallic films and silicon metal-oxide-field-effect-transistor (Si-MOSFET). For relatively clean samples, the resistivity showed the expected logarithmic increase with decreasing temperature and applied electric field [40, 41, 42].

In an alternate theory, Altshuler *et al.* [3] considered interaction effects in the framework of a dirty Fermi liquid in the regime when $k_F l \gg 1$ (where k_F is the Fermi wave vector, l is the electronic mean-free path) and $T\tau \ll 1$ (this is the diffusive regime, with τ being the scattering time) and obtained similar nonanalytic temperature dependence for the conductivity. The conductivity obtained is expressed in terms of the Fermi-liquid parameter F

$$\delta\sigma = \frac{e^2(1-F)\ln(T\tau)}{2\pi^2\hbar}, \tag{1.6}$$

where the factor F is small for weak screening. However, Altshuler *et al.* [3] did not consider localization effects (phenomena that can occur without electron-electron interaction). That is, the maximally crossed impurity lines in the current vertex that give rise to localization were disregarded.

Both correlation effects and localization effects lead to logarithmic temperature dependence of conductivity. The information about these effects can be disentangled by experiments performed in the presence of a magnetic field [43], since the correlation effects and localization effects show significantly different behaviors [44, 45]. With good agreement between theory and experiment, the nature of the conducting state of a 2D system was considered resolved.

Yet theoretical results, particularly those of Finkelstein [46, 47] were contrary to the general viewpoint. By performing field-theoretic renormalization-group calculations, he showed that the resistance of the system scales to weak coupling leading to a metallic state at zero temperature (his theory explicitly suppressed the maximally crossed diagrams that give rise to logarithms in the localization problem). Altshuler and Aronov [48] then showed that by considering spin-orbit or spin-flip scattering, the Finkelstein solution

to the resistance scales to strong coupling, and shows an insulating behavior [48, 49], thus paving the way for metal-to-insulator transition to be observed in $D \geq 2$ systems.

With the advent of better technology, it became possible to fabricate samples with mobilities an order of magnitude higher than the ones developed earlier. The earliest experiments which reported the metallic behavior of resistivity were performed on high mobility Si-MOSFET's by Kravchenko *et al.* [50, 51]. Both metallic and insulating behaviors were observed in the same Si-MOSFET sample by just varying the density of electrons. Since then, numerous studies have observed the metallic state in systems other than Si-MOSFET's: $p-$ and $n-$Si/SiGe [52], $p-$GaAs [53], $n-$GaAs [54], $n-$AlAs [55]. Nearly all of these studies have reported the observation of some key features. Metallic temperature dependence of the resistivity was observed for densities above a sample-dependent critical density n_c in the ballistic regime $T\tau \gg 1$, showing almost an order of magnitude variation of resistivity with temperature. For densities below n_c an insulating behavior was observed. The 2D system shows an unusually sharp response to the application of a parallel magnetic field. Conductivity is strongly suppressed with increased magnetic field, up to the saturation field, whereupon conductivity saturates. Interestingly, the field required for saturation of conductivity depends on the density of the 2D sample and is approximately equal to the field required for complete spin-polarization of the 2D sample [56]. Since the parallel magnetic field only couples to the spin degree of freedom and not with the orbital degree of freedom, the extreme sensitivity to parallel magnetic fields implies that exchange and spin-related interactions play a crucial role. Despite agreement as to the general behavior of 2D samples on the insulating and metallic side, there are questions on which general consensus has not been reached. First, does the resistivity on the metallic side continue to decrease ($d\rho/dT > 0$) down to the lowest temperatures (*i.e.*, no upturn toward insulating behavior at the lowest temperatures)? Prus *et al.* [57] have observed that the resistance of some curves with metallic behavior show an upturn upon further decrease in temperature, signifying a greater role played both by electron-electron interaction and weak localization; and signaling the possibility that the zero-temperature state of a 2D sample is indeed an

insulator. In contrast, Kravchenko *et al.* [50, 51], found no resistance upturn for Si-MOSFETS with similar mobilities. The lowest temperatures they achieved were an order of magnitude smaller than those achieved by Prus *et al.* [57], indicating a zero-temperature MIT. The second question which eludes general consensus is whether the crossover from metal to insulator is accompanied by a transition from a paramagnetic to a ferromagnetic phase and if so, what is the order of this phase transition. This is discussed in Section 1.4.

The theoretical approach to understand the MIT has been dependent on underlying assumptions about the ground state of 2D systems. Next we briefly summarize two approaches based on the Fermi-liquid picture and one not based on Fermi-liquid theory, which we call the non-Fermi liquid approach.

The non-Fermi liquid approach. Chakravarty *et al.* [58] assumed that the ground state of disordered electrons is a non-Fermi liquid. The single-particle Green's function, when analytically continued to the lower half-plane, instead of containing a quasi-particle pole consists of a branch point. The spectral function used for the calculation was

$$A(\omega, k) \propto \frac{1}{\omega_c^{\alpha} |\omega - v_F k|^{1-\alpha}} \tag{1.7}$$

where α is positive and ω_c is a high-frequency scale proportional to the inverse of the non-interacting density of states. For $\alpha < 1/2$ they found that the non-Fermi liquid state is localized; whereas for $\alpha > 1/2$, they found that the disordered system is a perfect conductor, with a stable non-Fermi liquid fixed point.

Dobrosavljevic *et al.* [59] took a phenomenological approach and assumed that at large conductance interactions can modify β and make it positive, leading to a metallic state. By assuming the form of the function β to be

$$\beta(g) = (d-2) + A/g^{\alpha}, \ A > 0 \tag{1.8}$$

at large conductance, the conductance obtained showed a logarithmic decrease with increase in temperature

$$g \sim (\ln(T_0/T))^{1/\alpha}. \tag{1.9}$$

They argued that this state cannot be a Fermi liquid because of the unusual temperature dependence of conductance and because the system will turn to an Anderson insulator once the interactions are turned off.

Fermi-liquid approaches. Among the Fermi-liquid approaches to describe the resistivity of a 2D system, the most prominent are those of Altshuler *et al.* [3], Finkelstein [46, 47], Castellani *et al.* [49], and Zala *et al.* [60]. We have already considered Altshuler and colleagues' solution which predicts localizing behavior in the diffusive regime with $k_F l \gg 1$. Next, we briefly review Finkelstein's solution in the diffusive regime and Zala and colleagues' approach in the ballistic regime, both of which predict metallic behavior.

- The Diffusive regime:
  The range of electron-densities for which the system is diffusive ($T\tau \ll 1$) and also show metallic behavior is rather limited. For densities such that $\rho \simeq h/e^2$ and temperatures $T \ll T_F$ (where T_F is the degeneracy temperature), the system lies in a diffusive regime. The temperature dependence of the resistivity in this regime can be described by the renormalization group (RG) equations developed by Finkelstein. The RG equation relating the resistivity and temperature is

$$\frac{d\rho}{d\xi} = \rho^2 \left[n_v + 1 - (4n_v^2 - 1)\left(\frac{1+\gamma_2}{\gamma_2} \ln(1+\gamma_2) - 1 \right) \right], \tag{1.10}$$

  where n_v is the valley degeneracy, $\xi = -\ln(T\tau/\hbar)$, the dimensionless resistivity ρ is in the units of $h/e^2\pi$ and γ_2 is the interaction parameter [61]. The coupling constant also gets renormalized and its equation is given by

$$\frac{d\gamma_2}{d\xi} = \rho \frac{(1+\gamma_2)^2}{2}. \tag{1.11}$$

  These RG equations [Eqs. (1.10), (1.11)] can describe non-monotonic resistivity behavior as a function of temperature. Starting from high-temperature regimes where the system shows insulating behavior, a decrease in temperature causes the resistivity and the interaction parameter to increase (the interaction parameter shows a monotonic behavior) until a critical interaction strength γ_2^* is reached. At this interaction strength the RHS of Eq. (1.10) changes its sign. Further decrease in temperature causes the resistivity to decrease and hence show metallic behavior. This result was not taken seriously, since for $n_v = 1$, γ_2 diverges at low energies. The situation however is completely different for a two-valley system $n_v = 2$ (Si-MOSFET along the (001) plane) where the interaction strengths required are within the perturbative regime.

- The Ballistic regime: Zala *et al.* [60] showed that insulating behavior in the diffusive regime and metallic behavior in the ballistic regime are both governed by the same physics: coherent scattering of electrons by the self-consistent potential created by all the other electrons (Friedel oscillations). For the ballistic limit they were able to show with the usual quantum-mechanical arguments that the scattering of electrons by impurities and by Friedel oscillations created due to impurities can be coherent, provided the scattering is a back-scattering event. As a result, the amplitude of back-scattering processes is enhanced compared to the case with no Friedel oscillation. The correction to conductivity is linear in the ballistic regime and is given by

$$\Delta\sigma(T) = \frac{e^2 T\tau}{\pi\hbar^2}\Big(1 + \frac{3F_0^\sigma}{1+F_0^\sigma}\Big), \tag{1.12}$$

  where the sign of the correction to conductivity crucially depends on the Fermi-liquid interaction parameter F_0^σ in the triplet channel and near the Stoner instability the corrections to conductivity is greatly enhanced. This result, essentially the effect of a single impurity, when extended to include the case of multiple impurities results in a conductivity correction that is logarithmic in temperature as obtained by Altshuler *et al.* [3]. The nonanalytic temperature dependence of the conductivity observed in both the ballistic and diffusive regimes arise due to the contributions from long range correlations or the soft modes [14]. The soft modes which are present in the dirty system have their analogues in a clean system as well and are responsible for nonanalyticities in the thermodynamic quantities like specific heat and spin susceptibility.

Although there has been considerable progress in understanding the transport properties of 2D systems in the ballistic limit, the question regarding the nature of the ground state of 2D electrons has not been resolved. This is because the conductivity can show various temperature dependences depending on the strength of disorder and also on the concentration of electrons; this can range from a purely Fermi-liquid behavior with large conductivity to a strongly localized behavior (hence a non-Fermi liquid) with exponential temperature dependence of conductivity in the dirty limit $k_F l \ll 1$. For impurity and electron concentrations intermediate between these two limits, the temperature dependence of conductivity can show various functional forms and the ground state can vary from bubbles of Wigner crystal [62], to stripe phase to bubbles of Fermi liquid [63]. Thus based solely from the temperature dependence of resistivity an unambiguous judgment on the ground state of the system cannot be made.

By fitting the experimentally determined conductivity with Zala *et al.*'s [60] theory, which implicitly assumes Fermi-liquid ground state, Fermi-liquid parameters F_0^σ and $m^*(r_s)$ were extracted [64, 65]. These were then compared with the parameters obtained independently from other experimental techniques, the most prominent being the Shubnikov-de Haas oscillation in the conductivity [66, 67]. An excellent match between the Landau parameters extracted by these two independent approaches points to the Fermi-liquid nature of the underlying state in the ballistic limit. At the same time there has been a interesting observation which does not fit well with the predictions of the Fermi-liquid theory. The theory predicts that the effective mass is renormalized by the density and hence the Fermi energy. A similar renormalization should also be achieved by a parallel magnetic field since the field alters the Fermi energy and the distribution of electrons. The prediction for a field dependent effective mass is for a clean system, still one expects a qualitatively similar dependence to hold for a dirty system which shows Fermi-liquid behavior. However no dependence of the effective mass on the field has been observed [68]. The issues related with the extraction of the Fermi-liquid parameters from the Shubnikov-de Haas data, the anomalous effective mass and the nature of the ground state of 2D electrons are explored in the next Section.

1.4 Quantifying Fermi-liquid Parameters

An analysis of quantum magneto-oscillation in terms of the Lifshitz-Kosevich (LK) formula yields information regarding the quasi-particle effective mass m^*, the Pauli (spin) susceptibility χ^* and the Lande g^* factor. These quasi-particle parameters are related to the harmonics of the Fermi-liquid interaction via the following relation:

$$F_0^\sigma = \frac{2}{g^*} - 1, \tag{1.13}$$

where F_0^σ is the interaction term in the triplet channel, and

$$F_1^S = 2(\frac{m^*}{m_b} - 1), \tag{1.14}$$

F_1^S is the first harmonic in the singlet channel and m_b is the band mass.

This analysis is based on the assumption that the LK formula originally developed to describe the magneto-oscillations in 3D Fermi liquid, can be extended to describe the

oscillations in 2D systems by a change in the electronic spectrum and in terms of the zero field Fermi-liquid parameters of the 2D system. Recently, there have been questions raised about the validity of LK formula in 2D [69, 70]. In the following we will discuss this issue in more detail.

1.4.1 Applicability of the Lifshitz-Kosevich Formula in 2D

In 3D systems, it was shown by Luttinger [71] and also by Bychkov and Gorkov [72] that the presence of a magnetic field does not affect the zero field Fermi-liquid parameters to leading order in $1/N$, where $N \gg 1$ is the number of occupied Landau levels. The correction to the magneto-oscillations obtained by including the oscillations in the self-energy is of the order of N^{-3} which is smaller by a factor of $\sqrt{N}$ compared to the leading oscillatory part. Thus additional oscillations of the self-energy can be ignored in 3D. The situation in 2D is different: the contribution coming from the oscillations in the self-energy is $1/N^2$ smaller than the monotonic part and is of the same order as the leading oscillatory term in the magneto-oscillation. Thus, for zero temperature the LK formula in 2D is not applicable for describing the oscillations [69, 70, 73]. On the other hand, experiments performed at finite temperatures seem to agree well with the LK formula, thus the range of validity for the LK formula requires a careful inspection. The amplitude of the k^{th} harmonic of the magneto-oscillation is given by

$$A_k = \frac{4\pi^2 kT}{\omega_c} \sum_{\varepsilon_n > 0} \exp\Big(-\frac{2\pi k[\varepsilon_n + i\Sigma_0(i\varepsilon_n, T)]}{\omega_c}\Big), \tag{1.15}$$

where $\varepsilon_n = \pi(2n+1)T$ is the Matsubara energy, $\omega_c = eB/mc$ is the cyclotron frequency and Σ is the self-energy of electrons. The self-energy for a generic Fermi liquid in the presence of short-ranged impurities is given by $i\Sigma_0(\varepsilon_n, T) = \alpha\varepsilon_n + \mathrm{sgn}(\varepsilon_n)/2\tau$. One obtains a simplified form of the amplitude By expressing the effective mass as $m^* = m(1+\alpha)$, one obtains a simplified form of the amplitude

$$A_k = \frac{4\pi^2 kT/\omega_c}{\sinh(2\pi^2 kT/\omega_c^*)} \exp\Big(-\frac{2\pi^2 T_D}{\omega_c}\Big), \tag{1.16}$$

where $T_D = 1/2\pi\tau$ is the Dingle temperature. For temperatures and impurity concentrations such that

$$2\pi^2(T/\omega_c^*, T_D/\omega_c) \geq 1, \tag{1.17}$$

the amplitudes of the oscillatory components will be exponentially suppressed, the suppression being stronger for higher amplitude terms [70]. A similar argument holds for the oscillatory part of the self-energy, and only the first harmonic needs to be retained. The contribution from the first harmonic of the self-energy oscillation to the magneto-oscillations is of the same order as the second harmonic of the quantum magneto-oscillation. This implies that the first harmonic of quantum magneto-oscillation does not obtain any additional contributions from the oscillations in the self-energy, hence, as long as only the first harmonic is the major contributor to the quantum magneto-oscillation one can still use the LK formula for analyzing the data.

The above analysis was performed for the de Haas-van Alphen effect, however, it is conjectured that many of the arguments, especially, the validity of the first harmonic term also holds for the description of Shubnikov-de Haas oscillations in the conductivity for large temperatures. Thus the quasi-particle parameters which get renormalized due to electron-electron interactions (within the Landau's Fermi-liquid theory) such as the spin susceptibility χ^*, effective mass m^* and Lande factor g^*, can be extracted from the Shubnikov-de Haas measurements. In this regard it is worth mentioning that in a recent experiment, an opposite phase of the second harmonic term as compared to the one predicted by LK formula was observed [74]. This can be attributed to the inapplicability of the LK formula beyond the first harmonic.

1.4.2 Absence of Polarization Dependent Effective Mass

The amplitude of the oscillations encodes the effective mass and the Dingle temperature, both of which are related to the amplitude via the following relation

$$-\frac{e\hbar H}{2\pi^2 k_B c} \ln\left(\frac{\delta\rho_{xx}}{\rho_{xx}}\right) = m^*(T + T_D), \tag{1.18}$$

the slope of $\ln(\rho_{xx}/\rho)$ vs T yields the effective mass, whereas the intercept gives the Dingle temperature. The amplitude and the oscillatory part are multiplied by a third term which

is also called the Zeeman term

$$Z_k = \cos\Big[\frac{\pi^2\hbar(n_\uparrow - n_\downarrow)}{eB_\perp}\Big] = \cos[\frac{\pi k\Delta_z^*}{\hbar\omega_c^*}], \tag{1.19}$$

where Δ_z^* is the Zeeman energy and $\hbar\omega_c$ is the cyclotron energy. The difference $(n_\uparrow - n_\downarrow) \propto \chi^* B_{tot}$, is directly proportional to the total applied field B_{tot} and for fields with no parallel component Z_k is a constant. The presence of non-zero parallel component causes Z_k to be field dependent leading to beats. From the position of the nodes in the beat pattern χ^* is extracted and the ratio χ^*/m^* gives g^*. The nodes occur at regular half-integer values of $k\Delta_z^*/\omega_c^*$ [66]. Perfect nodes implies that the oscillatory terms due to the up- and the down-spin electrons have the same amplitude and hence the same effective mass, a result in contradiction with Fermi-liquid theory. Indeed, the presence of a magnetic field causes the Fermi surface to split into two, one for the up-spin electrons and another smaller one for the down-spin electrons. A consequence of this phenomenon will be that the velocities of up-spin electrons will be higher compared to those of down-spin electrons. Thus within the frame work of Fermi-liquid theory it is natural to assume that there are three distinct interaction terms, an interaction between two up-spin electrons (fast moving electrons), one between two down-spin electrons (slow moving electrons and hence strong interaction) and the interaction between a down-spin and an up-spin electron (Section 4.1.1). These interaction terms in turn imply different effective masses for the up- and down-spin electrons. This intuitive expectation is confirmed by a perturbative calculation (Section 4.1.2). These results are in contradiction with the experimental findings on Si-MOSFETs with a (001) surface, which report absence of field dependence of the effective mass and also indicate that the effective masses of up- and down-spin electrons are the same, $m^\uparrow = m^\downarrow$ [68].

To resolve the paradox, we have turned to a large $N-$model. We have found the spin-valley degeneracy N plays an important role in the mass renormalization. Each of the N components shows polaronic behavior, with the mass renormalized primarily by the high energy plasmons. For typical $r_s = 2-6$ (where $r_s = \sqrt{2}m e^2/k_F$) the percentage change in the effective mass between unpolarized and a fully polarized state is within $1-3\%$, a result which is consistent with the experiment.

1.4.3 Effective mass and Lande-g Factor Near the Critical Densities

A number of groups have come up with interesting conclusions regarding the ultimate fate of χ^* and m^* as the densities approach the critical one. Shaskin *et al.* [75] and Vitkalov *et al.* [76] have both reported divergence of χ^* in Si-MOSFETS near the critical regimes, with the former arguing that the divergence in χ^* is due to the divergence in m^* whereas the g^*-factor shows only a nominal increase. Vitkalov *et al.* however report the divergence of g^* as the cause for the divergence in χ^*. These conflicting results point to different phases of the ground state on approach to the critical density: a divergence in m^* points toward Wigner crystallization, whereas the divergence in g^* points toward ferromagnetism. The mutually opposing results of the above experimental groups are in further disagreement with the results of a third group. Pudalov *et al.* [66] obtained an increase in both g^* and m^* near the critical density, however the increase in m^* was by a factor of 3 and only a small increase in the value of g^* was seen. Clearly the experimental evidence for the very existence of phase transition and its order is contradictory, nevertheless it remains an interesting point that if the phase transition does exist in 2D, what is the order of this phase transition.

The scenario of mass divergence near the MIT regime is similar to the one proposed by Brinkman and Rice [77], who showed using Gutzwiller's variational method [78] that at half-filling the effective mass diverges at the critical value of the interaction. This divergence is accompanied by the vanishing of the discontinuity in the single-particle occupation number thus indicating a deviation from the Fermi-liquid ground state. Galitski *et al.* [79] and Chubukov *et al.* [80] have proposed that at the critical interaction, the quantum critical behavior is associated with a density-wave instability at a finite wave vector q_c. At the critical point, the interaction diverges for finite wave vector q_c leading to the divergence of the fermion's self-energy and hence the effective mass. It was further argued by Chubukov *et al.* [80] that in the near vicinity of the critical point the self-energy has only frequency dependence, and the divergence of the effective mass right at the critical point and not before it indicates that the renormalization factor Z remains non-zero, thus the Fermi-liquid state survives till the critical point.

CHAPTER 2
INTERACTING FERMIONS IN TWO DIMENSIONS

2.1 Introduction

The nature of the low-energy electronic excitation in a 2D system has been of great interest, particularly since the discovery of high T_C superconductors. It was suggested by Anderson that forward scattering of two electrons leads to vanishing renormalization factor Z, *i.e.*, to the breakdown of the Fermi-liquid description [8]. Subsequently, the effect of forward scattering has been investigated by many authors within the framework of the t-matrix approximation, and an $\varepsilon^2 \log \varepsilon$ term as the leading correction to the imaginary part of the self-energy, $\mathrm{Im}\Sigma$, was obtained. This result indicates that the real part of the self energy is still dominant compared to the imaginary part of the self-energy and hence the quasi-particles are well defined [30, 31, 32].

In a recent work, it was shown that for fermions with a linearized dispersion, $\mathrm{Im}\Sigma$ acquires a log singularity on the mass shell even at the second order in the interaction [22, 29, 31, 32]. In this thesis we show that the divergences on the mass shell at higher orders in perturbation theory become power-law and are more singular. Although the divergences in the individual terms are cut off due to curvature effects (non-linear dispersion), the series itself does not converge. This result seems to support the Anderson's conjecture regarding the breakdown of Fermi liquid in 2D. However, this is not the complete picture.

At each order in the interaction, the singularity arises due to the interaction of quasi-particles with excitations near the upper-edge of the particle-hole continuum. By re-summing the singular perturbative terms to all orders, we were able to obtain a closed form for $\mathrm{Im}\Sigma$. This form shows that the singularities are due to the interaction of quasi-particles with the collective excitation of the system, the zero-sound mode (ZS). The re-summation regularizes the power-law divergences whereas remaining log divergences are removed by introducing finite curvature. As a result Fermi-liquid theory is restored. The outcome of the re-summation process is nonperturbative contributions to the self-energy,

one of them being a zero-sound contribution to the imaginary part of the self-energy $\mathrm{Im}\Sigma_{ZS}$ that is non-monotonic as a function of the distance from the mass shell. The non-monotonic behavior leads to a non-Lorentzian shape of the spectral function.

The contribution from the nonperturbative zero-sound mode to the real part of the self-energy $\mathrm{Re}\Sigma_{ZS}$ is strongly enhanced near the mass shell and is responsible for a nonanalytic $U^2\varepsilon|\varepsilon|$ contribution. This result suggests that the nonperturbative processes contribute to a nonanalytic T^2 term in the specific heat. This however is not the case. We discuss the zero-sound contribution to the specific heat in Chapter 3.

This Chapter is organized as follows. We begin in Section 2.2 by introducing the relevant scattering processes, these are forward- and back-scattering processes. Section 2.3 is essentially concerned with the self-energy of fermions interacting with a contact potential. We show in Section 2.3.1 and Section 2.3.2 that forward scattering leads to the divergence of the imaginary part of the self-energy on the mass shell at second and higher orders in the interaction. The procedure used for the resummation of diagrams at all orders is discussed in Section 2.3.3. This is followed by the calculation of the renormalized imaginary part of the self-energy in Section 2.3.4 and the real part of the self-energy in Section 2.3.5. The results from Secs. 2.3.4 and 2.3.5 are used to obtain the spectral function in Section 2.3.6. The spectral function obtained shows features that deviate from the usual Lorentzian function for a quasi-particle. The non-Lorentzian feature originates due to the interaction between a quasi-particle and the zero-sound mode which results in a non-monotonic behavior of $\mathrm{Im}\Sigma$; the effects on $\mathrm{Im}\Sigma$ are transferred to the spectral function. The nonperturbative processes for fermions interacting via a Coulomb potential also lead to non-monotonic behavior of $\mathrm{Im}\Sigma$, as discussed in Section 2.3.7. The final part of this Section, Section 2.3.8, discusses nonanalytic corrections to the tunneling density of states. We show that the tunneling density of states does not acquire a nonanalytic correction to order U^2. We end the Chapter by concluding in Section 2.4.

2.2 Scattering Processes

Scattering events between two low-energy quasi-particles of momenta $\vec{k}_1$ and $\vec{k}_2$ can be divided into three categories. (1) Exchange of large momentum of the order $\delta k = |\vec{k}_1 - \vec{k}_2| \propto k_F$, (2) exchange of small momentum $\delta k \simeq |\Omega|/v_F \ll k_F$ and, (3)

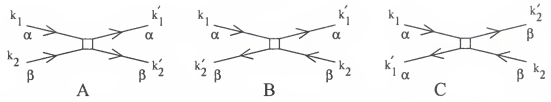

Figure 2–1: Scattering processes responsible for divergent or nonanalytic self-energy contributions in 2D. A) Parallel-moving quasi-particles scatter at each order by exchange of a small momentum. B) The quasi-particles are moving opposite to each other, initial and final momenta remain essentially unchanged. C) Each of the oppositely moving quasi-particles undergo momentum change close to $2k_F$.

exchange of momentum near $2k_F$ such that $||\delta k| - 2k_F| \simeq |\Omega|/v_F \ll k_F$. Scattering events of the first kind are responsible for analytic contributions to the self-energy and thermodynamics(Section 2.3). Scattering events of the second and third kinds are responsible for nonanalytic contributions to the self-energy and thermodynamics. The effect of the scattering events involving small momentum exchange or large $2k_F$ scattering becomes more pronounced with the lowering of the spatial dimensionalty, since the relative phase-space for these events increases in lower dimensions compared to the higher dimensions.

From an earlier analysis of small-momentum scattering events [22], it was established in 2D that the kinematics responsible for nonanalyticity in the self-energy are 1D in nature. These 1D processes can be subdivided into two kinds: A) those in which the two quasi-particles move almost in the same direction and undergo small momentum transfer so that all four momenta are close to each other $\vec{k}_1 \simeq \vec{k}_2 \simeq \vec{k}'_1 \simeq \vec{k}'_2$; this process is also called the g_4 process and its diagrammatic representation is shown in Fig. 2–1A, and B) g_2 processes which involves quasi-particles with anti-parallel momentum undergoing small momentum transfer $-\vec{k}_1 \simeq \vec{k}_2 \simeq -\vec{k}'_1 \simeq \vec{k}'_2$. The diagrammatic representation of a g_2 process is shown in Fig. 2–1B. The third kind of scattering event responsible for the nonanalytic term in the self-energy involves exchange of $2k_F$ momentum and is essentially 1D in character due to the quasi-particle occupancy restriction. The $2k_F$ process is depicted in Fig. 2–1C.

2.3 Self-Energy: Nonanalyticity and Singularity

In this Section, we will first derive the imaginary part of the self-energy to second order. We obtain two interesting results: a nonanalytic term in the self-energy and a mass-shell singularity. We will consider both of these issues in detail. The Hamiltonian of our system is the same as for the Coulomb potential case, except that the potential is now short ranged.

Before we go into the details of the calculation, we will discuss here through some simple arguments the origin of the nonanalytic term in the self-energy. An analytic self-energy forms a regular series in ε, the real part of the self-energy being expressed as $\mathrm{Re}\Sigma^R(\varepsilon) = a_1\varepsilon + a_2\varepsilon^3 + a_3\varepsilon^5 + \cdots$, whereas the imaginary part of the self-energy is expressed through the series $\mathrm{Im}\Sigma^R(\varepsilon) = b_1\varepsilon^2 + b_2\varepsilon^4 + b_3\varepsilon^6 + \cdots$. An example of a nonanalytic term in $\mathrm{Im}\Sigma^R$, which we will often encounter is $\varepsilon^2 \log|\varepsilon|$. Let us consider $\mathrm{Im}\Sigma^R$ at $T = 0$,

$$\mathrm{Im}\Sigma^R(\varepsilon) \sim \int_0^\varepsilon d\omega \int d^D q \mathrm{Im}G^R(\varepsilon - \omega, \vec{k} - \vec{q})\mathrm{Im}V^R(\omega, \vec{q}), \tag{2.1}$$

where $\mathrm{Im}G^R$ and $\mathrm{Im}V^R$ are the imaginary part of the Green's function and the potential respectively. From this form, it is clear that, if upon a momentum integration we obtain a ω term, then one ends up with a regular ε^2 term after the remaining frequency integration is performed, whereas if the momentum integration yields $\omega \log|\omega|$ (as in 2D) or ω^2 (as in 3D) then the frequency integration yields a nonanalytic $\varepsilon^2 \log|\varepsilon|$ or $|\varepsilon|^3$ term respectively.

Now to be a bit more explicit, the potential term $V(r,t)$ is real, thus $\mathrm{Im}V(q,\omega)$ is odd in frequency and we can express it in terms of a characteristic momentum Q of the system (which serves as an upper cut-off) in the following form

$$\mathrm{Im}V(q,\omega) = \omega F(\frac{q}{Q}, \frac{|\omega|}{Qv_F}), \tag{2.2}$$

where F is now a even function of frequency. The angular integration over $\mathrm{Im}G^R$ yields on the mass shell ($\varepsilon = \xi_k$; where $\xi_k = k^2/2m - k_F^2/2m$)

$$\int d\theta \mathrm{Im}G^R = -\int d\theta \pi\delta(\omega - \vec{v}_F.\vec{q} + q^2/2m) = \frac{2\pi}{v_F q} A_D(\frac{\omega + q^2/2m}{v_F q}), \tag{2.3}$$

where the subscript D stands for the dimension,

$$\begin{aligned} A_3(x) &= \theta(1-|x|) \\ A_2(x) &= \frac{\theta(1-|x|)}{\sqrt{1-x^2}}. \end{aligned}$$

The function A_D primarily serves to impose a lower cutoff $q \geq |\omega|/v_F$ and we can ignore the specific functional form. We plug the result of Eq. (2.2) and Eq. (2.3) back in Eq. (2.1) to obtain

$$\mathrm{Im}\Sigma^R(\varepsilon) \sim \int_0^{\varepsilon} d\omega\omega \int_{q\geq|\omega|/v_F} dq q^{D-2} F(\frac{q}{Q}, \frac{|\omega|}{Qv_F}). \tag{2.4}$$

Now if the momentum integral is dominated by large momenta of the order Q, then the function F to leading order can be considered to be independent of frequency (since $|\omega|/v_F Q \sim \varepsilon/v_F Q \ll 1$, as Q the upper momentum cut-off is large and ε is small) and one can replace the lower limit by 0 as well. The momentum and frequency integrations decouple, and one obtains an analytic ε^2 term. Thus a process which involves large momentum transfers yields analytic terms. Let us consider a case where the decoupling between the momentum and frequency is not possible. Such a scenario takes place at the second order in the interaction for a contact potential. The retarded part of the effective potential is a constant times the polarization bubble,

$$\mathrm{Im}V^R(\omega, q) = -U^2 \mathrm{Im}\Pi^R(\omega, q), \tag{2.5}$$

where Π^R has the following general structure in an arbitrary dimensionality

$$\mathrm{Im}\Pi^R(\omega, q) = -\nu_D \frac{\omega}{v_F q} B_D(\frac{\omega}{v_F q}), \tag{2.6}$$

where ν_D is the density of state in D dimensions and the dimensionless function B_D imposes a constraint $\omega \leq v_F q$. For $D = 3$, we obtain from Eq. (2.1)

$$\mathrm{Im}\Sigma(\varepsilon) \sim U^2 \int_0^{\varepsilon} d\omega \int_{q\geq|\omega|/v_F}^{k_F} dq q^2 \left[\frac{1}{qk_F}\right] \left[\frac{\omega}{v_F q}\right], \tag{2.7}$$

where we have neglected the constants, and the functions B_3 and A_3. The first square bracket represents the result from the angular integration, whereas the second one

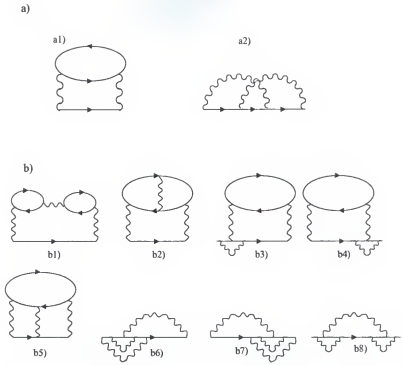

Figure 2–2: Self-energy diagrams with explicit and implicit polarization bubbles.

represents $\mathrm{Im}\Pi^R$. The upper cut-off is of the order of k_F. Performing the momentum integration we obtain

$$\begin{aligned} \mathrm{Im}\Sigma(\varepsilon) &\sim U^2 \int_0^{\varepsilon} d\omega\omega \left[k_F \Big|_{\mathrm{FL}} - \frac{|\omega|}{v_F}\Big|_{\text{Beyond FL}} \right] \\ &\sim a\varepsilon^2 - b|\varepsilon|^3, \end{aligned} \tag{2.8}$$

where the first term originates from the large momentum transfer regime and is the Fermi-liquid result, the sub-leading second term originates from the small-momentum-transfer regime and is nonanalytic. For reduced dimensions, the effective interaction plays a more singular role with the result that the nonanalytic terms become the leading terms in the imaginary part of the self-energy. In 2D, the nonanalytic term behaves as $\varepsilon^2 \log|\varepsilon|$, a more dominant term than the Fermi-liquid ε^2 term. In the Sections to follow, we will consider the origin of nonanalyticity in greater detail.

We will define the Fermion self-energy (Σ) via the Dyson equation in terms of the exact (G) and bare (G_0) Green's function

$$G^{-1} = G_0^{-1} + \Sigma, \tag{2.9}$$

note that we have defined Σ with an opposite sign compared to Refs. [16, 17].

2.3.1 Self-Energy at the Second Order

At second order in the interaction, there are only two non-trivial diagrams (Fig. 2–2), the rest of the irreducible diagrams in effect renormalize the chemical potential and hence are not important. For a contact interaction, $V(r) = U\delta(r)$, the two second order diagrams in Fig. 2–2 are related, namely, diagram $(a1)$ is -2 times diagram $(a2)$. This is particularly easy to see in momentum space as diagram $(a1) = 2U^2 \int_Q \Pi(Q)G(P+Q)$ and diagram $(a2) = -U^2 \int_Q \int_{Q_1} G(P+Q)G(P+Q+Q_1)G(P+Q_1) = -U^2 \int_Q \Pi(Q)G(P+Q)$, where $\int_Q$ is the integration over frequency and momentum and $\Pi(Q)$ is the polarization bubble without including the spin summation. In the retarded formalism, the total contribution at second order in the interaction is given by

$$\begin{aligned}\Sigma_2^R(\varepsilon,k) &= \frac{U^2}{(2\pi)^3\pi}\int d^2p_1 \int_{-\infty}^{\infty} d\Omega \int_{-\infty}^{\infty} d\varepsilon_1 \frac{\mathrm{Im}G_0^R(\varepsilon_1,p_1)\mathrm{Im}\Pi^R(\Omega,k-p_1)}{\Omega+\varepsilon_1-\varepsilon-i\delta} \\ &\quad \times \left[\tanh\left(\frac{\varepsilon_1}{2T}\right) + \coth\left(\frac{\Omega}{2T}\right)\right],\end{aligned} \tag{2.10}$$

and for $T = 0$, the imaginary part of the self-energy acquires the form

$$\mathrm{Im}\Sigma_2^R(\varepsilon,k) = -\frac{U^2}{(2\pi)^2\pi}\int_{-\varepsilon}^{0} d\Omega \int d^2q \mathrm{Im}G_2^R(\varepsilon+\Omega,k+q)\mathrm{Im}\Pi^R(\Omega,q), \tag{2.11}$$

where $\mathrm{Im}G^R(\varepsilon+\Omega,k+q)$ is

$$\mathrm{Im}G^R(\varepsilon+\Omega,k+q) = -\pi\delta(\Omega+\varepsilon-\xi_{k+q}), \tag{2.12}$$

with $\xi_k = k^2/2m - k_F^2/2m$. We will be interested in the contributions coming from $q \sim \Omega v_F \ll k_F$ and q close to $2k_F$. The form of the polarization bubble for small q is

$$\Pi^R(\Omega,q) = -\frac{m}{2\pi}\left(1 + \frac{i\Omega}{\sqrt{(v_Fq)^2-(\Omega+i0^+)^2}}\right), \tag{2.13}$$

whereas for $q \approx 2k_F$ we have

$$\Pi^R(\Omega, q) = -\frac{m}{2\pi}\left(1 - \left(\frac{q-2k_F}{2k_F} + \sqrt{\left(\frac{q-2k_F}{2k_F}\right)^2 - \left(\frac{\Omega + i0^+}{2k_F v_F}\right)^2}\right)^{1/2}\right). \tag{2.14}$$

The above two results for Π^R may be obtained by using the result of Stern [81]; alternatively, one can use the result for the polarization bubble in the Matsubara representation

$$\Pi^M(i\Omega_n, q) = -\frac{m}{2\pi}\left(1 - \frac{2}{q^2}\sqrt{\frac{\sqrt{x^2+y^2}-x}{2}}\right), \tag{2.15}$$

where $x = (qk_F)^2 - q^4/4 + m^2\Omega_n^2$ and $y = q^2 m\Omega_n$, expand for small $q \ll k_F$ and q near $2k_F$, and perform an analytic continuation to real frequencies.

The nonanalyticities in Eq. (2.13) and Eq. (2.14) represent Landau damping and the Kohn anomaly, respectively. For $\Omega < v_F q$ damping of excitations with frequency Ω and momentum q can take place only inside the particle-hole (PH) continuum, similar to the damping of a collective mode inside the PH continuum. The polarization bubble near $2k_F$ shows different nonanalyticities depending on whether $Q < 2k_F$ or $Q > 2k_F$ (where Q represents the transferred momentum). For $Q < 2k_F$, the nonanalytic part $\Pi^R \propto i\Omega/(2k_F - Q)^{1/2}$ and for $Q > 2k_F$ the nonanalytic part $\Pi^R \propto (Q - 2k_F)^{1/2}$. In what follows, we will calculate the forward and back-scattering contribution at 2^{nd} order.

Forward- and back-scattering contribution at second order. In an earlier work [15, 22], the leading nonanalytic contribution to the self-energy were identified to originate from processes with small and large $2k_F$ momentum transfers. To logarithmic accuracy, contributions from the Kohn ($2k_F$) anomaly to the nonanalytic term of the self-energy were found to be identical to the g_2 contributons. In the following, we will show that the nonanalyticity which originates from $q \approx 2k_F$ due to the dynamic nonanalytic term in the particle-hole response function is responsible for the nonanalyticity in the $\mathrm{Im}\Sigma^R$. The imaginary part of the polarization bubble near $Q = 2k_F + q \leq 2k_F$, is given by the dynamic term $m\Omega/4\pi v_F\sqrt{|q|k_F}$, thus the contribution to the imaginary part of the self-energy from the $Q \leq 2k_F$ region is

$$\mathrm{Im}\Sigma_2^R(\varepsilon, k) = \frac{U^2}{(2\pi)^2}\int_0^{\varepsilon} d\Omega \int d^2Q \delta(\varepsilon - \Omega - \xi_{k+Q})\Big[\frac{m\Omega}{4\pi v_F\sqrt{|q|k_F}}\Big], \tag{2.16}$$

where for $k = k_F$, $\xi_{k+Q} = (4k_F^2 + k_F q + q^2)/2m + (2k_F + q)k_F \cos\theta/m$. Performing the angular integration

$$\int d\theta \delta(a - b\cos\theta) = \frac{2\Theta(|b| - |a|)}{\sqrt{b^2 - a^2}};$$

$$\int QdQ = (2k_F)\int^0 dq$$

and keeping the most dominant terms (with typical q such that $|q|v_F \gg \Omega$), we obtain

$$\begin{aligned} \mathrm{Im}\Sigma^R_{2k_F}(\varepsilon, k) &= \frac{U^2}{(2\pi)^2}\int_0^\varepsilon d\Omega \int^{\Omega/v_F} dq(2k_F)\Big[\frac{2}{\sqrt{4k_F^3|q|/m^2}}\Big]\Big[\frac{m\Omega}{4\pi v_F\sqrt{|q|k_F}}\Big] \\ &= \frac{u^2}{8\pi E_F}\varepsilon^2 \log\frac{W}{\varepsilon}, \end{aligned} \tag{2.17}$$

where $Um/2\pi = u$ and $-W$ represents the lower cutoff on the momentum integration, which is typically E_F. The other nonanalytic piece of $\mathrm{Im}\Pi^R \propto (Q - 2k_F)^{1/2} = \sqrt{q}$ which originates from $Q > 2k_F$ does not contribute to the nonanalytic piece in the self-energy. The contribution to the nonanalytic term in the second order $\mathrm{Im}\Sigma^R_2$ [Eq. (2.11)] from the $q = 0$ region (we need to keep the nonanalytic piece of the polarization bubble near $q = 0$, *i.e.* $-m\Omega/2\pi\sqrt{(v_F q)^2 - \Omega^2}$) is expressed as

$$\mathrm{Im}\Sigma^R_2(\varepsilon, k) = \frac{U^2}{(2\pi)^2}\int_0^\varepsilon d\Omega \int d^2q\delta(\varepsilon - \Omega - \varepsilon_{k+q})\Big[\frac{m\Omega}{2\pi\sqrt{(v_F q)^2 - \Omega^2}}\Big], \tag{2.18}$$

where $\xi_{k+q} = k^2/2m + q^2/2m + kq\cos\theta/m - k_F^2/2m$. As before, we perform the angular integration on the delta function,

$$\int d\theta \mathrm{Im}G_0^R = -\frac{2\pi}{\sqrt{(v_F Q)^2 - (\Omega + \Delta)^2}}.$$

using this result, we find that Eq. (2.18) acquires the following form,

$$\begin{aligned} \mathrm{Im}\Sigma^R_2(\varepsilon, k) &= \frac{U^2}{(2\pi)^2}\int_0^\varepsilon d\Omega \int qdq\Big[\frac{2}{\sqrt{(\frac{kq}{m})^2 - (\Delta - \Omega - \varepsilon_q)^2}}\Big] \\ &\times\Big[\frac{m\Omega}{2\pi\sqrt{(v_F q)^2 - \Omega^2}}\Big], \end{aligned} \tag{2.19}$$

where $\xi_k = k^2/2m - k_F^2/2m$ and $\Delta = \varepsilon - \xi_k$ has the interpretation of the distance from the mass shell.

For $\Delta = 0$ and neglecting the curvature ($\varepsilon_q = 0$) we obtain

$$\begin{aligned} \mathrm{Im}\Sigma_2^R(\varepsilon,k) &= \frac{U^2}{(2\pi)^2}\int_0^{\varepsilon} d\Omega \int_{|\Omega|/v_F}^{k_F} dq^2 v_F^2/2\Big[\frac{m\Omega}{\pi v_F^2|(v_F q)^2-\Omega^2|}\Big] \\ &= \frac{U^2}{(2\pi)^2}\int_0^{\varepsilon} d\Omega\Big[\frac{m\Omega}{2\pi v_F^2}\Big]\int_0^{k_F} dx \frac{1}{|x|}, \end{aligned} \tag{2.20}$$

i.e., an unexpected log singularity on the mass shell. The origin of this divergence is due to the form of the polarization bubble at small momenta which is square root divergent at $|\Omega| = v_F Q$ and due to the divergent form of the Green's function obtained after performing the angular integration. Combining the two contributions and performing the d^2q integration one obtains a logarithmic singularity due to the soft modes on the mass shell ($\Delta = 0$). Higher orders in the interaction have larger number of particle-hole bubbles and hence stronger singularities. These case will be considered in the next Section.

By keeping Δ finite, we obtain the following form

$$\begin{aligned} \mathrm{Im}\Sigma_2^R(\varepsilon,k) &= \frac{mU^2}{v_F^2(2\pi)^3}\int_0^{\varepsilon} d\Omega\Omega\log\Big[\frac{E_F^2}{|\Delta(2\Omega-\Delta)|}\Big] \\ &= \frac{mU^2}{(4\pi)^3 v_F^2}\Big[\Delta^2\log\Big|\frac{\Delta-2\varepsilon}{\Delta}\Big| + 2\varepsilon(\varepsilon+\Delta) + 4\varepsilon^2\log\frac{E_F^2}{|\Delta||\Delta-2\varepsilon|}\Big] \\ &= \frac{mU^2}{16\pi^3 v_F^2}\Big[\Big(\varepsilon^2+\frac{\Delta^2}{4}\Big)\log\frac{E_F}{\Delta} + \Big(\varepsilon^2-\frac{\Delta^2}{4}\Big)\log\frac{E_F}{\varepsilon+\varepsilon_k}\Big], \end{aligned} \tag{2.21}$$

and near the mass shell

$$\mathrm{Im}\Sigma_2^R(\varepsilon,k) = \frac{u^2}{8\pi^2 E_F}\varepsilon^2\Big[\log\frac{E_F}{\Delta} + \log\frac{E_F}{\varepsilon+\varepsilon_k}\Big]. \tag{2.22}$$

It has been established that the two log contributions in Eq. (2.22) have different origins [22]. The first term is due to a process with two incoming particles of almost identical momentum undergoing small angle ($q \approx 0$) scattering (in $1D$ terminology it is the g_4 process), whereas the second term is due to a process in which two incoming particles of almost opposite momentum undergo small momentum scattering (a g_2 process). The following analysis will convince us that there are only two, $q \approx 0$ processes which contribute to the $\varepsilon^2\log\varepsilon$ term. We will reexamine the contribution to $\mathrm{Im}\Sigma^R$

$$\mathrm{Im}\Sigma^R \propto \int_0^{\varepsilon} d\Omega \int_{\Omega/v_F} q dq d\theta \delta(\Omega + \Delta - kq/m\cos\theta)\frac{\Omega}{\sqrt{(k_F q)^2-\Omega^2}},$$

where $\vec{k}$ is the momentum of the incoming particle. The imaginary part of the Green's function yields a $1/q$ term and for $k_F q \gg \Omega$ the imaginary part of the polarization bubble yields a $1/q$ term, the $1/q^2$ term obtained is responsible for the nonanalytic term. The above expression reduces to

$$\approx \int_0^{\varepsilon} d\Omega\Omega \int_{\Omega/v_F} \frac{dq}{q} \int d\theta\delta\Big(\frac{m}{kq}(\Omega+\Delta) - \cos\theta\Big),$$

for small Ω and Δ typical angles near $\pm\pi/2$ will yield the nonanalytic $\varepsilon^2 \log\varepsilon$ term, this is the angle between the incoming momentum $\vec{k}$ and the transferred momentum $\vec{q}$. A similar relationship exists between the momentum transfer and the incoming momentum $\vec{p}$ of the "other" electron. The information about the "other" electron is in the imaginary part of the polarization bubble and is given by

$$\begin{aligned} \mathrm{Im}\Pi^R(\Omega,q) &\propto \int_0^{p_F} pdpd\phi\Big\{\delta(\Omega-\varepsilon_q-pq\cos\phi)-\delta(\Omega+\varepsilon_q-pq\cos\phi)\Big\} \\ &= \frac{1}{q}\int_0^{pF} dpd\phi\Big\{\delta(\frac{\Omega-\varepsilon_q}{pq}-\cos\phi)-\delta(\frac{\Omega+\varepsilon_q}{pq}-\cos\phi)\Big\} \\ &\propto \frac{\Omega}{\sqrt{(p_F q)^2-\Omega^2}}, \end{aligned} \tag{2.23}$$

thus for $pq \gg \Omega$, we find $\mathrm{Im}\Pi^R \propto \Omega/q$ (the $1/q$ form of the polarization bubble is crucial for the nonanalytic term), clearly the typical angles involved in this contribution are $\phi \approx \pm\pi/2$. Thus both the fermionic momenta $\vec{p}$ and $\vec{k}$ are perpendicular to $\vec{q}$, implying two processes, g_4 and g_2, are responsible for the nonanalytic contribution to the self-energy from $q \approx 0$ regimes. In this work, we will classify g_2 as a back-scattering contribution since it involves scattering of two incoming momenta with total momentum close to zero. For a contact interaction, the total back-scattering contribution which is a sum of g_2 and $2k_F$ processes is given by

$$\mathrm{Im}\Sigma^R_{2,B}(\varepsilon) = \frac{u^2\varepsilon^2}{4\pi E_F}\log\frac{E_F}{|\varepsilon|}. \tag{2.24}$$

Since there is no mass-shell singularity from the back-scattering contribution, we do not need to consider higher order terms and hence we can stop the series at the second order in the interaction U. We will, however, pursue higher order contribution from forward scattering process because of the mass-shell singularity in this channel.

2.3.2 Higher-Order Forward-Scattering Contributions

In an earlier analysis, we have established that the singularities from the soft mode ($q \sim 0$) in the particle-hole bubble causes a log singularity of the $\mathrm{Im}\Sigma^R$ at the second order. At higher order in the interactions, these singularities proliferate leading to a power-law divergence of $\mathrm{Im}\Sigma^R$. The third order diagram of the self-energy consists of a maximum of two polarization bubbles, having the same momentum and frequency (Fig. 2–2),

$$\begin{aligned}(\Pi^R)^2 &= (\frac{m}{2\pi})^2\Big[1+i\frac{\Omega}{\sqrt{(v_Fq)^2-(\Omega+i0^+)^2}}\Big]^2 \\ &= (\frac{m}{2\pi})^2\Big[1+i\frac{2\Omega}{\sqrt{(v_Fq)^2-(\Omega+i0^+)^2}}-\frac{\Omega^2}{((v_Fq)^2-(\Omega+i0^+)^2)^2}\Big].,\end{aligned}$$

Thus at the third order, the most singular term in $\mathrm{Im}(\Pi^R)^2$ is given by

$$\mathrm{Im}[\Pi^R]^2 = -\frac{m^2}{4\pi^2}[\pi\Omega|\Omega|\delta(\Omega^2-v_F^2q^2)].$$

The singular term at the third order is given by

$$\begin{aligned}\mathrm{Im}\Sigma^R_{3,F}(\varepsilon,k) &= U^3\int_{-\varepsilon}^{0}\frac{d\Omega}{2\pi}\int\frac{qdq}{(2\pi)^2}\Big[\frac{-2\pi}{\sqrt{(v_Fq)^2-(\Delta+\Omega)^2}}\Big] \\ &\quad\times\Big[-\frac{m^2}{4\pi}\Omega|\Omega|\delta(\Omega^2-(qv_F)^2)\Big] \\ &= \frac{U^3m^2}{32\pi^3v_F^2}\int_{-\varepsilon}^{0}d\Omega\frac{\Omega|\Omega|}{\sqrt{\Omega^2-(\Delta+\Omega)^2}} \\ &= -\frac{U^3m^2}{32\pi^3v_F^2}\int_0^{\varepsilon}\frac{\Omega^2}{\sqrt{(2\Omega-\Delta)\Delta}} \\ &\approx -\frac{U^3m^2}{32\pi^3v_F^2}\Big[\frac{\varepsilon^2\sqrt{2}}{5}\sqrt{\frac{\varepsilon}{\Delta}}\Theta\left(\frac{\varepsilon}{\Delta}\right)\Big]\end{aligned} \tag{2.25}$$

where in the last step of the above equation the singular $1/\sqrt{\Delta}$ term has been extracted. The additional Θ function signifies that the expression is zero if Δ and ε are of the opposite sign. At higher orders we obtain

$$\mathrm{Im}\Sigma^R_{n,F} \propto \frac{U^n\varepsilon^{n/2+1}}{\Delta^{n/2-1}}\Theta\left(\frac{\varepsilon}{\Delta}\right) \tag{2.26}$$

for $n > 2$. Collecting forward-scattering contributions to all orders in u, we obtain

$$\mathrm{Im}\Sigma_F^R(\varepsilon) = \frac{u^2\varepsilon^2}{8\pi E_F}\Big[\log(\frac{E_F}{|\Delta|}) + \sum_{n=1}^{\infty} C_n\Big(\frac{(mU/2\pi)^2\varepsilon}{\Delta}\Big)^{n/2}\Big], \tag{2.27}$$

where C_n are the numerical coefficients. This series converges only for $(u^2\varepsilon/\Delta) \ll 1$, outside this regime the series will not converge. Thus there is a clear need for re-summation of the perturbative series. This is the topic of our next Section.

2.3.3 Re-summation of Forward-Scattering Contributions

A proper re-summation of the self-energy series involves keeping at each order in the interaction the most singular terms. We find that such terms correspond to diagrams with the maximum number of particle-hole bubbles (with small frequency and momentum). A convenient way to re-sum the contributions will be to first identify the singular four-fermion vertex Γ and then relate the fermion vertex to the self-energy Σ via the Dyson equation.

Four-fermion vertex. The diagrams that form particle-hole bubbles are of two kinds (for a short range interaction): the ones which have explicit bubbles and the others with implicit bubbles (those which are not easily identifiable). These explicit and implicit particle-hole bubbles also appear in the self-energy. A typical example is the 2^{nd} order self-energy where we consider two bubbles, one of which has an explicit bubble Fig. 2–2(a1) and the other an implicit bubble Fig. 2–2(a2). An explicit bubble comes with an additional factor of -2 from the spin summation. Due to these differences, the procedure of finding an overall pre-factor at order ν is rather involved, as it requires counting the number of diagrams at the same order in a conventional diagrammatic technique operating with a non-symmetrized vertex, $\bar{\Gamma}$. Once we obtain the non-symmetrized vertex, we anti-symmetrize it, and use the result in the Dyson equation to obtain the self-energy. In the following, we derive an expression for the forward-scattering part of the non-symmetrized vertex, $\bar{\Gamma}$, summing up diagrams with the maximum number of polarization bubbles to all orders in the contact interaction, U. The diagrams for a non-symmetrized vertex up to third order are presented in Fig. 2–3.

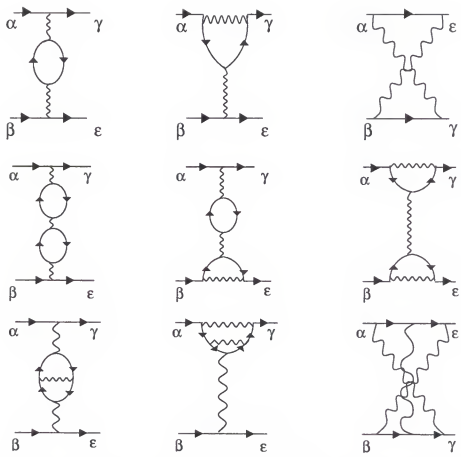

Figure 2–3: Second and third order Vertex diagrams with maximum number of particle-hole bubbles. Additional diagrams, obtained from those in the second column by a permutation $\alpha \rightarrow \beta, \gamma \rightarrow \varepsilon$, are not shown.

In the Matsubara technique, we associate a factor of $-U$ with each of the interaction lines, and a factor -2 with each of the polarization bubble. There is also an extra factor of -1 for exchange processes in which the two outgoing legs are permuted (the last diagrams of second and third order in Fig. 2–3). We present here a general recipe for calculating the ν^{th} ($\nu > 1$) order vertex diagram. The vertex consists of two parts (Fig. 2–3). The first part comes from the direct interaction and contains a spin factor $\delta_{\alpha\gamma}\delta_{\beta\varepsilon}$. The second part is due to the exchange interaction, and comes with a spin factor $\delta_{\alpha\varepsilon}\delta_{\beta\gamma}$. At each order, there is only one exchange diagram whose contribution is $-(-U)^{\nu}\Pi^{\nu-1}\delta_{\alpha\varepsilon}\delta_{\beta\gamma}$ (At second and third orders, these are the first and third diagrams in the third column of Fig. 2–3, respectively).

The rest of the diagrams are due to the direct interaction and contain various number of bubbles. At order ν (number of interaction lines $= \nu$), the number of bubbles in the diagram (both explicit and implicit) will be $\nu - 1$, thus the number of explicit bubbles or the rings (R) can vary from 0 to $\nu - 1$. We consider a diagram with R rings and $\nu - 1$ interaction lines, for this diagram $R + 1$ interaction lines will be used up in connecting the rings (we are considering connected diagrams) and also in connecting the rings to the two external solid lines. The remaining $N = \nu - R - 1$ interaction lines can be arranged anywhere either at the two ends of the chain of bubbles (or in other words, dressing up the two interaction lines which connect the solid line) or inside the R ring bubbles. Thus there will be $S = R + 2$ sites (two ends and inside the R rings) where N interaction lines can be placed. The number of diagrams with R ring diagrams is equal to the number of ways to arrange N lines among S sites:

$$\frac{(S+N-1)!}{(S-1)!N!} = \frac{\nu!}{(R+1)!(\nu-R-1)!}. \tag{2.28}$$

Consequently, the contribution to $\bar{\Gamma}$ from diagrams with R bubbles is

$$\frac{\nu!}{(R+1)!(\nu-R-1)!}(-U)^{\nu}(-2)^{R}\Pi^{\nu-1}\delta_{\alpha\gamma}\delta_{\beta\varepsilon}. \tag{2.29}$$

The total contribution from all bubble diagrams at the order ν is then

$$\sum_{R=0}^{\nu-1}\frac{\nu!(-2)^{R}}{(R+1)!(\nu-R-1)!}(-U)^{\nu}\Pi^{\nu-1}\delta_{\alpha\gamma}\delta_{\beta\varepsilon} = -\frac{(1-(-1)^{\nu})}{2}U^{\nu}\Pi^{\nu-1}\delta_{\alpha\gamma}\delta_{\beta\varepsilon} \tag{2.30}$$

where we have used an identity

$$\sum_{R=0}^{\nu} \frac{\nu!(-2)^R}{R!(\nu-R)!} = (1-2)^\nu = (-1)^\nu . \tag{2.31}$$

Adding up direct and exchange terms, we obtain the following form for the non-symmetrized vertex at order $\nu > 1$:

$$\bar{\Gamma}^{\nu}_{\alpha\beta,\gamma\varepsilon} = -\frac{1}{2}(1-(-)^\nu)U^\nu \Pi^{\nu-1}\delta_{\alpha\gamma}\delta_{\beta\varepsilon} - (-U)^\nu \Pi^{\nu-1}\delta_{\alpha\varepsilon}\delta_{\beta\gamma}. \tag{2.32}$$

The vertex function can now be readily summed to all orders, with the result

$$\begin{aligned} \bar{\Gamma}_{\alpha\beta,\gamma\varepsilon}(p_1,p_2;p_1-q,p_2+q) &= \bar{\Gamma}_{\alpha\beta,\gamma\varepsilon}(q) \\ &= -U\delta_{\alpha\varepsilon}\delta_{\beta\gamma} + \sum_{\nu=1}^{\infty} \bar{\Gamma}^{\nu}_{\alpha\beta,\gamma\varepsilon} \\ &= -\delta_{\alpha\gamma}\delta_{\beta\varepsilon}\frac{U}{1-(U\Pi)^2} - \delta_{\alpha\varepsilon}\delta_{\beta\gamma}\frac{U^2\Pi(q)}{1+U\Pi(q)}. \end{aligned} \tag{2.33}$$

where by including the additional factor $-U\delta_{\alpha\varepsilon}\delta_{\beta\gamma}$ we are able to extend the summation of the vertex function to $\nu = 1$. Using an SU(2) identity

$$\delta_{\alpha\varepsilon}\delta_{\beta\gamma} = (1/2)\left(\sigma^a_{\alpha\gamma}\sigma^a_{\beta\varepsilon} + \delta_{\alpha\gamma}\delta_{\beta\varepsilon}\right), \tag{2.34}$$

and introducing the dimensionless spin and charge vertices

$$\mathcal{G}_\sigma = -\frac{1}{2}\frac{1}{1+U\Pi(q)},$$

$$\mathcal{G}_\rho = \frac{1}{2}\frac{1}{1-U\Pi(q)}, \tag{2.35}$$

we obtain for the non-symmetrized vertex the following form

$$\begin{aligned} \bar{\Gamma}_{\alpha\beta,\gamma\varepsilon}(p_1,p_2;p_1-q,p_2+q) &= \bar{\Gamma}(q) \\ &= -U\left[\delta_{\alpha\gamma}\delta_{\beta\varepsilon}\left(\frac{1}{2}+\mathcal{G}_\rho\right) + \sigma^a_{\alpha\gamma}\sigma^a_{\beta\varepsilon}\left(\frac{1}{2}+\mathcal{G}_\sigma\right)\right]. \end{aligned} \tag{2.36}$$

Finally we anti-symmetrize the vertex by the following procedure

$$\Gamma_{\alpha\beta;\gamma\varepsilon}(q) = \bar{\Gamma}_{\alpha\beta;\gamma\varepsilon}(q) - \bar{\Gamma}_{\alpha\beta;\varepsilon\gamma}(q). \tag{2.37}$$

For a repulsive potential the retarded charge vertex, $\mathcal{G}_\rho^R$, has pole at the zeros of $1 - U\Pi^R(\mathbf{q},\Omega) = 0$. The pole exists even for an infinitesimally small U, since for $|\Omega| > |v_F Q|$, Π^R is real and can be arbitrarily large as $|\Omega| \to (v_F Q)^+$.

$$1 + U\frac{m}{2\pi}(1 - \frac{\Omega}{\sqrt{\Omega^2 - (v_F \mathbf{q})^2}}) = 0$$
$$\Omega^2 = v_F^2 \left(1 + \frac{u^2}{1+2u}\right)\mathbf{q}^2.$$

The collective mode which corresponds to the short-range interaction is called a zero-sound mode whose dispersion is $|\Omega| = cQ$ and the zero sound velocity is

$$c = v_F\sqrt{1 + \frac{u^2}{1+\frac{Um}{\pi}}} \approx v_F(1 + \frac{1}{2}u^2),$$

where the expansion is valid for $u \ll 1$. The charge vertex exhibits singular behavior near the zero-sound mode and has the following form

$$\begin{aligned}\mathcal{G}^R_{\rho,ZS} &= \frac{1}{2(\Omega - cQ)\frac{\partial}{\partial\Omega}[1 - U\Pi(Q,\Omega)]}\Big|_{\Omega=cQ} + \frac{1}{2(\Omega + cQ)\frac{\partial}{\partial\Omega}[1 - U\Pi(Q,\Omega)]}\Big|_{\Omega=-cQ} \\ &= \frac{(u^2 v_F^2 Q^2)}{(\Omega + i0+)^2 - c^2Q^2}.\end{aligned}$$

For small values of u the zero-sound mode cQ is just above the upper boundary of the particle-hole continuum, given by $v_F Q$. The residue of the charge vertex is not a constant and is proportional to Q^2, thus the quanta of the zero-sound mode are not free. The spin vertex $\mathcal{G}_\sigma^R$ on the contrary has a pole in the imaginary axis and remains over-damped.

Dyson equation. The self-energy due to forward scattering is related to the vertex function via the Dyson equation [17]

$$\Sigma_{F,\alpha\beta}(p) = \delta_{\alpha\beta}\int_q UG(p-q) - \int_{p',p''} U\Gamma_{\gamma\alpha;\gamma\beta}(p, p'+p''-p; p', p'')G(p')G(p'')G(p'+p''-p), \tag{2.38}$$

where

$$\int_k \cdots \equiv T\sum_{\Omega_m}\int d^2k/(2\pi)^2 \ldots \tag{2.39}$$

Although the Green's functions in the Dyson equation are exact ones, we can safely ignore the self-energy insertions into the diagrams which diverge near the mass shell as these insertions do not lead to any additional singularities near the mass shell. As we keep

u=$(Um/2\pi)$ small, regular corrections are thus irrelevant, and we can safely use bare G's instead of the exact ones in Eq. (2.38). Substituting Eq. (2.37) into the Dyson equation (2.38), we obtain for the self-energy

$$\begin{aligned}
\Sigma_{\alpha\beta}(p) &= \delta_{\alpha\beta}\int_q UG(p-q) - \int_{p'} U\overline{\Gamma}_{\gamma\alpha;\gamma\beta}G(p')\Pi(p-p') + \int_{p''} U\overline{\Gamma}_{\gamma\alpha;\beta\gamma}G(p'')\Pi(p-p'') \\
&= \delta_{\alpha\beta}\int_q UG(p-q) + \delta_{\alpha\beta}\int_{p'}\left\{\frac{2U^2}{1-(U\Pi)^2} + \frac{U^3\Pi}{1+U\Pi}\right\}G(p')\Pi(p-p') \\
&\quad -\delta_{\alpha\beta}\int_{p'}\left\{\frac{U^2}{1-(U\Pi)^2} + \frac{2U^3\Pi}{1+U\Pi}\right\}G(p'')\Pi(p-p'') \\
&= \delta_{\alpha\beta}\int_q UG(p-q) + \delta_{\alpha\beta}\int_q \frac{U^2\Pi(q)}{1-(U\Pi)^2}G(p-q) \\
&\quad -\delta_{\alpha\beta}\int_q \frac{U^3\Pi(q)^2}{1+U\Pi}G(p-q). \qquad (2.40)
\end{aligned}$$

Rearranging the result, we obtain the self-energy in the following form $\Sigma_{\mathrm{F},\alpha\beta} = \delta_{\alpha\beta}\Sigma_{\mathrm{F}}$ where

$$\Sigma_{\mathrm{F}}(p) = \int_q \left[U + U^2\Pi(q) + \frac{1}{2}\frac{U^3\Pi^2(q)}{(1-U\Pi(q))} - \frac{3}{2}\frac{U^3\Pi^2(q)}{(1+U\Pi(q))}\right]G(p-q). \qquad (2.41)$$

We remind the reader that in the perturbation theory $\mathrm{Im}\Sigma^R$ diverges upon approaching the mass shell– logarithmically to second order in U, and as $1/\sqrt{\varepsilon-\xi_k}$ to third order. It is convenient to rearrange the terms of Eq. (2.41) and decompose Σ_{F} into three parts making use of the charge and spin vertices, introduced in Eq. (2.35), as

$$\Sigma_{\mathrm{F}}(p) = \Sigma_\rho(p) + \Sigma_\sigma(p) + \Sigma_{\mathrm{ex}}; \qquad (2.42a)$$

$$\Sigma_\rho(p) = U\int_q \mathcal{G}_\rho(q)\,G(p-q); \qquad (2.42b)$$

$$\Sigma_\sigma(p) = 3U\int_q \mathcal{G}_\sigma(q)\,G(p-q); \qquad (2.42c)$$

$$\Sigma_{\mathrm{ex}} = \int_q \left[2U - U^2\Pi(q)\right]G(p-q). \qquad (2.42d)$$

Terms Σ_ρ and Σ_σ correspond to the interaction in the charge and spin channels, respectively, and are summed to all orders in U. The remainder, Σ_{ex}, contains extra contributions of the first and second orders in U, which are not included in the spin and charge terms and are required to reproduce the correct expansion of the first and second order term of the self-energy.

A similar expression was obtained for the self-energy in the paramagnon model (the spin-fluctuation model) [20], although the contribution from the remainder term, $\Sigma_{\rm ex}$, was not taken into account. The paramagnon model includes only two kinds of diagrams, RPA and ladder diagrams corresponding to the charge channel and the spin channel, respectively. In contrast, our choice of diagrams is based on a broader consideration of including the maximum number of particle hole bubbles at each order which for forward scattering leadto mass-shell singularity, thus we have included non-RPA and non-ladder-type diagrams as well. Including the maximally divergent diagrams also means that the perturbative expansion near the mass shell is in terms of the diverging parameter $((Um/2\pi)^2\varepsilon/\Delta)$ and any expansion which involves the regular $Um/2\pi$ is neglected. After the complete resummation, it turns out that the expression for the self-energy is very similar to the one obtained in Ref. [20].

2.3.4 Renormalized Imaginary Part of the Self-Energy

The imaginary part of the self-energy acquires non-zero contributions from the regions in momentum and frequency space where the effective interaction has a non-zero imaginary part. There are only two such regions, one of them at the collective mode $|\Omega| = cQ$ where the charge channel $\mathcal{G}_\rho^R$ has a pole, and the other region where $\mathrm{Im}\Pi^R \neq 0$, i.e., where particle-hole excitations are permissible. All three terms-the charge-vertex part, the spin-vertex part and the extra term− acquire contributions from the particle-hole region, whereas only the charge-vertex part has a contribution from the collective mode excitation. We can represent the imaginary part of the self-energy as follows

$$\begin{aligned} \mathrm{Im}\Sigma^R &= \mathrm{Im}\Sigma_\rho^R + \mathrm{Im}\Sigma_\sigma^R + \mathrm{Im}\Sigma_{\rm ex}^R \\ &= (\mathrm{Im}\Sigma_\rho^R + \mathrm{Im}\Sigma_\sigma^R + \mathrm{Im}\Sigma_{\rm ex}^R)_{\rm PH} + (\mathrm{Im}\Sigma_\rho^R)_{\rm ZS}, \end{aligned} \tag{2.43}$$

where the subscripts PH and ZS stand for the particle-hole and zero-sound contribution respectively. In the following analysis we will investigate the forward scattering contribution from the particle-hole excitation and the zero-sound mode, and show that $\mathrm{Im}\Sigma$ is completely renormalized.

Particle-hole contribution. The first term of Σ^R_{ex} is real [Eq. (2.42d)] and does not contribute to the imaginary part, whereas the second term differs from the second order self-energy term, Σ^R_2, by only a sign. Thus we can immediately infer $\mathrm{Im}\Sigma^R_{ex}$ from the forward scattering part of $\mathrm{Im}\Sigma^R_2$ [Eq. (2.22)],

$$\mathrm{Im}\Sigma^R_{ex} = -\mathrm{Im}\Sigma^R_2 = -\frac{U^2 m^2}{32\pi^3}\frac{\varepsilon^2}{E_F}\log\frac{E_F}{|\Delta|}. \tag{2.44}$$

The imaginary part of Σ_ρ and Σ_σ in the retarded formalism is given by

$$\mathrm{Im}\Sigma^R_\rho = -U\int_{-\varepsilon}^{0}\frac{d\Omega}{\pi}\int\frac{d^2Q}{(2\pi)^2}\mathrm{Im}G^R_0(\varepsilon+\Omega,\mathbf{k}+\mathbf{q})\mathrm{Im}\mathcal{G}_\rho \tag{2.45}$$

$$\mathrm{Im}\Sigma^R_\rho = -3U\int_{-\varepsilon}^{0}\frac{d\Omega}{\pi}\int\frac{d^2Q}{(2\pi)^2}\mathrm{Im}G^R_0(\varepsilon+\Omega,\mathbf{k}+\mathbf{q})\mathrm{Im}\mathcal{G}_\sigma \tag{2.46}$$

where for $q \le p_F$, $\mathrm{Re}\Pi^R = -m/2\pi$, thus for weak interaction $Um/2\pi \ll 1$, the terms $\mathrm{Im}\mathcal{G}_\rho$ and $\mathrm{Im}\mathcal{G}_\sigma$ will be equal in the leading order of interaction

$$\mathrm{Im}\mathcal{G}_\rho = \frac{1}{2}\frac{U\mathrm{Im}\Pi^R}{(1-U\mathrm{Re}\Pi^R)^2+(U\mathrm{Im}\Pi^R)^2} \approx \frac{1}{2}\frac{U\mathrm{Im}\Pi^R}{1+(U\mathrm{Im}\Pi^R)^2}$$
$$\mathrm{Im}\mathcal{G}_\sigma = \frac{1}{2}\frac{U\mathrm{Im}\Pi^R}{(1+U\mathrm{Re}\Pi^R)^2+(U\mathrm{Im}\Pi^R)^2} \approx \frac{1}{2}\frac{U\mathrm{Im}\Pi^R}{1+(U\mathrm{Im}\Pi^R)^2}.$$

Substituting the value for $\mathrm{Im}G^R_0$ and $\mathrm{Im}\Pi^R$ from Eqs. (2.12) and (2.13) in Eqs. (2.45) and (2.46) we obtain

$$\mathrm{Im}\mathcal{G}_{PH} = \mathrm{Im}\Sigma_\rho + \mathrm{Im}\Sigma_\sigma = \frac{u^2}{4\pi}\frac{\varepsilon^2}{E_F}\left[\log\frac{E_F}{u^2|\varepsilon|} + G_I\left(\frac{2\Delta}{u^2|\varepsilon|}\right)\right], \tag{2.47}$$

where

$$G_I(x) = 2\log 2 - 1/2 + \log|x|^{-1} - 2\mathrm{Re}\int_0^1\frac{zdz}{\sqrt{1-x/z}}\log\frac{1+\sqrt{1-x/z}}{1-\sqrt{1-x/z}}. \tag{2.48}$$

In the limit $|x| \gg 1$, the scaling function behaves as $G_I(x) \approx \log|x|^{-1}$ and hence

$$\mathrm{Im}\Sigma^R_{PH} = \frac{u^2}{4\pi}\frac{\varepsilon^2}{E_F}\log\frac{E_F}{\Delta}. \tag{2.49}$$

In the opposite limit $|x| \ll 1$, function $G_I(x)$ vanishes as $x \ln |x|$. As a result, net $\mathrm{Im}\Sigma^R_{\mathrm{PH}}$ remains finite at $\Delta = 0$, and for $|x| \ll 1$ (i.e., for $|\Delta| \ll u^2|\varepsilon|$) it behaves as

$$\mathrm{Im}\Sigma^R_{\mathrm{PH}} = \frac{u^2}{4\pi}\frac{\varepsilon^2}{E_F}\left[\ln\frac{E_F}{u^2|\varepsilon|} + \frac{2\Delta}{u^2\varepsilon}\ln\frac{|\Delta|}{u^2|\varepsilon|}\right]. \tag{2.50}$$

Comparing the limiting forms of Eq. (2.49) and Eq. (2.50), we see that higher order terms in u simply cut the logarithmic divergence in $\mathrm{Im}\Sigma^R_{\mathrm{PH}}$ for $|\Delta| < u^2|\varepsilon|$. To logarithmic accuracy, one can then approximate $\mathrm{Im}\Sigma^R_{\mathrm{PH}}$ by

$$\mathrm{Im}\Sigma^R_{\mathrm{PH}} = \frac{u^2}{4\pi}\frac{\varepsilon^2}{E_F}\ln\frac{E_F}{|w|}, \tag{2.51}$$

where $w \equiv \max(|\Delta|, u^2|\varepsilon|)$.

Zero-sound contribution. Unlike the particle-hole region, which contributes to all the terms in Eq. (2.43), the zero-sound mode makes a contribution only to $\mathrm{Im}\Sigma^R_\rho$:

$$\mathrm{Im}\Sigma^R_{\rho-ZS} = U\int_{-\varepsilon}^{0}\frac{d\Omega}{\pi}\int\frac{d^2Q}{(2\pi)^2}\mathrm{Im}G^R_0(\varepsilon+\Omega, \mathbf{k}+\mathbf{q})\mathrm{Im}\mathcal{G}_{\rho-ZS}, \tag{2.52}$$

where the subscript $\rho - ZS$, stands for the contribution to the charge channel from the zero-sound mode region. The collective mode $\mathrm{Im}\mathcal{G}_{\rho-ZS}$ has a pole given by

$$U\mathrm{Im}\mathcal{G}^R_{\rho-ZS} = \mathrm{Im}\left(\frac{U(\frac{Um}{2\pi})^2v_F^2Q^2}{(\Omega+i0^+)^2 - c^2Q^2}\right) = -\frac{U^3m^2Q}{8\pi}[\delta(\Omega - cQ) - \delta(\Omega + cQ)] \tag{2.53}$$

We will plug the form of interaction given in Eq. (2.53) into Eq. (2.52) and perform the angular integration on G^R_0 to obtain

$$\begin{aligned}\mathrm{Im}\Sigma^R_{\rho-ZS} &= -\int_{-\varepsilon}^{0}\frac{d\Omega}{\pi}\int\frac{QdQ}{(2\pi)^2}\frac{2\pi}{\sqrt{(v_FQ)^2 - (\Omega+\Delta)^2}} \\ &\quad \frac{m^2U^3Q}{8\pi}[\delta(\Omega - cQ) - \delta(\Omega + cQ)] \\ &= \frac{m^2U^3}{16\pi^3}\int_0^{\varepsilon/c}\frac{Q^2dQ}{\sqrt{(v_FQ)^2 - (-Qc+\Delta)^2}},\end{aligned} \tag{2.54}$$

near the mass-shell $Qc\Delta \gg \Delta^2$ and $c^2 - v_F^2 = (Um/2\pi)^2$. After some manipulations, on Eq. (2.54), we obtain

$$\mathrm{Im}\Sigma^R_{\rho-ZS} = \frac{m^2U^3}{16\pi^3}\int_0^{\varepsilon/c}\frac{QdQ}{\sqrt{\frac{2\Delta}{Qv_F} - (\frac{Um}{2\pi})^2}} = \frac{m^2U^3}{16\pi^3}\mathrm{Re}\int_0^{\varepsilon/c}\frac{QdQ}{\sqrt{\frac{2\Delta}{Qv_F} - (\frac{Um}{2\pi})^2}}. \tag{2.55}$$

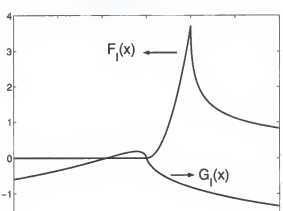

Figure 2–4: Scaling functions F_I and G_I as a function of x. Note the strong asymmetry of F_I about $x = 0$.

The above result was for $\varepsilon > 0$. For $\varepsilon < 0$ we have

$$\mathrm{Im}\Sigma^R_{\rho-ZS} = \frac{m^2U^3}{16\pi^3}\mathrm{Re}\int_0^{-\varepsilon/c} \frac{QdQ}{\sqrt{-\frac{2\Delta}{Qv_F} - (\frac{Um}{2\pi})^2}}. \tag{2.56}$$

Thus for any ε near the mass shell, the contribution to the imaginary part of the self-energy is given by

$$\begin{aligned} \mathrm{Im}\Sigma^R_{\rho-ZS} &= \frac{m^2U^3}{16\pi^3}\mathrm{Re}\int_0^{|\varepsilon|/c} \frac{QdQ}{\sqrt{sgn(\varepsilon)\frac{2\Delta}{Qv_F} - (\frac{Um}{2\pi})^2}} \\ &= \frac{m^2U^2\varepsilon^2}{16\pi^3 E_F}\Big[2\pi\int_0^{\min\{1,\sqrt{x}\}} \frac{y^4}{\sqrt{x-y^2}}\Big]. \end{aligned} \tag{2.57}$$

The integral of Eq. (2.57) can be performed using standard Mathematica software, the result is

$$F_I(x) = 2\pi\int_0^{\min\{1,\sqrt{x}\}} \frac{y^4 dy}{\sqrt{x-y^2}} = \begin{cases} 3\pi^2x^2/8, \text{ for } 0 \le x < 1; \\ \frac{\pi}{2}\left[\frac{3x^2}{2}\sin^{-1}\frac{1}{\sqrt{x}} - \sqrt{x-1}\left(\frac{3}{2}x+1\right)\right], \text{ for } x > 1. \end{cases} \tag{2.58}$$

Here $x = 2\Delta/u^2\varepsilon$, and for $x \gg 1$, $F_I(x) \approx 2\pi/5\sqrt{x}$. From the plot of $F_I(x)$, Fig. 2–4, it is clear that $\mathrm{Im}\Sigma^R_{ZS}$ remains finite in the entire range of x. Combining the asymptotic value of $F_I(x)$ and $G_I(x)$ for $x \gg 1$, we recover the 3^{rd} and higher order results obtained via the

perturbative process,

$$\begin{aligned} \mathrm{Im}\Sigma^R_{\rho-ZS} + \mathrm{Im}\Sigma^R_{PH} &= \left[\frac{\sqrt{2}u^3\varepsilon^2}{20E_F}\sqrt{\frac{\varepsilon}{\Delta}}\right] - \left[\frac{\sqrt{8}u^3\varepsilon^2}{20E_F}\sqrt{\frac{\varepsilon}{\Delta}}\right] \\ &= -\left[\frac{\sqrt{2}u^3\varepsilon^2}{20E_F}\sqrt{\frac{\varepsilon}{\Delta}}\right]. \end{aligned}$$

It should be noted that the above form of the third order self-energy is valid only for regions far away from the mass shell.

Unlike the perturbative case, where the regions near the mass shell are inaccessible due to divergence, no such divergence takes place for $F_I(x)$. At $|\Delta| = u^2|\varepsilon|/2$, $F_I(x)$ has a maximum and on the mass shell ($\Delta = 0$), $\mathrm{Im}\Sigma^R_{ZS}$ vanishes. The vanishing of $\mathrm{Im}\Sigma^R_{ZS}$ on the mass shell is due to the Cherenkov type restriction where the quasi-particle with velocity $v_F < c$ cannot emit a zero-sound boson, hence the zero-sound mode cannot decay the quasi-particle. The asymmetry of $F_I(x)$, $F_I(x) = 0$ for $x < 0$, can be understood if we refer to Eq. (2.54), for $\varepsilon > 0$ the integral will have non-zero contribution as long as $\Delta > 0$. For a detailed analysis let us consider Eq. 2.52. The delta functions originating from $\mathrm{Im}\Sigma^R_\rho$ and $\mathrm{Im}\mathcal{G}_\rho$ impose severe restrictions on the phase space for the emission of bosons. We find the following condition should hold for non-zero contribution to $\mathrm{Im}\Sigma^R_{\rho-ZS}$ or for the emission of Bosons (in the following we will use $c \approx v_F(1+u^2/2)$)

$$\begin{aligned} \varepsilon - \xi_k &= \Omega + \frac{v_F}{c}\Omega\cos\theta \\ -1 \le \cos\theta &= \frac{\frac{\Delta}{\Omega} - 1}{1 - \frac{u^2}{2}} < 1 \\ 0 < \frac{u^2\Omega}{2} &\le \Delta \le 2\Omega \le 2\varepsilon. \\ 0 < \frac{\Omega}{4\varepsilon} &\le \frac{x}{2} \le \frac{\Omega}{u^2\varepsilon} \le \frac{1}{u^2}. \end{aligned}$$

This condition clearly suggests that ε and Δ should have the same sign. To study the decay of a quasi-particle, we consider a fermion with energy ε such that $u^2|\varepsilon|/2 < \Delta$ or $x > 1$, in this case all Ω's satisfy $\Omega/4\varepsilon \le x/2$. As x is increased further the condition $x/2 \le \Omega/u^2\varepsilon$ imposes constraints on the low-energy bosons, thus fewer and fewer bosons are able to contribute to the decay processes, and hence $F_I(x)$ reduces. For Δ such that $u^2\varepsilon/2 > \Delta$, *i.e*, $x < 1$ decreasing Δ (or $x \to 0$) implies the frequency range available to the

bosons that contribute in the decay process shrinks, thus $F_I(x)$ decreases. This explains the non-monotonic variation of $\mathrm{Im}\Sigma^R_{ZS}$ as a function of the parameter $x = 2\Delta/u^2\varepsilon$.

An important thing to notice is that the contribution from the zero-sound region $\mathrm{Im}\Sigma^R_{ZS}$ is small compared to the contribution from the particle-hole region,

$$\frac{\mathrm{Im}\Sigma^R_{ZS}}{\mathrm{Im}\Sigma^R_{PH}} = \frac{F_I(x)}{\log E_F/|\varepsilon|},$$

since $F_I(x) \sim 1$, $\mathrm{Im}\Sigma^R_{PH}$ is log-dominant with respect to $\mathrm{Im}\Sigma^R_{ZS}$.

Finite-curvature effects. From the analysis thus far, we conclude that the divergences present from the 3^{rd} order onwards in the perturbative expansion of $\mathrm{Im}\Sigma^R$ [Eq. (2.27)] have been regularized by resumming the series. Nevertheless, there still remains a log divergence at second order due to the extra term $\mathrm{Im}\Sigma^R_{ex}$, which must be cut off due by the finite curvature of the fermionic dispersion. The log-singularity is cut at $q^2/2m \sim \Delta_c = \varepsilon^2/E_F$, and we obtain from Eq. (2.44)

$$\mathrm{Im}\Sigma^R_{\mathrm{ex}} = -\frac{u^2}{4\pi}\frac{\varepsilon^2}{E_F}\log\frac{E_F}{|\varepsilon|}. \tag{2.59}$$

Thus all the terms of Eq. (2.43) are renormalized and $\mathrm{Im}\Sigma$ is finite at the mass shell. A natural question that arises is: is it possible to remove the mass-shell divergence in the perturbative expansion of $\mathrm{Im}\Sigma^R$ [Eq. (2.27)] without resorting to resummation and instead removing the divergence by including the cut-off due to finite curvature? Let us insert the cut-off $\Delta_c = \varepsilon^2/E_F$ in Eq. (2.27). We obtain

$$\mathrm{Im}\Sigma^R_F(\varepsilon) = \frac{u^2\varepsilon^2}{4\pi E_F}\Big[\log(\frac{E_F}{|\varepsilon|}) + \sum_{n=1}^{\infty} C_n\Big(\frac{u^2E_F}{\varepsilon}\Big)^{n/2}\Big]. \tag{2.60}$$

This series does not converge for $|\varepsilon| < \omega_c$, where $\omega_c = u^2E_F$, thus the finite curvature does not lead to the convergence of the series and the need for resummation remains.

For $\Delta \gg \Delta_c$ curvature effects can be totally neglected (this is the regime that has been considered in our work) and the results for Im^R_{ZS} and Im^R_{PH} will remain the same as has been derived by the resummation procedure. For $\Delta \ll \Delta_c$ the results will change, since Δ_c can no longer be ignored in the integrations. To obtain the functional form all

one has to do is replace Δ by Δ_c in the functions

$$\begin{aligned} F_I\left(\frac{2\Delta}{u^2\varepsilon}\right) &\rightarrow F_I\left(\frac{2\Delta_c}{u^2\varepsilon}\right) = F_I\left(\frac{2|\varepsilon|}{\omega_c}\right) \\ G_I\left(\frac{2\Delta}{u^2\varepsilon}\right) &\rightarrow G_I\left(\frac{2\Delta_c}{u^2\varepsilon}\right) = G_I\left(\frac{2|\varepsilon|}{\omega_c}\right). \end{aligned}$$

We will use this information to obtain $\mathrm{Im}\Sigma^R_{PH}$ and $\mathrm{Im}\Sigma^R_{ZS}$ on and near the mass shell. Let us consider the limit $|\Delta| \ll \Delta_c$. Following our earlier analysis we will make the necessary changes $\mathrm{Im}\Sigma^R_{PH}(|\Delta|) \rightarrow \mathrm{Im}\Sigma^R_{PH}(|\Delta_c|)$, obtaining

$$\begin{aligned} \mathrm{Im}\Sigma^R_{PH} &= \frac{u^2\varepsilon^2}{4\pi E_F}\left[\log\frac{E_F}{u^2|\varepsilon|} + G_I\left(\frac{2\Delta_c}{u^2|\varepsilon|}\right)\right] \\ &= \frac{u^2\varepsilon^2}{4\pi E_F}\left[\log\frac{E_F}{u^2|\varepsilon|} + G_I\left(\frac{2|\varepsilon|}{\omega_c}\right)\right]. \end{aligned}$$

As a reminder the scaling function: $G_I(2|\varepsilon|/\omega_c) = G_I(x)$ behaves as

$$G_I(x) = \begin{cases} x\ln|x|, & \text{for} \quad x \ll 1, \quad |\varepsilon| \ll \varepsilon_c \\ \ln\frac{1}{|x|}, & \text{for} \quad x \gg 1, \quad |\varepsilon| \gg \omega_c. \end{cases} \tag{2.61}$$

From this result we obtain

$$\mathrm{Im}\Sigma^R_{PH} = \begin{cases} \frac{u^2\varepsilon^2}{4\pi E_F}\ln\frac{E_F}{u^2|\varepsilon|}, & \text{for} \quad |\varepsilon| \ll \omega_c; \\ \frac{u^2\varepsilon^2}{2\pi E_F}\ln\frac{E_F}{|\varepsilon|}, & |\varepsilon| \gg \omega_c. \end{cases} \tag{2.62}$$

There is no such scaling relation for $\mathrm{Im}\Sigma^R_{ex}(\Delta) \rightarrow \mathrm{Im}\Sigma^R_{ex}(\Delta_c)$ and the functional form remains the same for either limit, $\varepsilon \gg \omega_c$ or $\varepsilon \ll \omega_c$,

$$\mathrm{Im}\Sigma^R_{ex} = -\frac{u^2\varepsilon^2}{4\pi E_F}\log\frac{E_F}{|\varepsilon|}.$$

The zero-sound contribution to $\mathrm{Im}\Sigma^R_{ZS}$ obeys a scaling relation governed by the scaling function $F_I(x)$. For $x \ll 1$, $F_I(x)$ scales as $3\pi^2x^2/8$ and for $x \gg 1$ scales as $2\pi/5\sqrt{x}$, this then implies

$$\mathrm{Im}\Sigma^R_{ZS} = \frac{u^2\varepsilon^2}{4\pi E_F}\begin{cases} \frac{3\pi^2}{2}\frac{\varepsilon^2}{\omega_c^2}, & \text{for} \quad |\varepsilon| \ll \omega_c; \\ \frac{\pi\sqrt{2}}{5}\frac{\omega_c}{\varepsilon}, & |\varepsilon| \gg \omega_c. \end{cases} \tag{2.63}$$

Adding up contributions from all forward scattering terms, the final form reads

$$\mathrm{Im}\Sigma_F^R = \mathrm{Im}\Sigma_{PH}^R + \mathrm{Im}\Sigma_{ZS}^R + \mathrm{Im}\Sigma_{ex}^R = \begin{cases} \frac{u^2\varepsilon^2}{4\pi E_F}|\log u^2|, & \text{for} \quad |\varepsilon| \ll \omega_c; \\ \frac{u^2\varepsilon^2}{4\pi E_F}\log\frac{E_F}{|\varepsilon|}, & |\varepsilon| \gg \omega_c. \end{cases} \tag{2.64}$$

Notice since $F_I(x) \sim 1$ for all ranges of x, the contribution from $\mathrm{Im}\Sigma_{PH}^R$ and $\mathrm{Im}\Sigma_{ex}^R$ will be dominant by a large log term compared to $\mathrm{Im}\Sigma_F^R$ and has therefore not been included in Eq. (2.64).

ImΣ^R on the mass shell: final result. The leading contribution to the ImΣ^R comes from both forward- and back-scattering contributions. We have successfully renormalized the forward-scattering contribution and as discussed before no such renormalization scheme is required for the back-scattering contribution, so the total contribution is

$$\mathrm{Im}\Sigma^R \;=\; \mathrm{Im}\Sigma_F^R + \mathrm{Im}\Sigma_B^R = \frac{u^2\varepsilon^2}{2\pi E_F}\ln\frac{E_F}{|\varepsilon|}\begin{cases} \frac{1}{2}, & \text{for} \quad |\varepsilon| \ll \omega_c; \\ 1, & |\varepsilon| \gg \omega_c. \end{cases} \tag{2.65}$$

Thus near the mass shell ImΣ behaves as the usual $\varepsilon^2\log|\varepsilon|$.

2.3.5 Renormalized Real Part of the Self-Energy

In the following analysis, we will derive the real part of the self-energy near the mass shell from the back-scattering process by making use of the Kramers-Kronig relationship between the real and the imaginary part of the retarded self-energy. A detailed calculation of the zero-sound contribution to the real part of the self-energy is also presented, where instead of the Kramers-Kronig relationship we have considered the explicit form of the ReΣ in the retarded formalism.

Back scattering. In an earlier analysis we obtained $\mathrm{Im}\Sigma_{2k_F}^R$ and $\mathrm{Im}\Sigma_{g_2}^R$. A sum of these two back-scattering contributions is

$$\mathrm{Im}\Sigma_B^R(\varepsilon) = \frac{u^2}{4\pi}\frac{\varepsilon^2}{E_F}\log\frac{W}{|\varepsilon|}. \tag{2.66}$$

where W is an upper cut-off typically of the order of E_F. We will make use of the Kramers-Kronig relation to obtain the real part of the self-energy from the imaginary

part.

$$\mathrm{Re}\Sigma^R(\varepsilon) = \frac{1}{\pi}\mathcal{P}\int d E \frac{\mathrm{Im}\Sigma^R(E,\xi_k=\varepsilon)}{E-\varepsilon} = \frac{mU^2\varepsilon^2}{8\pi^4 v_F^2}\mathcal{P}\lim_{W\to\infty}\int_0^W dE \log\frac{W}{E}\left(1+\frac{\varepsilon^2}{E^2-\varepsilon^2}\right).$$

Focussing only on the cut-off independent and nonanalytic term, we obtain

$$\begin{aligned}\mathrm{Re}\Sigma^R(\varepsilon) &= \frac{mU^2\varepsilon}{8\pi^4 v_F^2}\mathcal{P}\lim_{W\to\infty}\int_0^W dE \log\frac{W}{E}\left(1+\frac{\varepsilon^2}{E^2-\varepsilon^2}\right)\\ &\approx \frac{mU^2\varepsilon|\varepsilon|}{8\pi^4 v_F^2}\mathcal{P}\lim_{W\to\infty}\int_0^{W/|\varepsilon|} dx \frac{\log x}{x^2-1}\\ &= -\frac{u^2}{8}\frac{\varepsilon|\varepsilon|}{E_F}\end{aligned} \tag{2.67}$$

Forward scattering. The real part of the self-energy consists of three contributions: from the remainder term (Σ^R_{ex}), from the particle-hole continuum (Σ^R_{PH}), and from the collective mode (Σ^R_{ZS}). The contribution from the remainder term and the particle-hole term is extracted similar to the previous approach, that is through the Kramers-Kronig relation, we obtain for the remainder term

$$\mathrm{Re}\Sigma^R_{ex} = \frac{u^2}{8}\frac{\varepsilon|\varepsilon|}{E_F} + O(\Delta^2\log\Delta) \tag{2.68}$$

and for the particle-hole term

$$\mathrm{Re}\Sigma^R_{PH} = -\frac{u^2}{8}\frac{\varepsilon|\varepsilon|}{E_F} - \frac{|\varepsilon|\Delta}{4E_F} \tag{2.69}$$

adding up the contributions from Eqs. (2.68) and (2.69) we obtain

$$\mathrm{Re}\Sigma^R_{ex} + \mathrm{Re}\Sigma^R_{PH} = -\frac{|\varepsilon|\Delta}{4E_F}. \tag{2.70}$$

Forward scattering: zero-sound contribution. In this Section, we will evaluate the nonanalytic $\varepsilon|\varepsilon|$ contribution from the zero-sound mode. The explicit form of $\mathrm{Re}\Sigma$ in the retarded formalism is

$$\begin{aligned}\mathrm{Re}\Sigma_R(\varepsilon,p) &= U\int\frac{d^2p_1}{(2\pi)^2}\int_{-\infty}^{\infty}\frac{d\omega}{\pi}\int_{-\infty}^{\infty}\frac{d\varepsilon_1}{2\pi}\frac{\mathrm{Im}G_R(\varepsilon_1,p_1)\mathrm{Im}\mathcal{G}^R_\rho(\omega,p-p_1)}{\omega+\varepsilon_1-\varepsilon}\\ &\quad\left[\tanh\frac{\varepsilon_1}{2T}+\coth\frac{\omega}{2T}\right],\end{aligned}$$

where $\mathrm{Im}\mathcal{G}_\rho^R$ is given by Eq. (2.52). Following the usual angular integration, we perform the dp_1 integration utilizing the delta function term from $\mathrm{Im}\mathcal{G}_\rho^R$. This yields

$$\begin{aligned}\mathrm{Re}\Sigma_R(\varepsilon,p) &= \alpha\int_0^\infty d\omega\int_{-\infty}^{\infty}d\varepsilon_1\frac{\omega^2}{\sqrt{(\frac{p\omega}{c})^2-(\varepsilon_1+\Delta)^2}(\omega+\varepsilon_1)}\left(\tanh\frac{\varepsilon_1+\varepsilon}{2T}+\coth\frac{\omega}{2T}\right)\\ &- \alpha\int_{-\infty}^0 d\omega\int_{-\infty}^{\infty}d\varepsilon_1\frac{\omega^2}{\sqrt{(\frac{p\omega}{c})^2-(\varepsilon_1+\Delta)^2}(\omega+\varepsilon_1)}\left(\tanh\frac{\varepsilon_1+\varepsilon}{2T}+\coth\frac{\omega}{2T}\right).\end{aligned}$$

where $\alpha = u^2U/4\pi$. For $T=0$, the trigonometric functions impose constraints on ε_1 and ω. Taking the zero temperature limit,

$$\begin{aligned}\mathrm{Re}\Sigma_R(\varepsilon,p) &= \alpha\int_0^\infty d\omega\int_{-\varepsilon}^{\infty}d\varepsilon_1\frac{2\omega^2}{\sqrt{(\frac{p\omega}{c})^2-(\varepsilon_1+\Delta)^2}(\omega+\varepsilon_1)}\\ &+\alpha\int_{-\infty}^0 d\omega\int_{-\infty}^{-\varepsilon}d\varepsilon_1\frac{2\omega^2}{\sqrt{(\frac{p\omega}{c})^2-(\varepsilon_1+\Delta)^2}(\omega+\varepsilon_1)}\\ &= \alpha\int_0^\infty d\omega\int_{-\varepsilon}^{\infty}d\varepsilon_1\frac{2\omega^2}{\sqrt{(\frac{p\omega}{c})^2-(\varepsilon_1+\Delta)^2}(\omega+\varepsilon_1)}\\ &-\alpha\int_0^\infty d\omega\int_{\varepsilon}^{\infty}d\varepsilon_1\frac{2\omega^2}{\sqrt{(\frac{p\omega}{c})^2-(-\varepsilon_1+\Delta)^2}(\omega+\varepsilon_1)}.\end{aligned}$$

Since we are working in the near vicinity of the mass shell the condition $\varepsilon \gg \Delta$ holds, thus

$$\begin{aligned}\mathrm{Re}\Sigma_R(\varepsilon,p) &= \alpha\int_0^\infty d\omega\int_{-\varepsilon}^{\varepsilon}d\varepsilon_1\frac{2\omega^2}{\sqrt{(\frac{p\omega}{c})^2-(\varepsilon_1+\Delta)^2}(\omega+\varepsilon_1)}\\ &= \alpha\int_0^\infty d\omega\int_{0}^{\varepsilon}d\varepsilon_1\frac{2\omega^2}{\sqrt{(\frac{p\omega}{c})^2-(\varepsilon_1+\Delta)^2}(\omega+\varepsilon_1)}\\ &+\alpha\int_0^\infty d\omega\int_{0}^{\varepsilon}d\varepsilon_1\frac{2\omega^2}{\sqrt{(\frac{p\omega}{c})^2-(-\varepsilon_1+\Delta)^2}(\omega-\varepsilon_1)}\\ &= I_1+I_2.\end{aligned}$$

Evaluation of both I_1 and I_2 integrals is similar, we will choose to integrate I_2 and simply state the result for I_1. We impose an upper-cutoff μ for the frequency integration (this constraint represents the damping of zero-sound modes at very high energies), and a lower cut-off at $\bar{\omega}$ to keep the integral real, contributions from the high frequency regions will be

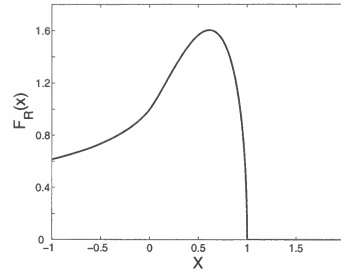

Figure 2–5: Scaling function F_R. Note the strong asymmetry of F_R about $x = 0$.

irrelevant and will not be considered.

$$
\begin{aligned}
I_2 &= \alpha \int_0^{\varepsilon} d\varepsilon_1 \int_{\omega}^{\mu} d\omega \frac{2\omega^2}{\sqrt{(\frac{p\omega}{c})^2 - (-\varepsilon_1 + \Delta)^2}(\omega - \varepsilon_1)} \\
&= -\alpha \frac{2c}{p}\left[-\frac{\varepsilon^2}{4} + \frac{\varepsilon^2 \log 4}{4}\right] \\
&\quad +2\alpha \int_0^{\varepsilon} \frac{\varepsilon_1^2 d\varepsilon_1}{\sqrt{(\frac{p\varepsilon_1}{c})^2 - (-\varepsilon_1 + \Delta)^2}} \log\left[-2\frac{(\varepsilon_1 - \Delta)^2 - (p/c)^2\bar{\omega}\varepsilon_1}{\sqrt{(\frac{p}{c}\varepsilon_1)^2 - (\varepsilon_1 - \Delta)^2}}\frac{1}{\bar{\omega} - \varepsilon_1}\right].
\end{aligned}
$$

It can be shown that the term inside the log and the square root in the denominator are purely imaginary, this further simplifies the above expression

$$
I_2 = -\alpha \frac{2c}{p}\left[-\frac{\varepsilon^2}{4} + \frac{\varepsilon^2 \log 4}{4}\right] + \pi\alpha \mathrm{Re} \int_0^{\varepsilon} \frac{\varepsilon_1^2 d\varepsilon_1}{\sqrt{u^2\varepsilon_1^2 - 2\varepsilon_1\Delta}}.
$$

Similarly we obtain for I_1

$$
I_1 = -\alpha \frac{2c}{p}\left[-\frac{\varepsilon^2}{4} + \frac{\varepsilon^2 \log 4}{4}\right] + \pi\alpha \mathrm{Re} \int_0^{\varepsilon} \frac{\varepsilon_1^2 d\varepsilon_1}{\sqrt{u^2\varepsilon_1^2 + 2\varepsilon_1\Delta}}.
$$

Adding up I_1 and I_2 we obtain

$$
I_1 + I_2 = \pi\alpha \mathrm{Re} \int_0^{\varepsilon} \frac{\varepsilon_1^2 d\varepsilon_1}{\sqrt{u^2\varepsilon_1^2 - 2\varepsilon_1\Delta}} + \pi\alpha \mathrm{Re} \int_0^{\varepsilon} \frac{\varepsilon_1^2 d\varepsilon_1}{\sqrt{u^2\varepsilon_1^2 + 2\varepsilon_1\Delta}}.
$$

The first term is more dominant and we will retain it, so the final expression for $\mathrm{Re}\Sigma^R_{ZS}$ is

$$\begin{aligned}\mathrm{Re}\Sigma^R_{ZS} &= \frac{u^2U}{4\pi}\mathrm{Re}\left[\int_0^{\varepsilon/v_F}\frac{qdq}{\sqrt{u^2-2\Delta/v_Fq}}\right] \\ &= \frac{u^2\varepsilon^2}{8E_F}F_R\left(\frac{2\Delta}{u^2\varepsilon}\right),\end{aligned} \tag{2.71}$$

where the scaling function $F_R(x)$ is,

$$F_R(x) = \mathrm{Re}\left[(1+\frac{3}{2}x)\sqrt{1-x}+\frac{3}{2}x^2\log\frac{1+\sqrt{1-x}}{\sqrt{-x}}\right]. \tag{2.72}$$

As shown in Fig. 2–5, the scaling function is asymmetric with respect to $x \to -x$, for $x > 1$ the function vanishes and for large and negative x,

$$F_R(x) \approx 4\mathrm{Re}\frac{1}{5\sqrt{-x}}.$$

The real part of the self-energy away from the mass shell is

$$\mathrm{Re}\Sigma^R_{ZS} = \frac{\sqrt{2}u^3}{20}\frac{\varepsilon|\varepsilon|}{E_F}\mathrm{Re}\sqrt{\left(-\frac{\varepsilon}{\Delta}\right)},$$

the ZS contribution away from the mass shell is smaller by a factor of u compared to the $u^2\varepsilon|\varepsilon|$ contribution to the self-energy from the back-scattering process. However, right on the mass shell the interaction with the zero-sound mode is strongly enhanced, the function $F_R(x) \to 1$ and $\mathrm{Re}\Sigma^R_{ZS} = u^2\varepsilon|\varepsilon|/8E_F$, this result is of the same order as the contribution from the PH region. The small x expansion of $F_R(x)$ is given by

$$F_R(x) = 1 + x + \frac{3x^2}{4}\log\frac{1}{x} + \cdots. \tag{2.73}$$

Using this expansion in Eq. (2.71) we obtain to linear order in Δ, the following correction to the self-energy

$$\mathrm{Re}\Sigma^R_{ZS} = \frac{u^2}{8}\frac{\varepsilon|\varepsilon|}{E_F} + \frac{|\varepsilon|\Delta}{E_F}. \tag{2.74}$$

Adding up contributions from Eqs. (2.70) and (2.74) we obtain

$$\mathrm{Re}\Sigma^R_F = \mathrm{Re}\Sigma^R_{PH} + \mathrm{Re}\Sigma^R_{ex} + \mathrm{Re}\Sigma^R_{ZS} = \frac{u^2}{8}\frac{\varepsilon|\varepsilon|}{E_F}. \tag{2.75}$$

Final result for the real part of the self-energy. Collecting up all nonanalytic u^2 contributions to the $\mathrm{Re}\Sigma_F^R$ from the forward scattering processes,

$$\begin{aligned} \mathrm{Re}\Sigma_F &= \mathrm{Re}\Sigma_{PH}^R + \mathrm{Re}\Sigma_{ex}^R + \mathrm{Re}\Sigma_{ZS}^R \\ &= \frac{u^2}{8}\frac{\varepsilon|\varepsilon|}{4E_F}, \end{aligned} \tag{2.76}$$

we find the above result from the forward-scattering process differs from the back-scattering result by a sign. Thus near the mass shell

$$\mathrm{Re}\Sigma^R = \mathrm{Re}\Sigma_B^R + \mathrm{Re}\Sigma_F^R = O(u^2\Delta^2 \log \Delta). \tag{2.77}$$

The conclusion from this result is that, for a short range potential the nonanalytic $u^2\varepsilon|\varepsilon|$ term is absent.

2.3.6 Spectral Function

Having determined $\mathrm{Im}\Sigma^R$ and $\mathrm{Re}\Sigma^R$, we are now in a position to evaluate the spectral function. The spectral function in terms of the Green's function is expressed as

$$\begin{aligned} A(\varepsilon,k) &= -\frac{1}{\pi}\mathrm{Im}G^R(\varepsilon,k) \\ &= \frac{1}{\pi}\frac{\mathrm{Im}\Sigma^R(\varepsilon,k)}{[\Delta + \mathrm{Re}\Sigma^R(\varepsilon,k)]^2 + [\mathrm{Im}\Sigma^R(\varepsilon,k)]^2}. \end{aligned} \tag{2.78}$$

We will plot the spectral function as a function of $x = 2\Delta/u^2\varepsilon$, keeping ε fixed and varying $\Delta = \varepsilon - \xi_k$ through its momentum dependence. We will also consider a situation where $\Delta \sim u^2|\varepsilon| \gg \Delta_c$ (as a reminder Δ_c is the energy scale at which the curvature effects become important), so that we can neglect curvature effects on the spectral function. Near the mass shell, $\mathrm{Re}\Sigma^R$ in the denominator can be neglected compared to Δ as $\mathrm{Re}\Sigma^R \approx u^2\Delta^2 \log\Delta \ll u^2\omega^2 \log|\omega|$. Thus the spectral function reduces to

$$A(\varepsilon,k) = \frac{1}{\pi}\frac{\mathrm{Im}\Sigma^R(\varepsilon,k)}{\Delta^2 + [\mathrm{Im}\Sigma^R(\varepsilon,k)]^2}. \tag{2.79}$$

The variation of $\mathrm{Im}\Sigma^R$ as a function of ε or ξ_k cannot be neglected, and is responsible for non-Lorentzian type features in the spectral function. The imaginary part of the retarded self-energy is a sum of four different contributions,

$$\mathrm{Im}\Sigma^R = \mathrm{Im}\Sigma_B^R + \mathrm{Im}\Sigma_{PH}^R + \mathrm{Im}\Sigma_{ex}^R + \mathrm{Im}\Sigma_{ZS}^R,$$

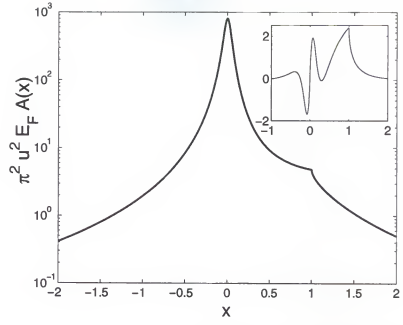

Figure 2–6: The log-plot of spectral function $A(\varepsilon, k)$ in units of $1/\pi^2 u^2 E_F$. $A(\varepsilon, k)$ is plotted as a function of $x = 2(\varepsilon - \xi_k)/u^2\varepsilon$ for $\log(E_F/u^2|\varepsilon|) = 2$ and $\varepsilon/2\pi E_F = 0.025$. A kink at $x = 1$ is due to the interaction of fermions with the zero-sound mode. Inset: part of the spectral function $A_1(\varepsilon, k)$ for $\varepsilon/2\pi E_F = 0.25$. A maximum in A_1 at $x = 1$ gives rise to a kink in total A (main panel).

where the last three terms are due to the forward scattering contribution. Near the mass shell, both $\mathrm{Im}\Sigma^R_B$ and $\mathrm{Im}\Sigma^R_{ex}$ are independent of Δ and to leading order the sum $\mathrm{Im}\Sigma^R_{ex} + \mathrm{Im}\Sigma^R_B$ vanishes, thus $\mathrm{Im}\Sigma^R$ shows dependence on Δ through the remaining terms,

$$\begin{aligned} \mathrm{Im}\Sigma^R_{ZS} &= \frac{u^2\varepsilon^2}{4\pi E_F} F_I(x) \\ \mathrm{Im}\Sigma^R_{PH} &= \frac{u^2\varepsilon^2}{4\pi E_F}\left[\log\frac{E_F}{u^2|\varepsilon|} + G_I(x)\right]. \end{aligned} \tag{2.80}$$

The spectral function acquires becomes

$$A(\varepsilon, k) = \frac{1}{\pi^2 u^2 E_F^2} \frac{\log\frac{E_F}{u^2|\varepsilon|} + G_I(x) + F_I(x)}{x^2 + \left(\frac{\varepsilon}{2\pi E_F}\right)^2 \left[\log\left(\frac{E_F}{u^2|\varepsilon|}\right) + G_I(x) + F_I(x)\right]^2}. \tag{2.81}$$

The scaling function $G_I(x)$ exhibits weak dependence on x for $x \sim 1$. Whereas, $F_I(x)$ is strongly dependent on x with a sharp peak at $x = 1$. The spectral function shows a narrow peak at $x = 0$ and a well-pronounced kink at $x = 1$, the kink corresponding to the sharp peak of $F(x)$. A plot of the spectral function $A(x)$ as a function of x is shown in Fig. 2–6.

For typical $\Delta \approx u^2|\varepsilon|$ or $x \approx 1$, $\log(E_F/u^2|\varepsilon|) \gg [G_I(x) + F_I(x)]$. Therefore, we can split the spectral-function into two parts: a part which describes the regular quasi-particle peak (A_0) and a part with scaling behavior (A_1)

$$\begin{aligned} A(\varepsilon,k) &= A_0(\varepsilon,k) + A_1(\varepsilon,k), \\ A_0(\varepsilon,k) &= \frac{1}{\pi^2 u^2 E_F} \frac{\log(E_F/u^2|\varepsilon|)}{x^2 + \left(\frac{\varepsilon}{2\pi E_F}\log(E_F/u^2|\varepsilon|)\right)^2}, \\ A_1(\varepsilon,k) &= \frac{1}{\pi^2 u^2 E_F}[G_I(x) + F_I(x)] \frac{x^2 - \left(\frac{\varepsilon}{2\pi E_F}\log(E_F/u^2|\varepsilon|)\right)^2}{\left(x^2 + \left(\frac{\varepsilon}{2\pi E_F}\log(E_F/u^2|\varepsilon|)\right)^2\right)^2}. \end{aligned} \tag{2.82}$$

Near $x = 1$, $A_0(x)$ is a smooth function whereas $A_1(x)$ shows a rapid variation. This variation associated with $A_1(x)$ is due to the fact that, for $|\Delta| > u^2|\varepsilon|$ $(x > 1)$, a fermion with frequency $\varepsilon > 0$ can emit a zero-sound boson of any frequency from $0 < \Omega < \varepsilon$ whereas for $|\Delta| < u^2|\varepsilon|$, a Cherenkov type restriction makes it impossible to emit and absorb bosons with frequencies above $|\Delta|/(1 - v_F/c) = \Delta/u^2$.

2.3.7 Coulomb Potential

Next, we will consider the interaction between the fermions and the plasmon modes and show that the kink-like behavior in the spectral function, which was obtained for fermions interacting with the zero-sound mode in the case of a short-range potential, is also present for the case of electrons interacting with plasmon modes. Herein, we will consider the low energy limit: with $|\varepsilon|, \xi_k \ll \omega_{pl}$; where $\omega_{pl} = \sqrt{2} r_s E_F$ is the maximum (undamped) plasmon frequency. Near the plasmon mode the potential is given by

$$\begin{aligned} V(\omega,q) &= \frac{V(q)}{1 - V(q)\Pi(q,\omega)} \\ &\approx \frac{2\pi e^2 \omega^2/q}{(\omega + i0^+)^2 - \Omega_0(q)^2}, \\ &\approx \frac{2\pi e^4 m v_F^2}{(\omega + i0^+)^2 - \Omega_0(q)^2} \end{aligned} \tag{2.83}$$

where $\Omega_0(q) = (e^2 m v_F^2 q)^{1/2}$ is the plasmon dispersion and we have used the following form for the polarization operator:

$$\Pi^R = -\frac{m}{\pi}\left(1 - \frac{\omega}{\sqrt{\omega^2 - v_F^2 q^2}}\right).$$

Using Eq. (2.83) as the potential, we can calculate the imaginary part of the self energy (we will keep $\varepsilon > 0$), i.e., the damping due to the interaction of the quasi-particle with the plasmons,

$$\begin{aligned} \mathrm{Im}\Sigma^R(\varepsilon,\xi_k) &= -\int_{-\varepsilon}^{0} d\Omega \int d^2q \mathrm{Im}G^R(\varepsilon+\Omega-\xi_{k+q})\mathrm{Im}V^R(\Omega,q) \\ &= \int_0^{\varepsilon} d\Omega \int d^2q \delta(\varepsilon-\xi_k-\Omega-v_F q\cos\theta)\delta(\Omega^2-\Omega_0^2(q)), \end{aligned} \tag{2.84}$$

where the first δ-function is due to the Green's function and the second is due to $\mathrm{Im}V^R$. The second delta function forces the transferred boson momentum to be small, i.e., $q \ll |\Omega_0(q) = \Omega|/v_F$, thus we can neglect the momentum dependence in the first delta function. The rest of the analysis is trivial and we obtain

$$\begin{aligned} \mathrm{Im}\Sigma^R(\varepsilon,\xi_k) &= \pi\frac{(\xi_k-\varepsilon)^2}{E_F} \quad \text{for} \quad 0 < \xi_k \leq \varepsilon \\ &= 0 \quad \text{otherwise} \end{aligned} \tag{2.85}$$

For a fixed value of ε, $\mathrm{Im}\Sigma^R$ has a kink at $\xi_k = 0$, also the kink is independent of the coupling constant. A kink in the spectral function could, in principle be detected in photoemission experiments on layered materials or in a momentum conserving tunneling between two parallel 2D gases [82].

2.3.8 Corrections to the Tunneling Density of States

The presence of $|\varepsilon|\Delta$ term in the real part of the self-energy of the particle-hole [Eq. (2.70)] and the ZS [Eq. (2.74)] contributions can in principle give rise to a nonanalytic correction to the tunneling density of states. The tunneling density of states is represented as

$$N(\varepsilon) = -\frac{2}{\pi}\int \frac{d^2k}{(2\pi)^2}\mathrm{Im}G^R(\varepsilon,k). \tag{2.86}$$

The term

$$\alpha|\varepsilon|\frac{\Delta}{E_F} = \alpha|\varepsilon|\frac{\varepsilon-\xi_k}{E_F}$$

in the real part of the self-energy is absorbed by the $Z-$factor in the Green function, yielding a simple form for the interacting Green's function in terms of the free Green's

function

$$G^R(k,w) = \frac{1}{1+\alpha\frac{|\varepsilon|}{E_F}}\frac{1}{\varepsilon - \xi_k + i0^+} = \frac{Z(\varepsilon)}{\varepsilon - \xi_k + i0^+}. \tag{2.87}$$

The tunneling density of state for a free system is m/π. Thus we can deduce the tunneling density of states for an interacting system to be

$$N(\varepsilon) = \frac{m}{\pi}Z(\varepsilon) \approx \frac{m}{\pi}\left(1 - \alpha\frac{|\varepsilon|}{E_F}\right). \tag{2.88}$$

This would be the case if a nonanalytic $|\varepsilon|\Delta$ were present in the real part of the self-energy. However, we see from Eqs. (2.70) and (2.74) that the $|\varepsilon|\Delta$ terms cancel out, moreover, the back-scattering term of the $\mathrm{Re}\Sigma$ does not contain a $|\varepsilon|\Delta$ term. Thus the tunneling density of state does not get any nonanalytic correction. The above result, valid for a contact potential, will also hold for a finite range potential, since as before the nonanalytic $|\varepsilon|\Delta$ terms cancel between the different forward scattering contributions, whereas the term is absent in the back-scattering contribution.

2.4 Conclusion

We will conclude this Chapter by restating our main results. Second-order perturbation theory yields two interesting results, namely, a nonanalytic term in the imaginary part of the self-energy and a logarithmic singularity on the mass shell for fermions with a linearized dispersion. The nonanalytic contributions originate from processes involving two incoming particles of nearly opposite momenta undergoing either a $q \approx 0$ or $q \approx 2k_F$ scattering, and also from the scattering process between two incoming particles with nearly identical momentum that undergo $q \approx 0$ momentum transfer. The latter process (the g_4 process in 1D terminology) is also responsible for a logarithmic singularity on the mass shell, indicating that the quasi-particles are ill-defined. We find that at higher orders in the interaction the singularity is enhanced and becomes a power law, causing a formal breakdown of the perturbation theory. These results, which are obtained for fermions with a linear dispersion, are modified by restoring finite curvature of the dispersion. The singularities from the individual terms in the perturbation theory are removed, yet the series itself remain divergent. A re-summation, performed by selecting the maximally divergent diagrams, removes these singularities even for a linearized dispersion, with the result that

Fermi-liquid theory is restored. However, we demonstrate that the interaction of fermions gives rise to a kink in the spectral function at $\Delta = u^2\varepsilon/2$. The non-Lorentzian shape of the spectral function should be amenable to a direct check in photoemission measurements or in momentum-conserved-tunneling between two parallel 2D electron gases.

CHAPTER 3
SPECIFIC HEAT OF A 2D FERMI LIQUID

3.1 Introduction

Thermodynamic quantities in a Fermi gas form a regular and analytic series as a function of temperature T and momentum q. For example,

$$\begin{aligned} C(T)/T &= \gamma + a_0 T^2 + a_1 T^4 + .. \\ \chi_s(T, q=0) &= \chi_s^0(0) + b_0 T^2 + .. \\ \chi_s(T=0, q) &= \chi_s^0(0) + c_0 q^2 + .. \end{aligned} \tag{3.1}$$

where the even powers of temperature T are due to the particle-hole symmetry of the Fermi function about the Fermi level and the even powers of q are due to the quadratic dispersion of the free particles. This result, valid for a Fermi gas, does not necessarily hold for interacting fermions. Fermi-liquid theory predicts only that

$$C(T)/T = \gamma^*,$$
$$\chi_S(T, q) = \chi_s^*(0),$$

where the constants γ^* and χ_s^*, differ from the free Fermi gas result and in general depend on the interaction parameters. To obtain higher orders in the temperature- and momentum-expansion of C_V and χ_s for an interacting system, the usual approach is to consider microscopic models (for example, fermions with short-range repulsion) and employ perturbation theory. Corrections to the linear-in temperature specific-heat term are conveniently obtained by calculating the self-energy on the mass shell, and relating the self-energy to the specific heat. A nonanalytic correction to the self-energy leads to nonanalytic terms in the thermodynamic quantities, for example, in 3D an $\varepsilon^3 \log|\varepsilon|$ term in the real part of the self-energy leads to a $T^3 \log T$ term and in 2D an $\varepsilon|\varepsilon|$ term in the self-energy gives a nonanalytic T^2 term [19, 20, 21, 22, 23, 24].

In the last Chapter we investigated the nonanalytic contributions to the self-energy from perturbative and nonperturbative processes. It was shown that upon resummation, the nonperturbative contributions to $\mathrm{Re}\Sigma^R$ become of the order U^2 near the mass shell and exactly cancel the second order $U^2\varepsilon|\varepsilon|$ term. This would then mean an absence of nonanalytic T^2 terms in the specific heat at second order in the interaction. We investigate the role of contributions of nonperturbative processes to the specific heat and find that the imaginary part of the self-energy contributes to the nonanalytic term in the specific heat, in such a way that it cancels the contribution from the nonperturbative real part of the self-energy, thus keeping the second-order result intact. We confirm our result in three different ways. In Section 3.2 a direct calculation of the specific heat from the self-energy is performed, and we find that the contributions from the nonperturbative processes cancel out. In Section 3.3 we use the Luttinger-Ward formula for the thermodynamic potential to show using real frequencies (Section 3.3.1) and imaginary frequencies (Section 3.3.2) that the nonperturbative processes do not contribute to the T^2 term in the specific heat through order U^2. We will consider the long-range Coulomb potential in Section 3.4 and show that the plasmons (nonperturbative processes) make an interaction independent contribution to the specific heat. We end the Chapter with a conclusion in Section 3.5.

3.2 Specific Heat Calculation From the Self-Energy

We will use the result of Ref. [16] which relates the thermodynamic potential to the Green's function and establish a relationship between the self-energy and the specific heat. The thermodynamic potential reads,

$$\Omega = 2T \sum_{\omega_m} \int \frac{d^2k}{(2\pi)^2} \ln G(\omega_m, k, T = 0),$$

where the Green's function is expressed in terms of Matsubara frequencies ω_m and has no additional temperature dependence. We can convert the summation over frequencies into a contour integration obtaining

$$\Omega = -2 \int_{-\infty}^{\infty} \frac{d\omega}{2\pi} \int \frac{d^2k}{(2\pi)^2} \Big[\ln G^R(\omega, k) - \ln G^A(\omega, k) \Big]. \tag{3.2}$$

The thermodynamic potential and the specific heat are related via

$$C = -T\frac{\partial^2\Omega}{\partial T^2}; \tag{3.3}$$

using Eq. (3.2) and Eq. (3.3) one obtains,

$$C = -\frac{2T^2}{\pi}\frac{\partial}{\partial T}\left[\frac{1}{T}\int\frac{d^2k}{(2\pi)^2}\int_{-\infty}^{\infty}d\omega\omega\frac{\partial n_0}{\partial\omega}\arg G^R(\omega,k)\right]. \tag{3.4}$$

For the case of a weak interaction such that $|\Sigma| \ll \omega$, one can expand the Green's function in Eq. (3.4) in powers of Σ. To the lowest order in Σ we obtain

$$C(T) = C_{\rm FG}(T) + \delta C(T), \tag{3.5}$$

where $C_{\rm FG}(T) = m\pi T/3$ is the specific heat for free fermions in 2D and $\delta C(T)$ is given by

$$\delta C(T)/T = \frac{2}{\pi}\frac{\partial}{\partial T}\left[\frac{1}{T}\int\frac{d^2k}{(2\pi)^2}\int_{-\infty}^{\infty}d\omega\omega\frac{\partial n_0}{\partial\omega}{\rm Im}\left[\Sigma^R(\omega,k)G_0^R(\omega,k)\right]\right]. \tag{3.6}$$

There are two contributions to $\delta C(T)$–one from Re Σ^R and another from ImΣ^R–which are labelled $C_1(T)$ and $C_2(T)$, respectively:

$$\delta C\,(T) = C_1\,(T) + C_2\,(T)\,; \tag{3.7a}$$

$$C_1(T)/T = \frac{2}{\pi}\frac{\partial}{\partial T}\left[\frac{1}{T}\int\frac{d^2k}{(2\pi)^2}\int_{-\infty}^{\infty}d\omega\omega\frac{\partial n_0}{\partial\omega}{\rm Im}G_0^R(\omega,k){\rm Re}\Sigma^R(\omega,k)\right];$$

$$= -2\frac{\partial}{\partial T}\left[\frac{1}{T}\int\frac{d^2k}{(2\pi)^2}\int_{-\infty}^{\infty}d\omega\omega\frac{\partial n_0}{\partial\omega}\,\delta\left(\omega-\varepsilon_k\right){\rm Re}\Sigma^R(\omega,k)\right]; \tag{3.7b}$$

$$C_2(T)/T = \frac{2}{\pi}\frac{\partial}{\partial T}\left[\frac{1}{T}\int\frac{d^2k}{(2\pi)^2}\int_{-\infty}^{\infty}d\omega\omega\frac{\partial n_0}{\partial\omega}\mathcal{P}\,\frac{1}{\omega-\varepsilon_k}{\rm Im}\Sigma^R(\omega,k)\right]. \tag{3.7c}$$

Eq. (3.7b) implies that to calculate the specific heat contribution from the real part of the self-energy, one needs only the mass-shell form of the real part of the self-energy. On the other hand, Eq. (3.7c) implies that the contribution from the imaginary part of the self-energy is zero if the specific heat is independent of momentum k, since the integral

$$\int d^2k\frac{1}{\omega-\xi_k}$$

vanishes if one assumes the density of states to be constant.

In the discussion to follow we will show that the nonperturbative contribution to the U^2T^2 term in the specific heat vanishes. Thus contrary to earlier results [21], the U^2T^2

term is not modified by the additional contribution from the nonperturbative process and remains exactly the same as obtained from the second order perturbative calculation [22].

3.2.1 Zero-Sound Mode Contribution to the Real Part of the Self-Energy

The zero-sound mode contributes both to the real and imaginary parts of the self-energy. In this Section, we will calculate nonanalytic contributions from the real part of the self-energy $\mathrm{Re}\Sigma^R_{ZS} = u^2\omega|\omega|/8E_F$ to the specific heat. Notice, for calculating the contributions to the specific heat from the real part of the self-energy we need only the mass-shell form of the self-energy. The contribution is,

$$\begin{aligned}
\delta C_1(T)/T &= -2\frac{\partial}{\partial T}\left[\frac{m}{T}\int_{-\infty}^{\infty}\frac{d\xi_k}{2\pi}\int_{-\infty}^{\infty}d\omega\omega\frac{\partial n_0}{\partial\omega}\delta(\omega-\xi_k)\left(\frac{u^2|\omega|\omega}{8E_F}+\frac{|\omega|\Delta}{4E_F}\right)\right] \\
&= \frac{1}{4E_F}\frac{\partial}{\partial T}\left[\frac{2mT^2}{\pi}\int_{-\infty}^{\infty}d\frac{\omega}{2T}\frac{(\frac{\omega}{2T})^2\frac{|\omega|}{2T}}{\cosh^2(\frac{\omega}{2T})}\right] \\
&= \frac{4Nu^2T}{\pi v_F^2}, \qquad (3.8)
\end{aligned}$$

where

$$N = \int_0^{\infty}\frac{x^3dx}{\cosh^2(x)} = \frac{9\zeta(3)}{8}. \qquad (3.9)$$

3.2.2 Zero Sound Mode Contribution to the Imaginary Part of the Self-Energy

For local self-energy (i.e., independent of momentum) the imaginary part of the self-energy does not contribute to the specific heat. In general, the imaginary part of the self-energy need not be local, this is the case for $\mathrm{Im}\Sigma^R_{ZS}$. Near the mass shell $|\omega| \approx |\xi_k|$, thus

$$\begin{aligned}
\mathrm{Im}\Sigma^R_{\rho-ZS} &= \frac{2u^3}{m}\mathrm{Re}\int_0^{|\omega|/c}\frac{QdQ}{\sqrt{sgn(\omega)\frac{2\Delta}{Qv_F}-u^2}} \\
&\approx \frac{2u^3}{m}\mathrm{Re}\int_0^{|\xi_k|/c}\frac{QdQ}{\sqrt{sgn(\omega)\frac{2\Delta}{Qv_F}-u^2}}. \qquad (3.10)
\end{aligned}$$

The specific heat contribution from the above term can be written as,

$$\begin{aligned}
\frac{\delta C_2}{T} &= \frac{2}{\pi}\frac{\partial}{\partial T}\left[\frac{1}{T}\int_{-\infty}^{\infty}\frac{md\xi_k}{2\pi}\int_{-\infty}^{\infty}d\omega\frac{\omega}{4T\cosh^2\frac{\omega}{2T}}\frac{1}{\omega-\xi_k}\mathrm{Im}\Sigma^R_{\rho-ZS}\right] \\
&= -\frac{1}{\pi}\frac{\partial}{\partial T}\left[\frac{u^3}{4\pi T^2}\int_0^{\infty}d\Delta\int_0^{\infty}d\omega\frac{\omega}{\cosh^2\frac{\omega}{2T}}\frac{1}{\Delta}\mathrm{Re}\int_0^{\omega/c}\frac{QdQ}{\sqrt{\frac{2\Delta}{Qv_F}-u^2}}\right] \\
&\approx -\frac{1}{\pi}\frac{\partial}{\partial T}\left[\frac{u^3}{4\pi T^2}\int_0^{\infty}d\Delta\int_0^{\infty}d\omega\frac{\omega}{\cosh^2\frac{\omega}{2T}}\frac{1}{\Delta}\mathrm{Re}\int_0^{\xi_k/c}\frac{QdQ}{\sqrt{\frac{2\Delta}{Qv_F}-u^2}}\right] \\
&= -\frac{1}{\pi}\frac{\partial}{\partial T}\left[\frac{u^3}{4\pi T^2}\int_0^{\infty}d\omega\frac{\omega}{\cosh^2\frac{\omega}{2T}}\int_0^{\infty}\frac{dz}{z}\mathrm{Re}\int_0^{\omega/c-z/2}\frac{Q^{3/2}dQ}{\sqrt{z-u^2Q}}\right], \qquad (3.11)
\end{aligned}$$

where we have made the substitution $z = 2\Delta/v_F$. We will first calculate the following integral,

$$I = \int_0^{\infty}\frac{dz}{z}\mathrm{Re}\int_0^{\omega/c-z/2}\frac{Q^{3/2}dQ}{\sqrt{z-u^2Q}}.$$

By splitting into regions in the (z, Q) plane where the integrand is real, we obtain

$$\begin{aligned}
I &= \int_0^{2\omega/(v_F+2v_F/u^2)}\frac{dz}{z}\int_0^{z/u^2}\frac{Q^{3/2}dQ}{\sqrt{z-u^2Q}} \\
&\quad + \int_{2\omega/(v_F+2v_F/u^2)}^{\omega/v_F}\frac{dz}{z}\int_0^{\omega/v_F-z/2}\frac{Q^{3/2}dQ}{\sqrt{z-u^2Q}} \\
&= \int_0^{2\omega u^2/2v_F}\frac{dz}{z}\int_0^{z/u^2}\frac{Q^{3/2}dQ}{\sqrt{z-u^2Q}} + \int_0^{\omega/v_F}Q^{3/2}dQ\int_{u^2\omega/v_F}^{\omega/v_F}\frac{dz}{z\sqrt{z-u^2Q}} \\
&= \frac{3\pi\omega^2}{16uv_F^2} + \left[\frac{\pi\omega^2}{2uv_F^2} - \frac{3\pi\omega^2}{16uv_F^2}\right] = \frac{\pi\omega^2}{2uv_F^2}.
\end{aligned}$$

Using this value back in Eq. (3.11) yields

$$\frac{\delta C_2}{T} = -\frac{4Nu^2T}{\pi v_F^2}. \qquad (3.12)$$

Adding up the two contributions from the zero-sound region, Eqs. (3.8)and (3.12), we obtain

$$\frac{\delta C_2}{T} + \frac{\delta C_1}{T} = 0, \qquad (3.13)$$

thus we find the zero sound makes no contribution to the leading nonanalytic term in the specific heat.

3.2.3 Finite Range Potential

The presence of a finite-range potential $U(q)$ does not modify our earlier result regarding the cancellation of the nonperturbative contributions. This is because the nonperturbative terms arise due to forward scattering processes with small momentum transfer hence $U(q)$ can be replaced by $U(0)$. The analysis for the cancellation of nonperturbative contribution to the U^2T^2 term in the specific remains the same. As a result, the nonanalytic contribution to the U^2T^2 term in the specific heat is the same as that obtained by the perturbative approach and is given by [22]

$$\frac{\delta C(T)}{T} = -\frac{9\zeta(3)}{\pi^2}\left[\frac{m}{2\pi}\right]^2\left[U^2(0) + U^2(2k_F) - U(0)U(2k_F)\right]\frac{C_{FG}}{E_F}. \tag{3.14}$$

3.3 Specific Heat Calculation from the Luttinger-Ward Formalism

The approach used in the previous Section to show the absence of a nonperturbative contribution to the T^2 term is quite involved, so we will use an alternative method, which is easier to execute, and in the process double check our earlier result. We will use the thermodynamic potential which is expressed in terms of the Luttinger-Ward formalism to calculate the specific heat. The most commonly cited expression in the literature for the thermodynamic potential of a system of interacting fermions with a potential $gV(x)$ is

$$\Omega(g) = \Omega_0 + \frac{V}{\beta}\int_0^g \frac{dg'}{g'}\sum_{i\omega_n,\vec{k}} \exp(i\omega_n\beta)\Sigma(g',\vec{k},\omega_n)G(g',\vec{k},\omega_n), \tag{3.15}$$

where g is the coupling constant, Σ and G are the full self-energy and Green's function respectively [83], and Ω_0 is the thermodynamic constant in the absence of interactions

$$\Omega_0 = -\frac{2V}{\beta}\sum_{\vec{k}} \log\{1 + \exp[-\beta(\varepsilon_{\vec{k}} - \mu)]\}.$$

As shown by Luttinger and Ward [84], Eq. (3.15) can be written in a compact form

$$\begin{aligned}\Omega &= -\frac{2V}{\beta}\sum_{i\omega_n,\vec{k}}\Big[\log[-G(i\omega_n,\vec{k})] + \Sigma(i\omega_n,\vec{k})G(i\omega_n,\vec{k})\Big] \\ &\quad + \frac{2V}{\beta}\sum_m\sum_{i\omega_n,\vec{k}}\left(\frac{1}{2m}\right)\Sigma_m(i\omega_n,\vec{k})G(i\omega_n,\vec{k}),\end{aligned} \tag{3.16}$$

where in the last expression $\Sigma_m(\vec{k},\omega_n)$ stands for the m^{th} order self-energy diagram

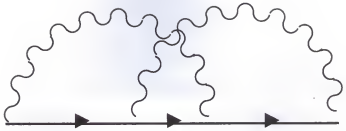

Figure 3–1: Example of a second-order-skeleton diagram. Notice the fully interacting Green's function.

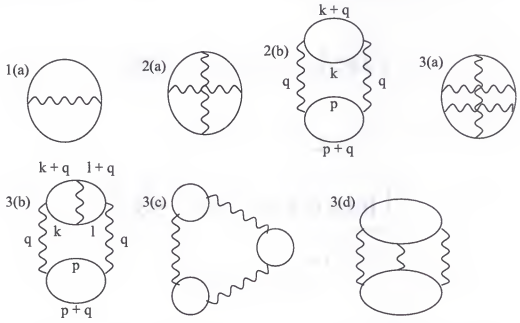

Figure 3–2: Diagrams through the third order that contribute to the thermodynamic potential.

determined from the skeleton diagram with fully interacting Green's function. An example of a second order skeleton diagram is shown in Fig. 3–1.

To calculate the specific heat from the thermodynamic potential we will be interested in those diagrams, that, at each order of interaction, have the maximum number of particle-hole bubbles (these are the most divergent diagrams of the thermodynamic series). Typical examples of third-order diagrams are shown in Fig. 3–2(3). It might seem that only one of the diagrams in Fig. 3–2(3) belong to the category of "maximum number of particle-hole bubbles", however a more careful analysis shows that the rest of the diagrams also have equal number of bubbles, though they are 'implicit' (they are obtained by integrating over the fermionic degrees of freedom). Furthermore, it is easy to show that

the diagrams of the kind shown in Fig. 3-2 (which are "part" of the skeleton diagrams) are obtained from the last term of Eq. (3.16). It turns out that, even for higher orders, the third expression is the only one which is relevant. Following the prescription described above, we obtain the following series for the thermodynamic potential of a short range potential,

$$\begin{aligned}\Omega &= \Omega_0 + VT\sum_{i\omega_n}\int\frac{d^2k}{(2\pi)^2}\Big[-U\Pi_m - \frac{1}{2}(U\Pi_m)^2 + \frac{1}{3}(U\Pi_m)^3 - \frac{1}{2}(U\Pi_m)^4 \\ &\quad + \frac{1}{5}(U\Pi_m)^5 - \frac{1}{3}(U\Pi_m)^6 + \cdots\Big]. \end{aligned} \tag{3.17}$$

3.3.1 Real-Frequency Approach

In an earlier work on nonanalytic contributions to the specific heat [15, 22], it was shown that the nonanalytic U^2T^2 contribution to the specific heat arises from two regions in momentum space, from $k \ll k_F$ and $k \approx 2k_F$. In the following analysis, we re-sum higher-order terms so as to obtain the nonperturbative contributions from the $k \ll k_F$ regime. We can split the thermodynamic potential into two parts, a part containing contributions coming from the small momentum region (summed to all orders) and a part which has contributions from the large-momentum region (only the second-order term).

$$\begin{aligned}\Omega &= \Omega_0 + \frac{2V}{\beta}\sum_{i\omega_n,|\vec{k}|\ll k_F}\frac{1}{2}\Big[-U\Pi - \frac{(U\Pi)^2}{2} + \frac{(U\Pi)^3}{3} - \frac{2(U\Pi)^4}{4} + \cdots\Big] \\ &\quad + \frac{2V}{\beta}\sum_{i\omega_n,|\vec{k}|\sim 2k_F}\frac{1}{2}\Big[-\frac{(U\Pi)^2}{2}\Big]. \end{aligned} \tag{3.18}$$

The above expression for the thermodynamic potential can be rearranged to obtain a compact form

$$\begin{aligned}\Omega &= \frac{V}{\beta}\sum_{i\omega_n,|\vec{k}|\ll k_F}\Big[-2U\Pi - \frac{(U\Pi)^2}{2} + \underbrace{\Big\{(U\Pi)^2 + \overbrace{\frac{3}{2}\log(1+U\Pi)}^{\text{spin-channel}} + \overbrace{\frac{1}{2}\log(1-U\Pi)}^{\text{charge-channel}}\Big\}}_{\text{nonperturbative Contribution}}\Big] \\ &\quad + \frac{2V}{\beta}\sum_{i\omega_n,|\vec{k}|\sim 2k_F}\frac{1}{2}\Big[-\frac{(U\Pi)^2}{2}\Big], \end{aligned} \tag{3.19}$$

where the terms inside the curly brackets are the nonperturbative contributions. The summations on discrete Matsubara frequencies can be converted to integrals through the

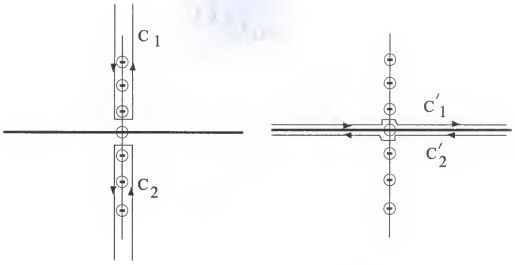

Figure 3–3: Contour for summing up the Log. The thick line represents the branch cut and the small circles represent the discrete Matsubara poles.

usual trick employed in [16]. We will show the procedure of summation for the log terms of Eq. (3.19). By making use of the relation between the Matsubara dielectric function $D^M(k, iw_m)$ and the retarded and advanced functions

$$D^M(k, i\omega \to \omega + i0^+) = D^R(k, \omega);$$

$$D^M(k, i\omega \to \omega + i0^-) = D^A(k, \omega),$$

the discrete sum can be expressed as an integral with contours, C_1 and C_2, as shown in Fig. 3–3. The discrete summation is

$$\begin{aligned} \frac{\partial}{\partial T} T \sum_{iw_n} \int \log(D^M(k, i\omega_n)) &= \frac{\partial}{\partial T} T \log D^M(k, 0) \\ &+ \frac{\partial}{\partial T} \int_{C_1} \frac{d\omega}{2\pi i} n_B(\omega) \log D^R(k, \omega) \\ &+ \frac{\partial}{\partial T} \int_{C_2} \frac{d\omega}{2\pi i} n_B(\omega) \log D^A(k, \omega), \end{aligned} \tag{3.20}$$

where $n_B(\omega)$ is the Bose distribution function. The retarded and the advanced function have neither poles nor zeroes in the upper and lower half plane respectively. Also the function, $\partial n_B(\omega)/\partial T$, decays rapidly as $\omega \to \pm\infty$. These properties of the integrand allows us to "open" the contour and express the integrals in terms of contours C'_1 and C'_2. Notice, the small bumps in the contours C'_1 and C'_2 cancel the first term of the

above equation. So the above equation with contours C'_1 and C'_2 minus the bumpy part is

$$\frac{\partial}{\partial T} T \sum_{i w_n} \int \log(D^M(k, i\omega_n)) = \frac{\partial}{\partial T} \int_{-\infty}^{+\infty} \frac{d\omega}{2\pi i} \int \frac{d^2k}{(2\pi)^2} n_B(\omega) \times \Big[\log D^R(k,\omega) - \log D^A(k,\omega)\Big].$$

Next, we will make use of the property of the log and the property of the function on the real axis $D^R = D^{A*}$, to obtain a simplified form. The contributions from the spin and charge channels will be evaluated using,

$$\frac{\partial}{\partial T} T \sum_{i w_n} \int \log(D^R(k, i\omega_n)) = \int \frac{d^2k}{(2\pi)^2} \int \frac{d\omega}{\pi} \frac{\frac{\omega}{4T^2}}{\sinh^2(\omega/2T)} \times \tan^{-1}\Big[\frac{\mathrm{Im} D^R(k,\omega)}{\mathrm{Re} D^R(k,\omega)}\Big]. \tag{3.21}$$

The contributions that will be considered are those from the spin channel, the charge channel and the Π^2 term. Out of these only the charge channel will get contributions from the zero-sound mode region. Let us first consider the spin channel:

$$\frac{3}{2\beta} \sum_{i w_n, \vec{k}} \log(1 + U\Pi) = \sum_{\vec{k}} \int_{-\infty}^{+\infty} \frac{dw}{2\pi} \frac{3}{exp(\beta w) - 1} \tan^{-1}\Big[\frac{U \mathrm{Im}\Pi^R}{1 + U \mathrm{Re}\Pi^R}\Big], \tag{3.22}$$

where the polarization operator in the particle-hole region is,

$$\Pi^R = -\frac{m}{2\pi}(1 + i\frac{w}{\sqrt{(kv_F)^2 - w^2}}).$$

The above term does not get any contribution from the zero-sound mode region. We will obtain the contributions from the particle-hole region under the assumption of weak coupling $mU \ll 1$

$$\frac{\partial}{\partial T} \frac{3}{2\beta} \sum_{i w_n, \vec{k}} \log(1 + U\Pi) = -\frac{3}{2} \int_0^{+\infty} \frac{dw}{\pi} \frac{2w}{(2T)^2 \sinh^2(w/2T)} \int_{\frac{w}{v_F}}^{k_F} \frac{dk^2}{4\pi} \times \tan^{-1}\Big[\frac{mUw}{2\pi\sqrt{k^2 - w^2}}\Big].$$

We are interested in the T^2 term, hence we will only be interested in the w^2 term from the dk^2 integration. The w^2 term from the dk^2 integration is

$$\int_{\frac{w}{v_F}}^{k_F} dk^2 \tan^{-1}\Big[\frac{uw}{\sqrt{(kv_F)^2-w^2}}\Big] = -\frac{m^2U^2w^2\pi}{8\pi^2}. \tag{3.23}$$

Therefore, the T^2 contribution is

$$\frac{\partial}{\partial T}\frac{3}{2\beta}\sum_{iw_n,\vec{k}}\log(1+U\Pi) = \frac{9m^2U^2T^2\zeta(3)}{16\pi^3}. \tag{3.24}$$

T^2 contributions from the charge channel (particle hole region) can be obtained by utilizing the same approach as for the spin channel. We obtain

$$\frac{\partial}{\partial T}\frac{1}{2\beta}\sum_{iw_n,\vec{k}}\log(1-U\Pi) = -\frac{3m^2U^2T^2\zeta(3)}{16\pi^3}. \tag{3.25}$$

Unlike the spin channel, the charge channel does get a contribution from the zero-sound mode region

$$\frac{\partial}{\partial T}\frac{1}{2\beta}\sum_{iw_n,\vec{k}}\log(1-U\Pi) = -\frac{1}{2}\sum_{\vec{k}}\int\frac{d\omega}{\pi}\frac{\frac{\omega}{4T^2}}{\sinh^2(\omega/2T)}\arg(\mathcal{G}_\rho), \tag{3.26}$$

where

$$\mathcal{G}_\rho = \frac{1}{2}\frac{1}{1-U\Pi} \approx \frac{u^2v_F^2k^2}{(\omega+i0^+)^2-c^2k^2}.$$

the integral of Eq. (3.26) is easy to perform as the argument of $\mathcal{G}_\rho$ in the momentum region $\omega/c < k < \omega/v_F$ is constant. In this region $\mathrm{Re}(\mathcal{G}_\rho) < 0$ and $\mathrm{Im}(\mathcal{G}_\rho) \to 0-$, giving an argument of $-\pi$. Thus,

$$\frac{\partial}{\partial T}\frac{1}{2\beta}\sum_{iw_n,\vec{k}}\log(1-U\Pi) = \int_0^\infty\frac{dw}{\pi}\int_{w/c}^{w/v_F}\frac{kdk}{2\pi}\frac{w}{(2T)^2\sinh^2(w/2T)}\pi, \tag{3.27}$$

where $c = v_F/\sqrt{1-(Um/2\pi)^2}$ is the zero sound velocity. This gives

$$\frac{\partial}{\partial T}\frac{1}{2\beta}\sum_{iw_n,\vec{k}}\log(1-U\Pi) = \frac{3U^2m^2\zeta(3)T^2}{8\pi^3v_F^2}. \tag{3.28}$$

The contributions coming from the small momentum region to the second order term is

$$\frac{\partial}{\partial T}\frac{1}{\beta}\sum_{iw_n,\vec{k}}\Pi^2U^2 = \int\frac{d^2k}{(2\pi)^2}\int_{-\infty}^{+\infty}\frac{dw}{2\pi}\frac{2U^2w}{(2T)^2\sinh^2(w/2T)}\mathrm{Im}(\Pi^R)^2. \tag{3.29}$$

The imaginary part of $(\Pi^R)^2$ is

$$\mathrm{Im}(\Pi^R)^2 = \frac{mw}{2\pi^2\sqrt{(kv_F)^2 - w^2}} - \frac{m^2\pi w^2}{4\pi^2}\delta((kv_F)^2 - w^2)sgn(w). \tag{3.30}$$

The first term of the above expression gives contributions to the T and the T^3 term, the δ function term is responsible for the T^2 term

$$\begin{aligned}\frac{\partial}{\partial T}\frac{1}{\beta}\sum_{i\omega_n,\vec{k}}\Pi^2U^2 &= -\int\frac{d^2k}{(2\pi)^2}\int_0^{+\infty}\frac{dw}{\pi}\frac{2U^2w}{(2T)^2\sinh^2(w/2T)}\frac{m^2\pi w^2}{4\pi^2}\frac{\delta(kv_F - w)}{2w} \\ &= -\frac{3}{\pi}(\frac{Um}{2\pi v_F})^2\zeta(3)T^2. \end{aligned}\tag{3.31}$$

We can now add up Eqs. (3.24), (3.25), (3.28), and (3.31) to obtain the nonperturbative contribution of Eq. (3.19). The result is that the nonperturbative contributions add up to zero, thus there is no nonperturbative contribution to the T^2 term in the specific heat, and, only the perturbative second order in the interaction strength, Π^2 terms of Eq. (3.19), contribute to the U^2T^2 term in the specific heat. We will show below that the $k \approx 0$ and $k \approx 2k_F$ regions give equal contributions to the U^2T^2 term in the specific heat.

3.3.2 Matsubara Formalism

In this final approach, we will keep Eq. (3.17) as it is and perform the summation directly on the Matsubara frequencies. A great advantage with this approach is that it is *a priori* apparent, for weak interaction $u \ll 1$, that we do not need to consider terms higher than the second order term for the U^2T^2 contribution, as none of the terms in the series are divergent and the series converges. On the other hand, a resummation will indeed be required if the interaction is strong, $u \simeq 1$, or long ranged. In the following discussion we will consider the two cases: weak potential $u \ll 1$ and the strong potential $u \simeq 1$. We will then extend our result to include a potential with an explicit momentum dependence.

Contact interaction: $u \ll 1$. For the weak potential it suffices to consider terms through second order in the interaction. The first order term does not contribute to the nonanalytic temperature dependence since the nonanalyticity arises only from the 2^{nd} order onwards.

We will calculate the contribution from the Π^2 term which originates from $k \ll k_F$ regions, followed by contributions from the $k \approx 2k_F$ region. The Matsubara polarization

operator in the small frequency and momentum region is

$$\Pi_m(\omega_n,k)=-\frac{m}{2\pi}\left(1-\frac{|\omega_n|}{\sqrt{\omega_n^2+(kv_F)^2}}\right). \tag{3.32}$$

Using this form of the polarization operator and performing the momentum integration, we obtain

$$\begin{aligned}\frac{1}{2\beta}\sum_{i\omega_n,k}\Pi^2U^2 &= \frac{1}{2\beta}(\frac{Um}{2\pi})^2\sum_{i\omega_n}\int_0^{k_F}\frac{dk^2}{4\pi}\left[1+\frac{w_n^2}{w_n^2+(kv_F)^2}-\frac{2|w_n|}{\sqrt{w_n^2+(kV_F)^2}}\right]\\ &= (\frac{Um}{2\pi})^2\frac{\pi T^3}{V_F^2}\left[\sum_{n=1}^{N}\Big(X+4n(n-\sqrt{n^2+X})+n^2\log|\frac{n^2+X}{n^2}|\Big)+\frac{X}{2}\right],\end{aligned}$$

where $N\gg 1$ is the upper cutoff and $X=(k_Fv_F/2\pi T)^2\gg 1$. Notice, the T^3 term has been extracted in front. A T^3 term in the thermodynamic potential corresponds to a T^2 term in the specific-heat. Thus, we will be interested only in extracting the term independent of temperature from the square bracket. To this end we will use the Euler-Maclaurin formula, which reads

$$\begin{aligned}\sum_{n=1}^{N}F(n) &= \int_1^N F(x)dx+\frac{1}{2}(F(N)+F(1))\\ &\quad+\sum_{k=1}^{N}\frac{F^{(2k-1)}(N)-F^{(2k-1)}(1)}{(2k)!}B_{2k},\end{aligned} \tag{3.33}$$

where B_{2k} are the Bernoulli's coefficient and $F^{(2k-1)}$ is the $2k-1^{th}$ derivative of the function F, and the function F in our case is

$$F(n)=X+4n(n-\sqrt{n^2+X})+n^2\log|\frac{n^2+X}{n^2}|.$$

From the above expression, it is clear that the only term which can contribute to a cut off and temperature independent term will be the $n^2\log 1/n^2$ term. We express the series as

$$\begin{aligned}-2\sum_{n=1}^{N}(n)^2\log(n) &= -2\int_1^N x^2\log x dx-N^2\log N\\ &\quad-2\sum_{k=1}^{N}\frac{(x^2\log x)^{(2k-1)}(N)-(x^2\log x)^{(2k-1)}(1)}{(2k)!}B_{2k},\end{aligned}$$

thus the constant term is

$$\sum_{n=1}^{N} F(n)\Big|_{\text{constant}} = -2\sum_{n=1}^{N} n^2 \log n\Big|_{\text{constant}} = -2[\frac{1}{9} - \frac{1}{12} + \frac{1}{360}\cdots] = -\frac{\zeta(3)}{2\pi^2}, \qquad (3.34)$$

and we obtain

$$\begin{aligned} -\frac{1}{2\beta}\sum_{i\omega_n,\vec{k}} \Pi^2 U^2 &= (\frac{Um}{2\pi})^2 \frac{\pi T^3}{v_F^2}\frac{\zeta(3)}{2\pi^2} \\ C_V &= -\frac{3\zeta(3)u^2T^2}{\pi v_F^2}. \end{aligned}$$

The remaining U^2T^2 contribution to the specific heat comes from the $2k_F$ region, to evaluate this contribution we need the asymptotic form of the polarization operator given by

$$\Pi(\omega_n, k) = -\frac{m}{2\pi}\left[1 - \left(x + \sqrt{x^2 + (\frac{\omega_n}{2k_F v_F})^2}\right)\right],$$

where $x = (k - 2k_F)/2k_F$. The square of the second term in the bubble yields another $n^2 \log n$ term, which as before is responsible for the T^2 term in the specific heat. The square of the second term in Π yields,

$$\begin{aligned} -\frac{1}{2\beta}\sum_{i\omega_n,\vec{k}} \Pi^2 U^2 &\rightarrow -\frac{1}{2\beta}(\frac{Um}{2\pi})^2 \int \frac{kdk}{2\pi}\Pi^2 \\ &= -\frac{1}{2\beta}\frac{U^2m^2}{(2\pi)^3}(2k_F)^2 \int_{-1}^{1} dx \left[x + |x| + \frac{\omega_n^2}{8|x|k_F^2 v_F^2}\right], \end{aligned} \qquad (3.35)$$

where the precise upper limits on x are not important, the log-divergence of x (at $x = 0$) is cut off at $x = \omega_n/2k_F v_F$. We obtain a similar log term,

$$-\frac{1}{2\beta}\sum_{i\omega_n,\vec{k}} \Pi^2 U^2 = (\frac{Um}{2\pi})^2 \frac{\pi T^3}{v_F^2}\frac{\zeta(3)}{2\pi^2}, \qquad (3.36)$$

Thus both $k \ll k_F$ and $k \approx 2k_F$ yield identical nonanalytic contributions to the specific heat. The total contribution is twice the contribution from either one of the regions.

3.3.3 Contact Interaction: Beyond Second Order

In this Section we will sum up the T^2 contributions from all the terms (U^n; $n \geq 2$) of the thermodynamic potential Eq. (3.17). We will widen the scope of our result by including self-energy insertions in to the bare Green's function. Although the general structure of such a Green's function is very complicated, near the Fermi surface, one can

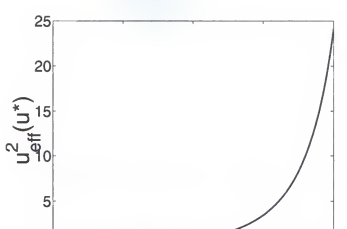

Figure 3–4: Plot of $u_{\text{eff}}^2(u^*)$ vs u^*

approximate the exact Green's function by its expression near the quasi-particle pole,

$$G(i\omega_n, k) = \frac{Z}{i\omega_n - \varepsilon_K^*},$$

where Z is the renormalization factor, $\varepsilon_k^* = v_F^*(k - k_F)$, $v_F^* = k_F/m^*$, and m^* is the renormalized mass. Parameters Z and m^* are some functions of the bare interaction u, whose forms, in general, are not known. This amounts to replacing the prefactor and the Fermi velocity in Eq. (3.32)

$$\Pi(\omega_m, k) \to \Pi^*(\omega_m, k) = -\frac{m^* Z^2}{2\pi}\left[1 - \frac{|\omega_m|}{\sqrt{\omega_m^2 + (v_F^* k)^2}}\right]. \tag{3.37}$$

As noted in the previous Section a T^3 term in the thermodynamic potential originates from a $\omega^2 \log\omega$ term, which is in turn obtained after the momentum integration of $(\frac{|\omega_m|}{\sqrt{\omega_m^2+(v_F k)^2}})^2$. In a higher order $U^n\Pi^{*n}$, the term $(\frac{|\omega_m|}{\sqrt{\omega_m^2+(v_F^* k)^2}})^2$ is obtained from the 3^{rd} term of the binomial expansion:

$$U^n\Pi^{*n} = (\frac{-Um^*Z^2}{2\pi})^n\left[1 - n\frac{|\omega_m|}{\sqrt{\omega_m^2 + (v_F^*)^2}} + \frac{n(n-1)}{2}\left(\frac{|\omega_m|}{\sqrt{\omega_m^2 + (v_F^*)^2}}\right)^2 + \cdots\right]. \tag{3.38}$$

Using this result in conjugation with Eq. (3.17), we obtain

$$\delta C\,(T)\,/T = -\frac{9\zeta(3)}{\pi^2} u_{\text{eff}}^2 C_{\text{FG}}^*/E_F^*. \tag{3.39}$$

Here $C^*_{\rm FG} = \pi m^* T/3$, $E^*_F = k_F v^*_F/2$, and

$$\begin{aligned} u^2_{\rm eff} &= (u^*)^2 \left[1 + 2u^* + 6(u^*)^2 + 4(u^*)^3 + \ldots\right] \\ &= (u^*)^2 \left[\frac{3}{2}\left(\frac{1}{1-u^*}\right)^2 + \frac{1}{2}\left(\frac{1}{1+u^*}\right)^2 - 1\right], \end{aligned} \tag{3.40}$$

where

$$u^* \equiv Z^2 m^* U/2\pi. \tag{3.41}$$

This result is valid for $0 \leq u^* < 1$. The divergence of $u^2_{\rm eff}$ at $u^* = 1$, resulting from the spin-channel, signals an instability toward a magnetically-ordered state. A plot of $u^2_{\rm eff}\,(u^*)$ is presented in Fig. 3–4.

3.3.4 Generic Interaction

In Section 3.3.3, we obtained the specific heat of a contact interaction for arbitrary interaction strengths, this result has a rather limited use as most realistic interactions have a finite range. To obtain a form that is valid for finite-range potential we begin by investigating the structure of vertices.

Let us consider higher-order terms, which can lead to two kinds of corrections; self-energy insertions and vertex corrections. The effect of self-energy corrections is reflected in a renormalized effective mass and a Z-factor for the quasi-particle. The second correction is attributed to vertex terms. A typical diagram of n^{th} order consists of n bubbles. To obtain a T^2 contribution to the specific heat one needs a product of two $|\Omega_m|/Q$ terms which are obtained from any two out of the n bubbles. Any extra factor of $|\Omega_m|/Q$ will not lead to a nonanalytic term, thus we can set $\Omega_m = 0$ and $Q \to 0$ in the rest of the diagram. Thus, even at arbitrary order we are dealing with only two bubbles. The effect of higher order terms can be hidden in the static vertices (these are static because we need to first set $\Omega_m = 0$ and then $Q \to 0$) joining the two bubbles. These vertices are of two types: $\Gamma^k(k, -k; k, -k)$ and $\Gamma^k(k, -k; -k, k)$. What we are left with is a "2nd" order diagram, where the wavy lines are replaced by two blocks represented either by a $\Gamma^k(k, -k; k, -k)$ or a $\Gamma^k(k, -k; -k, k)$. In the conventional notation the vertices

$\Gamma^k(k,-k;k,-k)$ and $\Gamma^k(k,-k;-k,k)$ are related to $\Gamma^k(\theta)$ via,

$$\hat{\Gamma}^k(\theta) = \lim_{|\Omega|/Q\to 0} \hat{\Gamma}(k_F\hat{n}_1, 0; k_F\hat{n}_2, 0|Q,\Omega), \tag{3.42}$$

where $\hat{\Gamma}(\vec{k}_1,\omega_1;\vec{k}_2,\omega_2|Q,\Omega)$ is the vertex for a process $(\vec{k}_1,\omega_1;\vec{k}_2,\omega_2 \rightarrow \vec{k}_1-\vec{Q},\omega_1-\Omega;\vec{k}_2+\vec{Q},\omega_2+\Omega)$ and θ is the angle the two incoming quasi-particles. Since the incoming momenta are nearly anti-parallel to each other, we can set the angle to be equal to $\theta=\pi$. The vertex with the full spin representation is then,

$$\Gamma^k_{\alpha\beta,\gamma\delta}(\pi) = \Gamma^k(k,-k;k,-k)\delta_{\alpha\gamma}\delta_{\beta\delta} - \Gamma^k(k,-k;-k,k)\delta_{\alpha\delta}\delta_{\beta\gamma}. \tag{3.43}$$

We can express the scattering amplitude in terms of the vertex function via the relation,

$$A_{\alpha\beta,\gamma\delta}(\pi) = Z^2\Gamma^k_{\alpha\beta,\gamma\delta}(\pi), \tag{3.44}$$

where the scattering amplitude itself is represented in terms of spin and charge components,

$$\begin{aligned} A_{\alpha\beta,\gamma\delta}(\vec{k},-\vec{k}) &= A_{\alpha\beta,\gamma\delta}(\pi) = \frac{\pi}{m^*}[A_c(\pi)\delta_{\alpha\gamma}\delta_{\beta\delta} + A_s(\pi)\sigma_{\alpha\gamma}\sigma_{\beta\delta}] \\ &= \frac{\pi}{m^*}\left[(A_c(\pi)-A_s(\pi))\delta_{\alpha\gamma}\delta_{\beta\delta} + 2A_s(\pi)\delta_{\alpha\delta}\delta_{\beta\gamma}\right]. \end{aligned} \tag{3.45}$$

From Eqs. (3.43), (3.44) and (3.45) we obtain the relationship between the spin and charge components and the vertex function,

$$\begin{aligned} Z^2\Gamma^k(\vec{k},-\vec{k};\vec{k},-\vec{k}) &= \frac{\pi}{m^*}[A_c(\pi)-A_s(\pi)] \\ Z^2\Gamma^k(\vec{k},-\vec{k};\vec{k},-\vec{k}) &= -2\frac{\pi}{m^*}A_s(\pi). \end{aligned} \tag{3.46}$$

Finally we will substitute $Z^2\Gamma^k(\vec{k},-\vec{k};\vec{k},-\vec{k})$ for $U(0)$ and $Z^2\Gamma^k(\vec{k},-\vec{k};-\vec{k},\vec{k})$ for $U(2k_F)$ in Eq. (3.14), to obtain the nonanalytic form of the specific heat in a generic Fermi liquid [85],

$$\begin{aligned} \frac{\delta C(T)}{T} &= -\frac{9\zeta(3)}{\pi^2}\left[\frac{m}{2\pi}\right]^2\Big[(Z^2\Gamma^k(\vec{k},-\vec{k};\vec{k},-\vec{k}))^2 + (Z^2\Gamma^k(\vec{k},-\vec{k};-\vec{k},\vec{k}))^2 \\ &\quad -(Z^2\Gamma^k(\vec{k},-\vec{k};\vec{k},-\vec{k}))(Z^2\Gamma^k(\vec{k},-\vec{k};-\vec{k},\vec{k}))\Big]\frac{C_{FG}}{E_F} \\ \frac{\delta C(T)}{T} &= -\frac{3\zeta(3)}{2\pi(v_F^*)^2}[A_c^2(\pi)+3A_s^2(\pi)]T. \end{aligned} \tag{3.47}$$

Notice the universal sub-leading term in the specific heat is not an angular average over all the angles and is different from the leading, Fermi-liquid specific heat term ($C(T)/T \propto$ constant) which is expressed as an "angular-average-($\langle F_C(\theta)\cos\theta\rangle$)" over the Fermi-liquid interaction function.

The result for C_V has been expressed in terms of the scattering amplitude. Alternatively, the specific heat can be expressed in terms of the harmonics of the quasi-particle interaction function $F(\theta)$. The harmonics of the scattering amplitude and the interaction function are related via

$$A_{c/s}^{(n)} = \frac{F_{c/s}^{(n)}}{1 + F_{c/s}^{(n)}},$$

thus

$$A_{c/s}(\pi) = \sum_{n=0}^{\infty}(-1)^n \frac{F_{c/s}^{(n)}}{1 + F_{c/s}^{(n)}}.$$

In contrast to the T term in the specific heat which requires only one harmonic, F_c^1, the T^2 term requires the full set of harmonics. The parameters of Eq. (3.47) can be extracted from the specific heat measurement on the fluid monolayer of ^{3}He [27]. To a reasonable accuracy, the data can be fitted by a form $C/(NTE_F^*) = \gamma(T/E_F^*)$, where N is the density per unit area in a fluid monolayer, $E_F^* = E_F(m/m^*)$ and $\gamma(x) = a - bx$. A fit to the data then yields $b = 0.9[A_c^2(\pi) + 3A_s^2[\pi]] \approx 9 - 14$, thus $[A_c^2(\pi) + 3A_s^2[\pi]] \approx 11 - 15.5$. In the case of "almost localized fermions" [86], the charge channel is the dominant interaction and $F_c^{(n)} \gg 1$. Thus the scattering amplitude term, $A_c(\pi)$, is expected to be small due to cancellation between the subsequent terms in the expansion. Neglecting $A_c(\pi)$, the spin part of the amplitude is obtained to be $|A_s(\pi)| \approx 1.9 - 2.3$. In addition, if the $n = 0$ harmonic of F_s is the leading contributor to $A_s(\pi)$, then $F_s^{(0)} \approx -(0.66 - 0.7)$. This is consistent with the 3D value $F_s^{(0)} \approx -0.75$ [25].

3.4 Specific Heat for the Coulomb Potential

We have shown earlier that the collective mode for a finite range potential leads to a nonanalytic behavior of the self-energy near the mass shell. However, this nonanalyticity is not manifested in the contribution to the T^2 term in the specific heat. For a long

range Coulomb potential, we obtain a T^2 correction to the specific heat both from the particle-hole and from the plasmon regime. In the temperature range $T \ll \kappa v_F \ll E_F$, where $\kappa = me^2$ is the screening wavenumber, the correction is independent of the interaction strength. For the Coulomb potential, the singular nature of the interaction for small momentum transfer allows one to consider an effective RPA potential for the self-energy, and for the thermodynamic potential we need to consider the usual series of ring diagrams. A knowledge of the thermodynamic potential allows us to evaluate the entropy and the specific heat. The finite temperature thermodynamic potential in the ring diagram series is given by

$$\frac{\Delta\Omega}{A} = \frac{T}{2}\sum_{iw_n}\int\frac{d^2k}{(2\pi)^2}\log(1-V(k)\Pi_m(k,iw_n)), \tag{3.48}$$

where the summation is over the bosonic frequencies, Π_m is the polarization operator (we include contributions from both up and down-spin electrons), and $V(k) = 2\pi e^2/k$ the 2D Coulomb potential.

Using Eq. (3.21) to convert the frequency summation into frequency integrals, we obtain

$$S = -\frac{1}{2}\int\frac{d^2k}{(2\pi)^2}\int\frac{d\omega}{\pi}\frac{\frac{w}{4T^2}}{\sinh^2(\omega/2T)}\tan^{-1}\Big[\frac{\mathrm{Im}D^R(k,\omega)}{\mathrm{Re}D^R(k,\omega)}\Big], \tag{3.49}$$

where $D^R = 1 - V(k)\Pi_m(k,iw_n)$. The regions contributing to the entropy are the plasmon region and the particle-hole region (Fig. 3–5). Near the plasmon region,

$$D^R = 1 - V(q)\Pi^R(\omega,q) \approx \frac{(\omega+i0^+)^2-\omega_p^2}{\omega_p^2}, \tag{3.50}$$

thus $\mathrm{Im}D^R \to 0^+$ and $(1-V(k)\mathrm{Re}\Pi^R) < 0$ giving a value of π for the argument in the integrand. The contribution from the plasmon region is thus

$$S|_{plasmon} = -\int_0^{\kappa v_F}\frac{dw}{\pi}\frac{\frac{w}{4T^2}}{\sinh^2(w/2T)}\int_{\frac{w^2}{\kappa v_F^2}}^{\frac{w}{v_F}}\frac{kdk}{2\pi}\pi$$

$$S|_{plasmon} = -\Big(\frac{T}{v_F}\Big)^2\frac{3\zeta(3)}{2\pi}$$

$$C_{V-pl} = -\Big(\frac{T}{v_F}\Big)^2\frac{3\zeta(3)}{\pi}.$$

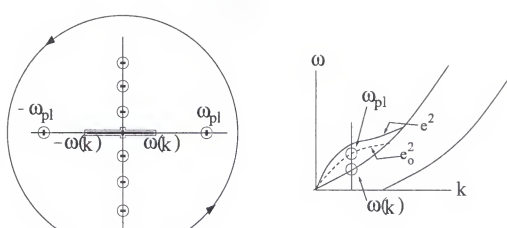

Figure 3-5: Contour for summing up the discrete sum of the Matsubara thermodynamical potential. A) Matsubara poles at the Matsubara frequencies and at the plasmon positions $-\omega_{pl}$ and ω_{pl} (for the integration variable e_0^2); the branch cut from $-\omega_k$ to ω_k represents the particle-hole region. B) Particle-hole spectrum for 2D.

The other contribution to the entropy is from the particle-hole region. The argument [Eqn. 3.49] decays as one goes deep into the particle-hole region. In the particle-hole region the polarization bubble is given by

$$\Pi^R(\omega,q) = -\frac{m}{\pi}\left(1 + i\frac{\omega}{\sqrt{(v_F q)^2 - \omega^2}}\right), \tag{3.51}$$

thus,

$$\tan^{-1}\left(\frac{\mathrm{Im}D^R(\omega,k)}{\mathrm{Re}D^R(\omega,k)}\right) = \tan^{-1}\left(\frac{V(k)\frac{m}{\pi}\frac{\omega}{\sqrt{(v_F q)^2-\omega^2}}}{1+V(k)\frac{m}{\pi}}\right) \tag{3.52}$$

$$S|_{particle-hole} = -\int \frac{d^2k}{(2\pi)^2}\int_0^{kv_F}\frac{dw}{\pi}\frac{\frac{w}{4T^2}}{\sinh^2(w/2T)}\tan^{-1}\Big[\frac{2me^2 w/\sqrt{k^2-w^2}}{k+2me^2}\Big], \tag{3.53}$$

We will make the substitutions $w/2T \to z$ and $v_F k/2T \to k'$, and also a change in the order of integration to obtain

$$S|_{particle-hole} = -\frac{1}{2\pi}(\frac{2T}{v_F})^2\int_0^{\frac{\mu}{T}}\frac{dzz}{\pi\sinh^2(z)}\int_z^{\frac{\mu}{T}}dk'k'\Big(\tan^{-1}\Big[\frac{z/\sqrt{k'^2-z^2}}{2Tk'/\mu r_s+1}\Big]\Big), \tag{3.54}$$

where $r_s = \kappa/k_F$ and $\mu = k_F v_F/2$. It will be convenient to split the integrals into two parts, the first part gives the linear in T correction to the entropy and a T^2 term, whereas

the second integral gives T^2 correction to the entropy.

$$\begin{aligned} S|_{particle-hole} &= -\frac{1}{2\pi}(\frac{2T}{v_F})^2 \int_0^{\frac{\mu}{T}} \frac{dzz^2}{\pi \sinh^2(z)} \int_z^{\frac{\mu}{T}} dk' \frac{1}{Tk'/(\mu r_s)+1} \\ &\quad -\frac{1}{2\pi}(\frac{2T}{v_F})^2 \int_0^{\frac{\mu}{T}} \frac{dzz}{\pi \sinh^2(z)} \\ &\quad \times \int_z^{\frac{\mu}{T}} dk' k' \Big(\tan^{-1}\Big[\frac{z}{\sqrt{k'^2-z^2}} \Big] - \frac{z/k'}{Tk'/(2\mu r_s)+1} \Big) \end{aligned}$$

the expression in the big bracket is convergent and the main contribution comes from $k' \sim 1$, hence for $T \ll \kappa v_F$ we can make a further simplification,

$$\begin{aligned} S|_{particle-hole} &= -\frac{1}{2\pi}(\frac{2T}{v_F})^2 \int_0^{\frac{\mu}{T}} \frac{dzz^2}{\pi \sinh^2(z)} \int_z^{\frac{\mu}{T}} dk' \frac{1}{Tk'/(2\mu r_s)+1} \\ &\quad -\frac{1}{2\pi}(\frac{2T}{v_F})^2 \int_0^{\frac{\mu}{T}} \frac{dzz}{\pi \sinh^2(z)} \\ &\quad \times \int_z^{\frac{\mu}{T}} dk' k' \Big(\tan^{-1}\Big[\frac{z}{\sqrt{k'^2-z^2}} \Big] - \frac{z}{k'} \Big). \end{aligned} \tag{3.55}$$

Finally we have

$$\begin{aligned} S|_{particle-hole} &= \frac{r_s \log(r_s) T}{3m} + \frac{1}{2\pi}(\frac{2T}{v_F})^2 \frac{3\zeta(3)}{2\pi} - \frac{1}{2\pi}(\frac{2T}{v_F})^2 \Big(-\frac{3\zeta(3)}{8} + \frac{3\zeta(3)}{2\pi} \Big) \\ &= \frac{r_s \log(r_s) T}{3m} + (\frac{T}{v_F})^2 \frac{3\zeta(3)}{4\pi}. \end{aligned} \tag{3.56}$$

So the linear in T contribution to the specific heat from the particle-hole region is $C = r_s \log(r_s) T/(3m)$. The T^2 term due to the particle-hole term is

$$S|_{particle-hole} = \Big(\frac{T}{v_F}\Big)^2 \frac{3\zeta(3)}{4\pi}. \tag{3.57}$$

Adding the contributions from the plasmon and the particle-hole region, we get for the nonanalytic correction to the entropy

$$S|_{particle-hole+plasmon} = -\Big(\frac{T}{v_F}\Big)^2 \frac{3\zeta(3)}{4\pi}. \tag{3.58}$$

Hence the T^2 contribution to the specific heat $C = T\partial S/\partial T|_{\mu,A}$ is

$$C = -\Big(\frac{T}{v_F}\Big)^2 \frac{3\zeta(3)}{2\pi}. \tag{3.59}$$

We notice that in this temperature range the specific heat is independent of the interaction strength. A further discussion is provided in Appendix A where we reconsider the plasmon-pole and particle-hole contribution to the specific heat from an alternate approach. We obtain the same results as before

3.5 Conclusion

In this Chapter, the important question regarding the role of nonperturbative interaction effects in the specific heat has been considered. Often while evaluating the contributions to the specific heat from the self-energy, the contribution from the imaginary part of the self-energy is neglected. We have found that for a short range potential, the imaginary part of the self-energy emanating from the zero-sound mode region, $\mathrm{Im}\Sigma_{ZS}$, does contribute to the nonanalytic term in the self-energy. In fact, this contribution exactly cancels the contribution coming from the real part of the self-energy (whose contribution also originates from the zero-sound region). This result implies that a nonanalytic correction to the self-energy arises only due to perturbative processes. We have verified this result directly by calculating the specific heat from the thermodynamic potential. To this end use has been made of both the real and Matsubara frequency formalism. An advantage of using the Matsubara formalism is the ease in identifying the terms which gives rise to the nonanalytic contributions to the specific heat. This has helped us in extending our second order result to all orders. This extension to all orders is required for cases when the interaction strengths are not weak. In a further extension of this work, a finite-range potential was considered. We have been able to obtain a closed form solution for the contributions to the specific heat to this problem as well. Finally, we have considered the case of long range Coulomb potential and shown that perturbative process do contribute to the specific heat and, in the low-T limit, this contribution is interaction-independent.

CHAPTER 4
ANOMALOUS EFFECTIVE MASS

The observation of a metallic-like resistivity and an apparent metal-insulator transition in high-mobility Si-MOSFETs in 1994 [50, 51] challenged the scaling theory of localization and has since led a number of groups to study both the transport and thermodynamic properties of Si-MOSFET's and other semi-conductor heterostructures. The origin of the anomalous metallic behavior still remains a subject of active research. As discussed in Section 1.3, although models based on the conventional dirty Fermi-liquid can account for many observed effects both qualitatively and quantitatively, there are quite a few proposals for the non-Fermi liquid origin of the anomalous metallic state. On the experimental side, the main qualitative argument for the Fermi-liquid nature of the metallic state is the observation of conventional Shubnikov-de Haas oscillations, which implies an existence of well defined quasi-particles. The parameters of the 2DES, the effective mass m^* and the Landé g-factor are obtained by fitting the Lifshitz-Kosevich formula to the Shubnikov-de Haas (SdH) oscillation data. Excellent fit to the SdH data using the renormalized parameters and the matching of these parameters with the parameters ($\chi^* \propto m^* g^*$) obtained via other experimental techniques like saturation of magnetoresistance approach [64, 66, 67], give strong evidence for the Fermi-liquid behavior of the 2D system. In particular, studies indicate the spin susceptibility χ^* shows a strong increase as the density approaches the critical one (insulating regime) with a large fraction of this increase attributed to the increase in the effective mass term than g^*, an attribute very similar to the He^3 case.

The magnetic field dependence of the effective mass serves as an additional check for Fermi-liquid behavior. Experimental observation of such behavior in 2D Si-MOSFET's in the presence of a parallel magnetic field shows that, contrary to the expectations, the effective mass shows no dependence on the degree of polarization [68] (Fig. 4–1). Although the effective mass exhibits strong dependence on the density and hence the

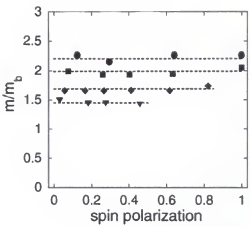

Figure 4–1: Effective mass vs the degree of spin-polarization. The electron densities in units of 10^{11}cm^{-2} are: 1.32 (dots), 1.47 (squares), 2.07(diamonds), and 2.67 (triangles).

Fermi energy E_F, the lack of dependence on the magnetic-field, which alters the Fermi energy, is quite surprising as it does not follow the prediction of Fermi-liquid theory. That the masses should depend on polarization can be seen from considering two limiting cases: of zero- and 100% polarization. At fixed total density, the Fermi energy is doubled by fully polarizing the 2D system. Thus the ratio of Coulomb to Fermi energy $g = e^2\sqrt{\pi n}/E_F$, which is a measure of interaction strength is halved compared to the unpolarized case. Yet the effective mass remains polarization independent. In this Chapter we analyze this paradox in detail.

The present Chapter is divided into two parts. Section 4.1 deals with the polarization dependence of the effective mass. We will consider two independent approaches, Landau's phenomenological approach in Section 4.1.1 and the weak coupling approach in Section 4.1.2, to show that in a Fermi liquid the effective mass not only acquires a field dependence but also exhibits spin-splitting. In the second part of this Chapter, Section 4.2.1 and Section 4.2.2, we examine the influence of valley degeneracy on the effective mass and on the spin susceptibility, respectively. The importance of valley degeneracy on the transport properties in the (001) plane of Si-MOSFET has been emphasized in a recent

study by Punnoose and Finkelstein [61]. The diffuson propagator in a spin-1/2 system has 4 channels, 1 singlet and 3 triplet, whereas for a system with spin-1/2 and 2-valley degeneracy (total degeneracy is 4), as in the (001) plane of Si-MOSFET, there are 1 singlet and 15 triplet channels. These additional channels have been held responsible for a large (almost an order of magnitude) drop in resistivity near the critical region. Motivated by these findings, we consider a Coulomb gas in the large-N limit (for Si-MOSFETs, $N = 4$). In a system with no valley degeneracy, the effective mass is renormalized by emission of both virtual electron-hole pairs and plasmons, in the large N-limit of the Coulomb gas, the effective mass is renormalized primarily due to a polaronic effect: via emission and absorpbtion of (virtual) high energy plasmons, while electron-hole pairs play only a nominal role. As plasmons are classical objects, the quantum degeneracy and, hence the polarization, does not affect the effective mass to the leading order in $1/N$. The large-N expansion obtained is rapidly convergent even for non-valley degenerate system ($N = 2$) and, as such, it provides a non-trivial way of going beyond the weak coupling limit.

In Section 4.2.2 we investigate the behavior of the spin susceptibility in the large-N limit. We find that the spin susceptibility is renormalized; however this renormalization in leading and subleading order is due to the renormalized effective mass, whereas the Landé-g factor remains unrenormalized. This indicates that the enhancement of the spin susceptibility does not reflect the tendency towards ferromagnetic ordering.

4.1 Spin-Polarized Effective Mass

In the following two Sections we show how a standard treatment results in a polarization dependent effective mass in the presence of a magnetic field applied parallel to the 2D surface. The parallel magnetic field is assumed to couple only to the spin degree of freedom and not to the orbital degree of freedom, and acts as a knob which can be used to change the population of either kind of electrons, while keeping the total density of electrons fixed.

4.1.1 Landau's Phenomenological Approach

First, we derive an effective mass expression for a partially spin-polarized Fermi liquid system, generalizing the approach used for the single component case [87]. The form of the Landau interaction function for a spin-polarized case is, however, much more complicated

due to the breakdown of SU(2) symmetry. We will show that this interaction function effectively reduces to three independent terms which describe the interaction between two up-spin electrons, between two down-spin electrons, and between an up-spin electron and a down-spin electron. The strategy to obtain the mass is to compare the change in the quasi-particle energy between a moving frame and a fixed frame via two different ways. In the first way, Galilean invariance is utilized to find the difference in the energy of a quasi-particle between the rest frame and a moving frame. In the second way, one notices that the distribution functions are different in different frames, and thus we can calculate the change in the quasi-particle energy which arises due to a variation in the distribution function.

The general form of the interaction function in a spin-polarized system is given by [88]

$$\begin{aligned} f_{\alpha,\mu;\beta,\nu}(\vec{p},\vec{p}\,') &= \bar{F}(\vec{p},\vec{p}\,')\delta_{\alpha,\beta}\delta_{\mu,\nu} + G(\vec{p},\vec{p}\,')\vec{\sigma}_{\alpha,\beta}.\vec{\sigma}_{\mu,\nu}\,' + \hat{\mathbf{z}}.[X(\vec{p},\vec{p}\,')\vec{\sigma}_{\alpha,\beta}\delta_{\mu,\nu} \\ &\quad + X(\vec{p}\,',\vec{p})\vec{\sigma}_{\mu,\nu}\delta_{\alpha,\beta}] + Y(\vec{p},\vec{p}\,')[\vec{\sigma}_{\alpha,\beta}.\hat{\mathbf{z}}][\vec{\sigma}_{\mu,\nu}.\hat{\mathbf{z}}], \end{aligned} \tag{4.1}$$

where the field is in the $\hat{\mathbf{z}}$ direction, and $\vec{\sigma}$ are the Pauli matrices.

The change in quasi-particle energy due to a change in the quasi-particle distribution function is given by

$$\delta\hat{\epsilon}(\vec{p}) = \mathrm{Tr}' \int \hat{f}(\vec{p},\sigma;\vec{p}\,',\sigma')\delta\hat{n}(\vec{p}\,')\frac{d^2p'}{(2\pi)^2}, \tag{4.2}$$

and the distribution matrix $\delta\hat{n}$ is

$$\begin{pmatrix} \delta n_\uparrow & 0 \\ 0 & \delta n_\downarrow \end{pmatrix},$$

where the change in distribution function for the majority (spin-up) quasi-particle is given by $\delta n_\uparrow$ and for the minority (spin-down) quasi-particle by $\delta n_\downarrow$. We explicitly calculate the product of the density matrix $\delta n_{\mu,\nu}$ with the interaction function, to obtain the following

terms:

$$\begin{aligned}
\bar{F}(\vec{p},\vec{p}\,')\delta_{\alpha,\beta}\delta_{\mu,\nu}\delta n_{\mu,\nu} &= \bar{F}(\vec{p},\vec{p}\,')\delta_{\alpha,\beta}[\delta n_\uparrow + \delta n_\downarrow] \\
G(\vec{p},\vec{p}\,')\vec{\sigma}_{\alpha,\beta}.\vec{\sigma}_{\mu,\nu}\,'\delta n_{\mu,\nu} &= G(\vec{p},\vec{p}\,')[2\delta n_{\beta,\alpha} - \delta_{\alpha,\beta}(\delta n_\uparrow + \delta n_\downarrow)], \\
\hat{\mathbf{z}}X(\vec{p},\vec{p}\,')\vec{\sigma}_{\alpha,\beta}\delta_{\mu,\nu}\delta n_{\mu,\nu} &= X(\vec{p},\vec{p}\,')\sigma^z_{\alpha,\beta}[\delta n_\uparrow + \delta n_\downarrow]
\end{aligned}$$

and

$$\begin{aligned}
\hat{\mathbf{z}}X(\vec{p}\,',\vec{p})\vec{\sigma}_{\mu,\nu}\delta n_{\mu,\nu}\delta_{\alpha,\beta} &= X(\vec{p}\,',\vec{p})\sigma^z_{\mu,\nu}\delta n_{\mu,\nu}\delta_{\alpha,\beta} = X(\vec{p}\,',\vec{p})[\delta n_\uparrow - \delta n_\downarrow]\delta_{\alpha,\beta} \\
Y(\vec{p},\vec{p}\,')\sigma^z_{\alpha,\beta}\sigma^z_{\mu,\nu}\delta n_{\mu,\nu} &= Y(\vec{p},\vec{p}\,')\sigma^z_{\alpha,\beta}[\delta n_\uparrow - \delta n_\downarrow]. \qquad (4.3)
\end{aligned}$$

It is easy to deduce that the quasi-particle energy matrix is in a diagonal form since $\delta_{\alpha,\beta}$, $\sigma^z_{\alpha,\beta}$ and $\delta n_{\alpha,\beta}$ are all in a diagonal form. Thus for a spin-up quasi-particle we obtain the following relation

$$\begin{aligned}
\delta\varepsilon_\uparrow(\vec{p}) &= \int \frac{d^2p'}{(2\pi)^2}\Bigg[\delta n_\uparrow(\vec{p}\,')\Big\{\bar{F}(\vec{p},\vec{p}\,') + G(\vec{p},\vec{p}\,') + X(\vec{p},\vec{p}\,') + X(\vec{p}\,',\vec{p}) + Y(\vec{p},\vec{p}\,')\Big\} \\
&\quad +\delta n_\downarrow(\vec{p}\,')\Big\{\bar{F}(\vec{p},\vec{p}\,') - G(\vec{p},\vec{p}\,') + X(\vec{p},\vec{p}\,') - X(\vec{p}\,',\vec{p}) - Y(\vec{p},\vec{p}\,')\Big\}\Bigg].
\end{aligned}$$

Similarly, for a spin-down quasi-particle

$$\begin{aligned}
\delta\varepsilon_\downarrow(\vec{p}) &= \int \frac{d^2p'}{(2\pi)^2}\Bigg[\delta n_\uparrow(\vec{p}\,')\Big\{\bar{F}(\vec{p},\vec{p}\,') - G(\vec{p},\vec{p}\,') - X(\vec{p},\vec{p}\,') + X(\vec{p}\,',\vec{p}) - Y(\vec{p},\vec{p}\,')\Big\} \\
&\quad +\delta n_\downarrow(\vec{p}\,')\Big\{\bar{F}(\vec{p},\vec{p}\,') + G(\vec{p},\vec{p}\,') - X(\vec{p},\vec{p}\,') - X(\vec{p}\,',\vec{p}) + Y(\vec{p},\vec{p}\,')\Big\}\Bigg].
\end{aligned}$$

To simplify the algebra we will define a new interaction function $F^{ij}(\vec{p},\vec{p}\,')$, where $i,j = \uparrow,\downarrow$ such that

$$\begin{aligned}
\delta\varepsilon_\uparrow(\vec{p}) &= \int \frac{d^2p\,'}{(2\pi)^2}\Big[F^{\uparrow,\uparrow}(\vec{p},\vec{p}\,')\delta n_\uparrow(\vec{p}\,') + F^{\uparrow,\downarrow}(\vec{p},\vec{p}\,')\delta n_\downarrow(\vec{p}\,')\Big] \\
\delta\varepsilon_\downarrow(\vec{p}) &= \int \frac{d^2p'}{(2\pi)^2}\Big[F^{\downarrow,\uparrow}(\vec{p},\vec{p}\,')\delta n_\uparrow(\vec{p}\,') + F^{\downarrow,\downarrow}(\vec{p},\vec{p}\,')\delta n_\downarrow(\vec{p}\,')\Big],
\end{aligned}$$

where

$$
\begin{aligned}
F^{\uparrow,\uparrow}(\vec{p},\vec{p}\,') &= \bar{F}(\vec{p},\vec{p}\,') + G(\vec{p},\vec{p}\,') + X(\vec{p},\vec{p}\,') + X(\vec{p}\,',\vec{p}) + Y(\vec{p},\vec{p}\,') \\
F^{\uparrow,\downarrow}(\vec{p},\vec{p}\,') &= \bar{F}(\vec{p},\vec{p}\,') - G(\vec{p},\vec{p}\,') + X(\vec{p},\vec{p}\,') - X(\vec{p}\,',\vec{p}) - Y(\vec{p},\vec{p}\,') \\
F^{\downarrow,\uparrow}(\vec{p},\vec{p}\,') &= \bar{F}(\vec{p},\vec{p}\,') - G(\vec{p},\vec{p}\,') - X(\vec{p},\vec{p}\,') + X(\vec{p}\,',\vec{p}) - Y(\vec{p},\vec{p}\,') \\
F^{\downarrow,\downarrow}(\vec{p},\vec{p}\,') &= \bar{F}(\vec{p},\vec{p}\,') + G(\vec{p},\vec{p}\,') - X(\vec{p},\vec{p}\,') - X(\vec{p}\,',\vec{p}) + Y(\vec{p},\vec{p}\,').
\end{aligned}
$$

Thus, we can invoke Galilean invariance to obtain the effective mass [87]. Using Galilean invariance we can relate the quasi-particle energy in a moving frame ε' with the quasi-particle energy in a laboratory frame ε. Let us assume the moving-frame has a velocity $\vec{u}$ with respect to the lab frame. Introducing a quasi-particle with momentum $\vec{p}$ in the lab frame, we increase the total mass of the system by the bare mass m, since a new particle has been added. The quasi-particle energy in the moving frame is

$$
\begin{aligned}
\varepsilon'(\vec{p} - m\vec{u}) &= \varepsilon(\vec{p}) - \dot{\vec{p}}u + \frac{mu^2}{2} \\
p' &= p - m\vec{u},
\end{aligned}
$$

where $\vec{p}$ ($\vec{p}\,'$) is the quasi-particle momentum in the lab frame (moving frame) and m is the bare mass of the particle. We thus obtain

$$
\varepsilon'(\vec{p}) = \varepsilon(\vec{p} + m\vec{u}) - (\vec{p} + m\vec{u}) \cdot \vec{u} + \frac{mu^2}{2}.
$$

The right hand side of the equation can be expanded to linear order in $\vec{u}$ to obtain the relation

$$
\varepsilon'(\vec{p}) = \varepsilon(\vec{p}) + \frac{(m - m^*)\vec{p} \cdot \vec{u}}{m^*}.
$$

Hence for the particle of the first kind (spin-up) we have

$$
\varepsilon'_\uparrow(\vec{p}) = \varepsilon_\uparrow(\vec{p}) + \frac{(m - m^*_\uparrow)\vec{p} \cdot \vec{u}}{m^*_\uparrow} \Rightarrow \delta\varepsilon'(\vec{p}) = \frac{(m - m^*_\uparrow)\vec{p} \cdot \vec{u}}{m^*_\uparrow}, \tag{4.4}
$$

where the bare mass for spin-up and spin-down quasi-particles is the same and equals m. A second relation is obtained by observing that the quasi-paricle energy $\varepsilon'(\vec{p})$ in the moving frame differs from the quasi-paricle energy $\varepsilon(\vec{p})$ in the lab frame because of a

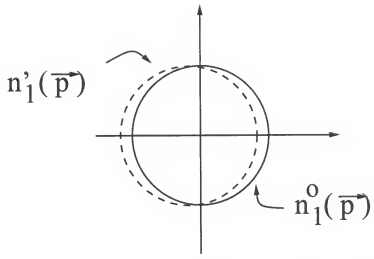

Figure 4–2: Distribution function in the primed frame and lab frame are represented by dashed and full circle respectively.

different distribution function. The shift in the energy spectrum $\delta\varepsilon(\vec{p}) = \varepsilon'(\vec{p}) - \varepsilon(\vec{p})$ due to a different distribution [the new distribution is shifted by $-m\vec{u}$ in momentum space for both up- and down-spin particles, (Fig. 4–2)] is

$$\delta\varepsilon(\vec{p}) = \mathrm{tr}' \int \hat{f}(\vec{p},\vec{p}\,')\delta\hat{n}_{\vec{p}\,'}\frac{d^2p'}{(2\pi)^2} \tag{4.5}$$

where tr' is the trace. For spin-up

$$\delta\varepsilon_\uparrow(\vec{p}) = \int \frac{d^2p'}{(2\pi)^2}\left[F^{\uparrow,\uparrow}(\vec{p},\vec{p}\,')\delta n_\uparrow(\vec{p}\,') + F^{\uparrow,\downarrow}(\vec{p},\vec{p}\,')\delta n_\downarrow(\vec{p}\,')\right], \tag{4.6}$$

and for spin down

$$\delta\varepsilon_\downarrow(\vec{p}) = \int \frac{d^2p'}{(2\pi)^2}\left[F^{\downarrow,\uparrow}(\vec{p},\vec{p}\,')\delta n_\uparrow(\vec{p}\,') + F^{\downarrow,\downarrow}(\vec{p},\vec{p}\,')\delta n_\downarrow(\vec{p}\,')\right], \tag{4.7}$$

where we have used

$$\delta n_\uparrow(\vec{p}\,') = n'_\uparrow(\vec{p}\,') - n^0_\uparrow(\vec{p}\,'). \tag{4.8}$$

There is a very simple relationship between the distribution function in the primed frame and that in the lab frame: a particle moving with momentum $\vec{p}\,'$ in the primed frame will have momentum $\vec{p}\,' + m\vec{u}$ in the rest frame, thus the distribution functions in the different frames will obey the relation $n'_\uparrow(\vec{p}\,') = n^0_\uparrow(\vec{p}\,' + m\vec{u})$, where $n'_\uparrow$ ($n^0_\uparrow$) is the distribution in

the primed (rest) frame. The two distribution functions are shown in Fig. 4-2. Continuing with Eq. (4.8) we obtain

$$\begin{aligned} n'_\uparrow(\vec{p}\,') - n^0_\uparrow(\vec{p}\,') &= n^0_\uparrow(\vec{p}\,' + m\vec{u}) - n^0_\uparrow(\vec{p}\,') \\ &= m\vec{u}\cdot\frac{\vec{p}\,'}{m^*_\uparrow}\frac{\partial n^0_\uparrow(\vec{p}\,')}{\partial\varepsilon_\uparrow(\vec{p}\,')} \\ &= -\frac{m\vec{u}\cdot\vec{p}\,'}{m^*_\uparrow}\delta(\varepsilon_\uparrow(p_{\vec{F}\uparrow}) - \varepsilon_\uparrow(\vec{p}\,')), \end{aligned} \tag{4.9}$$

where $p_{\vec{F}\uparrow}$ is the Fermi wave vector of the up-spin electron. Similarly for the spin-down particle, the change in distribution is

$$\delta n_\downarrow(\vec{p}\,') = m\vec{u}\cdot\frac{\vec{p}\,'}{m^*_\downarrow}\frac{\partial n^0_\downarrow(\vec{p}\,')}{\partial\varepsilon_\downarrow(\vec{p}\,')} = -\frac{m\vec{u}\cdot\vec{p}\,'}{m^*_\downarrow}\delta(\varepsilon_\downarrow(\vec{p}_{F\downarrow}) - \varepsilon_\downarrow(\vec{p}\,')),$$

where $\vec{p}_{F\downarrow}$ is the Fermi wave vector of the down-spin electron. For a spin-polarized system the Fermi wave vector of the up-spin electron, $\vec{p}_{F\uparrow}$, will be greater than that of the down-spin electron, $\vec{p}_{F\downarrow}$. Substituting the simplified form of $\delta n_\uparrow(\vec{p}\,')$ and $\delta n_\downarrow(\vec{p}\,')$ in Eq. (4.6) and Eq. (4.7), and using the relations

$$\begin{aligned} \frac{d^2\vec{p}}{(2\pi)^2} &= \frac{m^*}{2\pi}\frac{d\varepsilon d\theta}{2\pi} \\ \int_0^{2\pi} d\theta' F(\vec{p}\cdot\vec{p}\,')\vec{u}\cdot\vec{p}\,' &= \int_0^{2\pi} d\theta' F(|\vec{p}\,'||\vec{p}|\cos\theta')|\vec{u}||\vec{p}\,'|\cos(\theta-\theta') \\ &= |\vec{u}||\vec{p}\,'|\cos(\theta)\int_0^{2\pi} d\theta' F(|\vec{p}\,'||\vec{p}|\cos\theta')\cos\theta', \end{aligned} \tag{4.10}$$

we obtain

$$\begin{aligned} \delta\varepsilon_\uparrow &= -\frac{m}{2\pi}\vec{u}\cdot\vec{p_{F\uparrow}}\int\frac{d\theta'}{2\pi}\cos\theta' F^{\uparrow,\uparrow}(\vec{p}_{F\uparrow},\vec{p}_{F\uparrow}) \\ &\quad -\frac{m}{2\pi}\vec{u}\cdot\vec{p_{F\downarrow}}\int\frac{d\theta'}{2\pi}\cos\theta' F^{\uparrow,\downarrow}(\vec{p}_{F\uparrow},\vec{p}_{F\downarrow}\,') \\ \delta\varepsilon_\downarrow &= -\frac{m}{2\pi}\vec{u}\cdot\vec{p_{F\uparrow}}\int\frac{d\theta'}{2\pi}\cos\theta' F^{\downarrow,\uparrow}(\vec{p}_{F\downarrow},\vec{p}_{F\uparrow}\,') \\ &\quad -\frac{m}{2\pi}\vec{u}\cdot\vec{p_{F\downarrow}}\int\frac{d\theta'}{2\pi}\cos\theta' F^{\downarrow,\downarrow}(\vec{p}_{F\downarrow},\vec{p}_{F\downarrow}\,'), \end{aligned} \tag{4.11}$$

where $\vec{p}_{F\uparrow}$ and $\vec{p}_{F\downarrow}$ point in the same direction, and in general $F^{\uparrow,\uparrow}(\vec{p}_{F\uparrow},\vec{p}_{F\uparrow}\,') \neq F^{\downarrow,\downarrow}(\vec{p}_{F\downarrow},\vec{p}_{F\downarrow}\,') \neq F^{\downarrow,\uparrow}(\vec{p}_{F\downarrow},\vec{p}_{F\uparrow}\,')$. Comparing Eqs. (4.4) and (4.11) we obtain for the

up-spin fermions

$$\left(\frac{m^*_\uparrow}{m}\right)^{-1} = 1 - m_\uparrow \int \frac{d\theta'}{(2\pi)^2} \cos\theta' F^{\uparrow,\uparrow}(\vec{p}_{F\uparrow}, \vec{p}_{F\uparrow}\,') - \frac{m p_{F\downarrow}}{p_{F\uparrow}} \int \frac{d\theta'}{(2\pi)^2} \cos\theta' F^{\uparrow,\downarrow}(\vec{p}_{F\uparrow}, \vec{p}_{F\downarrow}\,'),$$

similarly for the down-spin fermions

$$\left(\frac{m^*_\downarrow}{m}\right)^{-1} = 1 - \frac{m p_{F\uparrow}}{p_{F\downarrow}} \int \frac{d\theta'}{(2\pi)^2} \cos\theta' F^{\downarrow,\uparrow}(\vec{p}_{F\downarrow}, \vec{p}_{F\uparrow}\,') - m \int \frac{d\theta'}{(2\pi)^2} \cos\theta' F^{\downarrow,\downarrow}(\vec{p}_{F\downarrow}, \vec{p}_{F\downarrow}\,').$$

It is clear from the above equations that the effective mass for the up and down-spin electrons is, generally, different. An explicit evaluation of the effective mass requires a knowledge of the F function which, however, is not provided within Landau's phenomenological theory. In the following Section, we will perturbatively evaluate the effective mass of a system of electrons interacting with the long range Coulomb interaction and confirm our prediction regarding the spin splitting of the effective mass.

4.1.2 Weak-Coupling Approach

A knowledge of the exact eigen states of a Hamiltonian allows us to calculate relevant physical quantities. In many cases, though, it is simply too difficult to calculate these eigen states. In these situations one resorts to perturbative techniques and obtains the physical quantities as a perturbative expansion in terms of a small parameter of the system. We resort to this approach to calculate the effective mass in terms of the dimensionless constant $r_s = \sqrt{2}me^2/k_F$ (a measure of the interaction strength). The stronger the interaction, the more the deviation of the electron effective mass from the bare electron mass. For a system with different numbers of up- and down-spin electrons, there will be unequal renormalization of the masses and hence spin-split masses.

The Hamiltonian of our system is given by

$$\begin{aligned} H &= \int \Big[\frac{1}{2m}\nabla\Psi^\dagger_\alpha(r)\nabla\Psi_\alpha(r) - \frac{g\mu_B B_\parallel}{2}\Psi^\dagger_\alpha(r)\Psi_\alpha(r)\Big] d^3r \\ &\quad + \frac{1}{2}\int\int \Psi^\dagger_\alpha(r)\Psi^\dagger_\beta(r')U(r-r')\Psi_\beta(r')\Psi_\alpha(r) d^3r d^3r', \end{aligned} \tag{4.12}$$

where the summation on repeated spin indices is implied and $U(r-r')$ is the usual Coulomb interaction potential. The Fermi wave vectors for spin-up and spin-down electrons are different: $k_F^{\uparrow,\downarrow} = k_F\sqrt{1 \pm \xi}$, where $\xi = (n^\uparrow - n^\downarrow)/n$ is the degree of polarization.

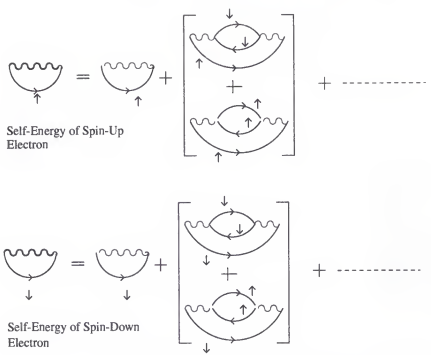

Figure 4–3: Self-Energy of spin-up and spin-down electrons.

We will consider all interactions present in this system: between two up-spin electrons, between two down-spin electrons and between an up-spin and a down-spin electron.

The electrons interact via a Coulomb potential. This potential is screened due to the creation of electron-hole pairs. To calculate the self-energy (required to obtain the effective mass), we choose those diagrams which at each order in the interaction have maximum divergence. Self-energy diagrams given in Fig. 4–3 contain all such contributions. The series when summed to all orders [the choice of this particular series is known as the Random Phase Approximation (RPA)] yields an effective potential which is dynamically screened.

The effective mass in terms of the self-energy is defined as

$$\frac{m}{m^{*\uparrow\downarrow}} = \frac{1+\frac{\partial\Sigma^{\uparrow\downarrow}(p,i\bar{w})}{\partial\xi_p^{\uparrow\downarrow}}}{1-\frac{\partial\Sigma^{\uparrow\downarrow}(p,i\bar{w})}{\partial i\bar{w}}}\Bigg|_{\bar{w}\to 0;\xi_p^{\uparrow\downarrow}\to 0}, \tag{4.13}$$

where $\Sigma^{\uparrow\downarrow}$ is the self-energy of up and down-spin electrons with momentum p, frequency $i\bar{w}$ and quasi-particle energy ξ_p. For $p \simeq k_F^{\uparrow\downarrow}$, $\xi_p^{\uparrow\downarrow} = k_F^{\uparrow\downarrow}(v - v_F^{\uparrow\downarrow})$, where k_F^{α} and v_F^{α} are the Fermi momenta and velocities respectively. Let us consider the self-energy diagram for

spin-up electrons given in Fig. 4–3. Because the Fermi momenta of spin up and spin down electrons are different, a probe electron causes different variations in the densities of the two spin orientations. The resulting potential contains the sum of two contributions from both spin orientations. Summing up the RPA series, we obtain the following expression for the self-energy:

$$\begin{aligned}\Sigma^{\uparrow\downarrow}(p,i\tilde{w}) &= -\int_{-\infty}^{+\infty}\frac{dw}{2\pi}\int_0^{\infty}\frac{kdk}{(2\pi)^2}V(k)\int_0^{2\pi}d\theta G^{\uparrow\downarrow}_{(0)}(p+k,iw+i\tilde{w}) \\ &\quad -\int_{-\infty}^{+\infty}\frac{dw}{2\pi}\int_0^{\infty}\frac{kdk}{(2\pi)^2}\frac{V^2(k)\Pi(k,iw)}{1-V(k)\Pi(k,iw)} \\ &\quad \times\int_0^{2\pi}d\theta G^{\uparrow\downarrow}_{(0)}(p+k,iw+i\tilde{w}),\end{aligned} \tag{4.14}$$

where $V(k)=2\pi e^2/k$ is the bare potential, G is the free single-particle Green's function and Π is the polarization operator. The momentum-frequency integrals in Eq. (4.14) are dominated by the regions $k\sim\kappa\ll k_F$, where $\kappa\sim r_s k_F$ is the screening length and $\omega\sim kv_F$. Therefore the long-wavelength limit of the polarization operator $\Pi(k,w)$ can be used. This form is

$$\Pi=\Pi^{+}+\Pi^{-},\ \Pi^{\pm}(iw,k)=-\frac{m}{2\pi}\left(1-\frac{|w|}{\sqrt{(kv_F^{\pm})^2+w^2}}\right).$$

At this point we will summarize the approach that has been taken to calculate the effective mass. In effect, we need to evaluate two quantities, a self-energy differentiated with respect to the external frequency and a self-energy differentiated with respect to ξ_k. We find that when differentiating Eq. (4.14) with respect to ξ_k, the two individual terms diverge, however the divergences cancel each other. The first term of the self-energy yields a log singularity which is exactly cancelled by a similar log singularity arising from the second term. Similar care needs to be taken when differentiating Eq. (4.14) with respect to the frequency. Details of the calculation are provided in Appendix B. The result essentially states that the effective mass of spin-up and spin-down electrons depends on the interaction parameter r_s and the degree of polarization,

$$\frac{m^{*\uparrow\downarrow}}{m} = \frac{1+\frac{r_s^{\uparrow\downarrow}}{\sqrt{2}}\left(\frac{1}{2}+\frac{1}{\pi}\right)+0.23\frac{r_s^{\uparrow\downarrow}}{\sqrt{2}}\xi}{1+\frac{r_s^{\uparrow\downarrow}}{\pi\sqrt{2}}\left(\frac{\pi}{2}+\log\frac{1}{r_s^{\uparrow\downarrow}}\right)+0.23\frac{r_s^{\uparrow\downarrow}}{\sqrt{2}}\xi}, \tag{4.15}$$

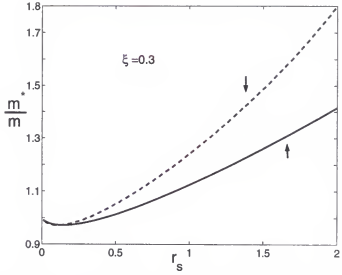

Figure 4–4: Effective mass for a spin-up and a spin-down electron at polarization $\xi = 0.3$.

hence expanding to the lowest order in polarization we obtain

$$\frac{m^{*\uparrow\downarrow}}{m} = 1 + \frac{r_s}{\sqrt{2}}\left(\frac{1}{\pi} + \frac{\log r_s}{\pi}\right) \mp \frac{r_s\xi}{2\sqrt{2}\pi}(2 + \log r_s). \tag{4.16}$$

The general behavior of the effective mass for $\xi = 0$, even the decrease of the effective mass compared to the bare mass at high density, is in agreement with a recent experiment on the 2D electron system in an GaAs/AlGaAs heterostructure [89]. On the other hand the above theoretical predictions regarding the presence of a spin-split effective mass (Fig. 4–4) is not consistent with the experimental findings. The LK formula for the case of magnetic field tilted with respect to the 2D electron gas plane reads

$$\rho_{xx}/\rho_0 = \sum_{k,\sigma} A_k \cos[2\pi^3 k\hbar n_\sigma/eB_\perp - \pi], \tag{4.17}$$

where $\sigma = \uparrow, \downarrow$ is the spin index, and A_k is the amplitude of the k^{th} harmonic which is a function of the electron mass and is assumed to be the same for spin-up and spin-down electrons. If however, the masses were different then the corresponding amplitudes would differ and the LK formula would change to

$$\begin{aligned}\frac{\rho_{xx}}{\rho_0} &= \sum_{s,\sigma} A_s(m^\uparrow)\cos[2\pi^3 s\hbar n_\sigma/eB_\perp - \pi] \\ &+ \sum_s \Big(A_s(m^\downarrow) - A_s(m^\uparrow)\Big)\cos[\frac{2\pi^3 s\hbar n^\downarrow}{eB_\perp} - \pi].\end{aligned} \tag{4.18}$$

The frequency of the oscillation is dependent on the density of the components and for a spin-polarized system a mismatch in frequency results in a beat pattern to be observed in the experimental data. Due to the difference in amplitude term (ΔA_s), the beats will not be complete. Nevertheless the experimental data show full beats, implying that $\Delta A_s = 0$ and that the effective masses for the up-spin and down-spin electrons are equal [66]. On a similar note, the experimental group of Shashkin *et al.*[68] found no dependence of the effective mass on the degree of polarization (Fig. 4–1).

4.2 Multi-Valley System

The absence of polarization dependence of the effective mass suggests that m^* is renormalized via an interaction with some classical degree of freedom which is not affected by the quantum degeneracy of the electron state. As will be shown below, such a mechanism is provided by the renormalization of electrons by the virtual emission and absorption of high energy plasmons. We reanalyze the issue of spin independent effective mass by considering the spin-valley degeneracy in the 2D system. A valley degeneracy provides an additional parameter (N) to the problem. This parameter is 4 for the case of a 2D Si-MOSFET (2 spins $\bigotimes$ 2 valleys) grown along a (001) plane. The additional parameter $N = 4$ turns out to be critical in explaining transport data in both the diffusive and ballistic limits. We will consider the effect of valley degeneracy in the context of the effective mass problem and will also calculate the spin susceptibility. To this end our Hamiltonian is defined as follows

$$\begin{aligned} H &= \int \frac{1}{2m} \nabla \Psi_\alpha^\dagger(r) \nabla \Psi_\alpha(r) d^3r \\ &\quad + \frac{1}{2} \int \int \Psi_\alpha^\dagger(r) \Psi_\beta^\dagger(r') U(r - r') \Psi_\beta(r') \Psi_\alpha(r) d^3r d^3r', \end{aligned} \tag{4.19}$$

where $\alpha, \beta = 1....N$, are the spin-valley indices.

4.2.1 Effective Mass

In the long-wavelength limit the Matsubara polarization operator at $T = 0$ for a system with degeneracy N (N components) is

$$\Pi^M(q, i\omega) = -\frac{mN}{2\pi}(1 - |\omega|/\sqrt{\omega^2 + q^2 p_F^2/m^2}),$$

where the Fermi wave vector in terms of the density of electrons n is $p_F = 2\sqrt{\pi n/N}$, *i.e.*, the Fermi momentum decreases by a factor of $\sqrt{N}$. This decrease in the Fermi momentum is due to the fact that the electrons are distributed in N-valleys. Within the random phase approximation (RPA), the typical momentum transfer is of the order of $\kappa \sim e^2 m N$. The ratio $\alpha = \kappa/p_F = r_s N^{3/2}/2$, is a parameter describing the crossover between the regimes of weak ($\alpha \ll 1$) and strong ($\alpha \gg 1$) screening. Both weak- and strong-screening regimes are within the reach of perturbation theory ($r_s \ll 1$), provided the degeneracy $N \gg 1$.

In the weak-screening regime, the scattering processes leading to mass renormalization are essentially elastic and the typical momentum transferred $q \sim \kappa$ is small. The main contribution to the mass renormalization is via the interaction of electrons with the particle-holes [shaded region in Fig. 4–5A], whereas the emission/absorption of plasmons provides subleading contributions. The effective mass is

$$\frac{m^*}{m} = 1 + \frac{r_s\sqrt{N}}{2\pi}\ln(r_s N^{3/2}) + O(r_s).$$

Thus in the weak screening regime, the ratio of the change in effective mass in a fully spin-polarized case ($N \to N/2$) to that in the unpolarized case is rather large. This is similar to the earlier considered case of $N = 2$.

In the strong-screening regime, $r_s N^{3/2} \gg 1$, the typical momentum transfers are much greater than k_F. In this regime, as the momentum transferred is large the scattering is almost isotropic (s-wave). The particle-hole continuum contribution to the mass renormalization is greatly reduced for s-wave scattering. However, the interaction of the quasi-particle with high energy plasmons [shaded region in Fig. 4–5B] plays the dominant role and leads to the enhancement of m^*. As a plasmon is a classical collective mode, it is not affected by a change in N. Consequently, the leading term in the N^{-1} expansion for m^* does not depend on N, whereas the next-to-leading term is numerically small.

The Matsubara polarization operator for $q \gg p_F$ is

$$\begin{aligned}\Pi_0^M(q, i\omega) &= N\int\int \frac{d\varepsilon}{2\pi}\frac{d^2p}{(2\pi)^2}\frac{1}{(i\varepsilon + i\omega - \xi_{p+q})(i\varepsilon - \xi_p)} \\ &= -2n\varepsilon_q/(\varepsilon_q^2 + \omega^2),\end{aligned} \tag{4.20}$$

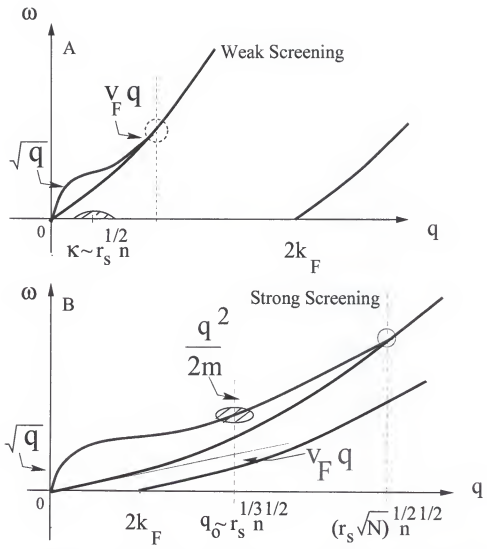

Figure 4–5: Particle-hole spectrum for a multi-component and a 2-component system.

where $\xi_p = p^2/2m - E_F$, $\varepsilon_q = q^2/2m$ and E_F is the Fermi energy.

The dressed interaction lines consisting of the RPA diagrams still remain the most dominant, due to the large N-factor associated with each polarization bubble. The modified RPA potential with the above polarization operator

$$V(q, i\omega) = \frac{\frac{2\pi e^2}{q}}{1 + \frac{2\pi e^2}{q} \frac{2n\varepsilon_q}{(\varepsilon_q^2 + \omega^2)}}, \tag{4.21}$$

has dominant contributions coming from $q_0 \sim r_s^{1/3}\sqrt{N}p_F$, with the screening radius $r \sim (r_s^{1/3}\sqrt{n})^{-1} \gg \sqrt{n}^{-1}$ larger than the typical interelectron distance yet much smaller compared to the screening radius $r \sim (r_s\sqrt{n})^{-1}$ for the case with only spin-degeneracy.

The zeroes of $1 - (2\pi e^2/q)\Pi^R(q,\omega)$ determine the plasmon spectrum. As shown in Fig. 4–5, the long-wavelength limit of plasmon spectrum (proportional to $\sqrt{q}$) depends only on the density of electrons and is independent of the spin-valley degeneracy. For momenta above $\kappa^{2/3}k_F^{1/3}$, the plasmon dispersion for the 2-component system is completely damped by particle-hole excitations. In contrast, for multi-component systems due to the considerably smaller velocities of the components, the plasmons remain undamped until large momenta of the order $\sqrt{r_s\sqrt{N}}n$. The plasmon dispersion in the large momentum region is given by $\omega_p = \sqrt{\varepsilon_q^2 + 2\pi e^2 nq/m}$. The slow-moving electrons in the multi-valley system are better screened by the high-energy plasmon excitations, with the particle-hole excitation playing only a nominal role. The area of the particle-hole continuum in the (ω, q) plane is reduced and its contribution to the real part of the self-energy (via $\mathrm{Im}V_R$) and hence to the mass renormalization is correspondingly small [16].

We obtain the quasi-particle effective mass from the self-energy via the standard relation

$$m^*/m \approx 1 - \Big(\frac{\partial\Delta\Sigma^M(\xi_p, i\varepsilon)}{\partial\xi_p} + \frac{\partial\Delta\Sigma^M(\xi_p, i\varepsilon)}{\partial i\varepsilon}\Big)\Big|_{p\to p_F, \varepsilon\to 0}, \tag{4.22}$$

where $\Delta\Sigma_p^M(\varepsilon) = \Sigma_p^M(\varepsilon) - \Sigma_{pF}^M(0)$ is the difference of the Matsubara self-energies.

The difference of the static and dynamic self-energy is,

$$\begin{aligned}
\Delta\Sigma^M(\xi_p, i\varepsilon) &= \Delta\Sigma^M_{static}(\xi_p) + \Delta\Sigma^M_{dyn}(\xi_{pF}, i\varepsilon) \\
\Delta\Sigma^M_{static}(\xi_p) &= \int \frac{d\omega}{2\pi}\frac{d^2q}{(2\pi)^2} V(q,0)\Big[G(\xi_{p+q}, i\varepsilon + i\omega) - G(\xi_{p_F+q}, i\omega)\Big] \\
&= \int \frac{d\omega}{2\pi}\frac{d^2q}{(2\pi)^2} V(q,0)\Big[\frac{-i\varepsilon + \xi_{\vec{p}+\vec{q}} - \xi_{\vec{p}_F+\vec{q}}}{(\varepsilon + \omega + i\xi_{\vec{p}+\vec{q}})(\omega + i\xi_{\vec{p}_F+\vec{q}})}\Big] \\
&= \frac{m}{2\pi^2}\xi_p \int_0^\pi d\theta \cos\theta V(2k_F \sin\theta/2, 0)
\end{aligned} \tag{4.23}$$

$$\begin{aligned}
\Delta\Sigma^M_{dyn}(\xi_p, i\varepsilon) &= \int \frac{d\omega}{2\pi}\frac{d^2q}{(2\pi)^2}[V(q,i\omega) - V(q,0)]\Big[G(\xi_{p+q}, i\varepsilon + i\omega) - G(\xi_{p_F+q}, i\omega)\Big] \\
&= \int \frac{d\omega}{2\pi}\frac{d^2q}{(2\pi)^2}\Big[\frac{(V(q,i\omega) - V(q,0))(\xi_{\vec{p}+\vec{q}} - \xi_{p_{\vec{F}}+\vec{q}} - i\varepsilon)}{(\varepsilon + \omega + i\xi_{\vec{p}+\vec{q}})(\omega + i\xi_{\vec{p}_F+\vec{q}})}\Big].
\end{aligned} \tag{4.24}$$

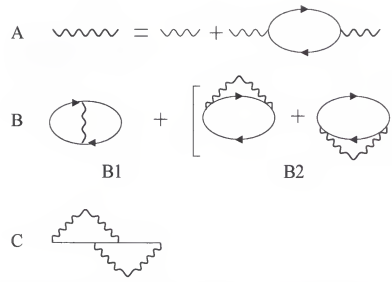

Figure 4–6: Diagrammatic corrections. A) The RPA potential. B) Corrections to the polarization bubble due to the interaction terms. C) Vertex corrections to the self-energy.

The pole at $\omega = ir\varepsilon_q$, where $r = \sqrt{1+4\pi e^2 n/q\varepsilon_q}$, provides the dominant contribution to the frequency integration of the dynamic term in Eq. (4.24). Taking the derivative of the dynamic term we obtain

$$\left(\frac{\partial\Delta\Sigma^M_{dynamic}}{\partial i\varepsilon}+\frac{\partial\Delta\Sigma^M_{dynamic}}{\partial\xi_p}\right)\Bigg|_{\varepsilon\to 0,\xi_p\to 0} = -2n\pi e^4\int\frac{qdq}{r(r+1)^3\varepsilon_q^3}$$
$$= -r_s^{2/3}\frac{\Gamma(1/3)\Gamma(7/6)}{10\sqrt{\pi}}. \qquad (4.25)$$

The result of Eq. (4.25) is larger by a factor of $(r_s N^{3/2})^{2/3}$ compared to that from the static part and will contribute to the leading-order correction to the effective mass. Thus the leading term in the $1/N$-expansion is (this form was obtained earlier by Iordanskii and Kashuba [90])

$$\frac{m^*}{m} = 1+r_s^{2/3}\frac{\Gamma(1/3)\Gamma(7/6)}{10\sqrt{\pi}}. \qquad (4.26)$$

The form of the polarization operator as given by Eq. (4.20) is insensitive to the degree of polarization, thus the mass renormalization in the leading order remains unchanged even for full polarization. Corrections to this leading order term is obtained by including, A) corrections to the polarization bubble due to the contributions coming from small

momentum regions, B) vertex corrections to the bubble [Fig. 4–6B], and C) vertex corrections to the self-energy [Fig. 4–6C].

From a scaling analysis we can infer that the vertex corrections from B) and C) contribute to a $r_s^{4/3}$ term to the leading result. The correction from B) is $\delta m_2^*/m \propto \int d\omega d^2q G^2 V^2 \delta\Pi$, where $V \sim \varepsilon_{q_0}/n$, $q \sim q_0$, $\omega \sim G^{-1} \sim \varepsilon_{q_0}$ and $\delta\Pi \sim r_s^{2/3} n/\varepsilon_{q_0}$, this yields a $r_s^{4/3}$ correction term. The corrections from C) is $\delta m_3^*/m \propto \int d\omega_1 d^2q_1 d\omega_2 d^2q_2 G^4 V^2$, where $\omega_1 \sim \omega_2 \sim G^{-1} \sim \varepsilon_{q_0}$, $q \sim q_0$ and $V \sim \varepsilon_{q_0}/n$, this also results in a $r_s^{4/3}$ term. We have checked explicitly that the scaling analysis holds. These corrections remain independent of the degree of polarization. We will next consider contributions from A) which gives polarization-dependent corrections and form the next-to-leading term in the $1/N$-expansion.

Contributions from the small-momentum region to the polarization bubble are given by Eq. 4.27,

$$\begin{aligned} \delta\Pi_0^M(q,i\omega) &= 2N \int \frac{d^2p\Theta(-\xi_p)}{(2\pi)^2} \left[\frac{(3\omega^2\varepsilon_q - \varepsilon_q^3)(\frac{pq\cos\theta}{m})^2}{(\omega^2+\varepsilon_q^2)^3} \right] \\ &= \frac{4n^2\pi}{mN} \frac{(3\omega^2-\varepsilon_q^2)\varepsilon_q^2}{(\omega^2+\varepsilon_q^2)^3}. \end{aligned} \tag{4.27}$$

The correction in the polarization bubble modifies the position of the plasmon-pole from $\omega = ir\varepsilon_q$ to $\omega = ir^*\varepsilon_q$. Where $r^{*2}\varepsilon_q^2 = r^2\varepsilon_q^2 + \Delta^2$, with $r\varepsilon_q \gg \Delta$ and

$$\Delta^2 = -\frac{8n^2e^2\pi^2}{qmN} \frac{3\omega^2-\varepsilon_q^2}{(\omega^2+\varepsilon_q^2)^2} \approx \frac{8n^2e^2\pi^2}{qmN} \frac{3r^2\varepsilon_q^2+\varepsilon_q^2}{(r^2\varepsilon_q^2-\varepsilon_q^2)^2}. \tag{4.28}$$

Thus the additional corrections to the mass term due to the new position of the pole will be

$$\begin{aligned} \left[\frac{\partial}{\partial i\varepsilon} + \frac{\partial}{\partial \xi_p}\right]\delta\Sigma &= -\frac{m}{2\pi^2} \int d\varepsilon_q \varepsilon_q d\omega \frac{V(q)(\omega^2+\varepsilon_q^2)}{(i\omega-\varepsilon_q)^3} \left[\frac{-\Delta^2}{(\omega^2+r^2\varepsilon_q^2+\Delta^2)(\omega^2+r^2\varepsilon_q^2)} \right] \\ &\approx -\frac{2}{N}\int \frac{dq}{q} \frac{1+3r-2r^2}{r^3(1+r)^3}, \end{aligned} \tag{4.29}$$

where the partial derivatives of $\delta\Sigma$ are taken at $(\varepsilon, \xi_p) \to 0$. The UV-divergence in the above expression is cut off at typical momentum transfers $q \sim \sqrt{r_s N^{3/2}} p_F$, as at these momentum the plasmon spectrum is damped due to the particle-hole excitations. The leading-order corrections to the effective mass from the corrections to the polarization

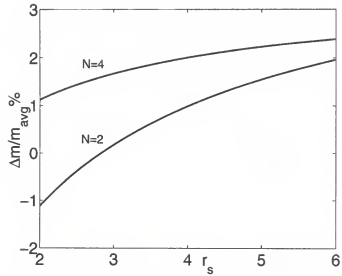

Figure 4–7: Percentage change in effective mass between a fully polarized and an unpolarized system as a function of r_s.

bubble will thus be

$$\Big[\frac{\partial}{\partial i\varepsilon}+\frac{\partial}{\partial \xi_p}\Big]\delta\Sigma^M(\xi_p,i\varepsilon)\Big|_{\varepsilon\to 0,\xi_p\to 0} \;=\; -\frac{1}{8N}\log N r_s^{2/3}.$$

This contribution is larger by a factor of $\log r_s^{2/3} N$ compared to that from the static part [Eq. (4.23)] and is the dominant subleading correction to the effective mass. Thus we obtain the mass to next-to-leading order in $1/N$ as

$$\frac{m^*}{m} = 1 + 0.14 r_s^{2/3} + \frac{1}{12N}\log r_s N^{3/2} + O(\frac{1}{r_s N^{5/2}}). \tag{4.30}$$

Because of the small coefficient in front of the leading term in Eq. (4.30), the actual condition for small r_s is rather weak: a two-fold enhancement of the mass occurs only for $r_s \approx 20$, thus smaller values of r_s allows a reasonable description within the mean-field theory. Equation (4.30) practically coincides with the observed $m^*(r_s)$ dependence in the interval $r_s = 2 - 6$. Beyond $r_s = 6$ the experimental value (Pudalov *et al.* [66]) exceeds the theoretical value (Fig. 4–8). For full polarization $N \to N/2$, unlike the earlier model for a 2-component system (spin-degeneracy only), the percentage change in the ratio of effective mass for a fully polarized to the unpolarized case is small. This ratio is given by

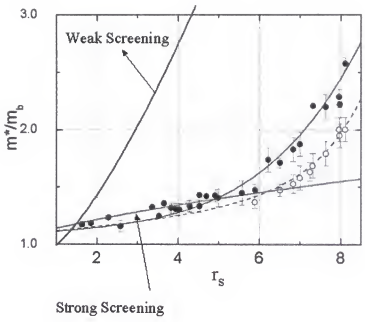

Figure 4–8: Plot of the effective mass formula obtained from the weak-screening case and from the strong screening case.

Eq. (4.31),

$$\frac{\Delta m}{m_{avg}} = \frac{m^*(\xi = 1) - m^*}{(m^*(\xi = 1) + m^*)/2} 100\%. \tag{4.31}$$

For an Si-MOSFET sample N changes from $4 \rightarrow 2$ at full polarization, the calculated effective mass remains almost the same and for the range of r_s from $2 - 5$, Δm is not more than $1 - 3\%$ (Fig. 4–7), a similar result is obtained for $N = 2 \rightarrow N = 1$. The difference in effective mass is particularly small for the $N = 4 \rightarrow N = 2$ degenerate system due to the peculiar cancellation of the $\log N/N$ term.

The explicit polarization dependence of the effective mass, given by

$$\frac{m^{*\uparrow}}{m} = 1 + 0.14 r_s^{2/3} + \frac{1+\zeta^2}{8N} \log\Big(\frac{r_s^{2/3} N}{1+\zeta^2}\Big), \tag{4.32}$$

is plotted in Fig. 4–9. The effective mass remains essentially constant throughout and

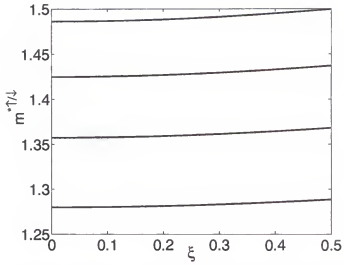

Figure 4–9: Effective mass as a function of degree of polarization for different values of r_s, starting from the lower one $r_s = 2$ to $r_s = 3, 4$ and 5.

there is no spin-splitting of the masses at this order in $1/N$ Eq. (4.32) is valid as long as the separation between two spin-down electrons is less than the screening length. The condition for the applicability of mean-field theory is $1 - \xi \gg r_s^{2/3}$]. This result is in qualitative agreement with the experimental finding on Si-MOSFETs [68], where the effective mass showed no dependence on the degree of polarization.

4.2.2 spin susceptibility

The second Fermi-liquid parameter which is of great interest in the context of a possible ferromagnetic transition and is experimentally determined, is the Landé-g^* factor. The g^*-factor is extracted from a knowledge of the static spin susceptibility χ^* via the relation $\chi^*/\chi = m^*g^*/mg$. In the previous Section, we obtained the effective mass as a function of interaction strength r_s and the valley degeneracy parameter N. As before, we will use perturbative techniques to obtain the spin susceptibility as a function of the above two parameters.

The spin susceptibility is obtained by studying the response of the system to the external magnetic field and in the Matsubara formalism is given by:

$$\chi^{M(ab)}(i\omega_n) = \int_0^{1/\tau} e^{i\omega_n \tau} \langle T_\tau \hat{m}^{M(a)}(\tau) \hat{m}^{M(b)}(0) \rangle d\tau, \tag{4.33}$$

where $\hat{m} = g\mu_B(\bar{\psi}_\alpha\sigma_{\alpha\beta}\psi_\beta)/2$ is the magnetization, σ is the Pauli matrix, μ_B is the Bohr magneton, a, b are the vector indices and $g \approx 2$ is the Lande-g factor. Plugging the form of the magnetization in Eq. (4.33), one obtains

$$\chi^{M(ab)}(i\omega_n) = (\frac{g\mu_B}{2})^2 \int_0^{1/\tau} e^{i\omega_n\tau}\langle T_\tau\bar{\psi}_\alpha(\tau)\sigma^{(a)}_{\alpha\beta}\psi_\beta(\tau)\bar{\psi}(0)_\gamma\sigma^{(b)}_{\gamma\delta}\psi_\delta(0)\hat{S}(1/T,0)\rangle d\tau, \quad (4.34)$$

In the zeroth order of interaction $\hat{S}(1/T,0) = 1$, the electron spin susceptibility is given (using "Wick's" theorem) by

$$\chi_0^{M(ab)}(i\omega_n) = (\frac{g\mu_B}{2})^2 \int_0^{1/\tau} e^{i\omega_n\tau}G(-\tau)G(\tau)\text{Trace}\,(\sigma^{(a)}\sigma^{(b)})d\tau. \quad (4.35)$$

Since Trace $(\sigma^{(a)}\sigma^{(b)}) = 2\delta_{ab}$, the relation is simply expressed in terms of the single particle Green's function G.

$$\chi_0^{M(ab)}(i\omega_n) = \frac{(g\mu_B)^2}{2}\delta_{ab}\int_0^{1/\tau} e^{i\omega_n\tau}G(-\tau)G(\tau)d\tau, \quad (4.36)$$

Thus $\chi_0^{M(ab)}(i\omega_n) = \frac{(g\mu_B)^2}{4}\delta_{ab}\Pi(i\omega_n)$, where $\Pi(i\omega_n)$ is the usual Lindhard function.

Due to electron-electron interaction, the susceptibility has the Lindhard form only in the lowest order of interaction. In what follows we obtain corrections to the free susceptibility by including interaction effects.

Higher-order corrections. We incorporate higher order terms by including the corrections due to the vertex function as in Fig. 4–6(B1) and due to the self-energy insertion to one of the Green's function as in Fig. 4–6(B2). The effective interaction in both cases considered is the RPA potential. Before evaluating the additional contributions to the susceptibility, let us briefly discuss the relevant range for the momentum and frequency transfer. The typical momentum transfer κ in the dense single component limit is of the order of $r_s k_F$ which is much less than k_F. The case of an N-valley system, however, greatly differs from the single component limit. Due to the presence of N valleys, the electrons get distributed over the valleys and hence the Fermi energy of each valley gets suppressed by a factor of $1/\sqrt{N}$. Typical momentum transfers becomes much greater than the Fermi momentum for the interaction regimes such that $N^{-3/2} \ll r_s \ll 1$. Contributions from the regions with small momentum transfers $k \ll k_F$, are sub-leading to those from the large-momentum-transfer regions. Details of the calculation are provided in

Appendix C. The correction to the Lindhard form of the susceptibility is

$$\begin{aligned}\Pi^* &= \Pi_0 + \delta\Pi \\ &= -\frac{m}{\pi}\Big[1 - \int \frac{q_1 dq_1}{2\pi}\frac{d\omega_1}{2\pi} D(q_1,\omega_1)\Big[\frac{q_1^2/m}{(i\omega_1 + \varepsilon_{q_1})^3}\Big]\Big] \\ &= -\frac{m^*}{\pi}. \end{aligned} \tag{4.37}$$

Thus from this form of the susceptibility, we can say that the corrections to the polarization due to small momentum regimes will give the same $-1/N \ln N$ correction as the mass term. The g^* factor remains unaffected. This result is in qualitative agreement with the experiment on Si-MOSFETs. A similar behavior is exhibited by ^{3}He where the renormalization of the spin susceptibility is essentially due to the effective mass. Near the critical point the spin susceptibility of ^{3}He diverges, due to ^{3}He being "almost localized" (m^* diverges) rather than being "almost ferromagnetic" (where g^* diverges). It can similarly be argued that the divergence of the spin susceptibility of Si-MOSFETs near the critical point is due to the divergence of effective mass rather than the g^* factor.

However, a recent experiment on g^* (AlAs sample) has shown that the g^* factor is affected by lifting the valley degeneracy [91]. We believe more work is required to qualify this behavior to a many-body effect.

4.3 Conclusion

Theoretical arguments based on general grounds predict that in a generic spin-polarized Fermi liquid, the effective mass of spin-up and spin-down electrons will be different. Contrary to these expectations, the effective mass of electrons in 2D Si-MOSFETs remains polarization-independent even under full spin-polarization. This indicates that Fermi statistics do not play a role in the mass renormalization and that the mass renormalization is due to classical degrees of freedom. For a system with spin-valley degeneracy N and in the strong screening regime such a polarization-independent effective mass is shown to result from the interaction of electrons with the high energy plasmons. In the strong screening regime plasmons are the main contributors to the mass renormalization and, since they are not affected by the change in N, the effective mass remains polarization-independent to the leading order in $1/N$. We used a large N-expansion and

showed that the leading correction is independent of N, the information about the degeneracy N comes only in the next to leading term. The expansion of the effective mass in $1/N$ turns out to be rapidly convergent even for non-valley degenerate systems ($N = 2$). In particular, we find that within this model, the percentage change in the effective mass of a 2-valley system under full spin-polarization is not more than 1-3%, a result consistent with experiment.

The spin susceptibility within this model is almost entirely renormalized by the mass. This finding is also in qualitative agreement with the experimental results on Si-MOSFET's .

CHAPTER 5
CONCLUSIONS

In this work, we have investigated the origin of processes which lead to the deviation from Fermi-liquid universality in two dimensional interacting systems.

In the first part of this work we have analyzed the low-energy properties of Fermi liquids in two dimensions. We have found that even at second order in perturbation theory (for a short-ranged potential), two interesting results are obtained: a nonanalytic term in the imaginary part of the self-energy and a logarithmic singularity on the mass shell for fermions with a linearized dispersion. The nonanalytic term and the log-singular term originate from special scattering events. Scattering events that involve exchange of small momentum between two parallel-moving quasi-particles, also known as forward-scattering events, give rise to the log-singular term on the mass shell. We find that at higher orders in the interaction the singularity due to forward scattering processes is enhanced and becomes a power-law causing the perturbation theory to formally diverge. We have dealt with the divergences by a re-summation process which involves adding up all the maximally divergent diagrams. An outcome of this resummation process is a zero-sound mode. We find that the interaction of the fermions with the zero-sound mode results in a non-Lorentzian shape of the spectral function.

We have investigated the contribution of the zero-sound mode to the nonanalytic T^2 term in the specific heat. We have found that for a short-ranged potential, both the imaginary and the real part of the self-energy emanating from the zero-sound mode region contribute to the nonanalytic T^2 term in the specific heat. In fact the contributions from the real and imaginary parts exactly cancel each other, thus we conclude that the nonperturbative zero-sound mode does not contribute to the T^2 term in the specific heat. We have verified the result by calculating the specific heat directly from the thermodynamic potential using both the real- and imaginary-frequency formalisms. This work was extended to the case of finite-ranged potential. The main result here is that the T^2 term

can be represented in terms of the Fermi-liquid parameters. We have also considered the case of the long-ranged Coulomb potential and show that nonperturbative processes do contribute a T^2 term to the specific heat and for, sufficiently low T, this contribution is interaction independent.

Direct evidence for the Fermi-liquid behavior (or its potential breakdown) of a two-dimensional electron system comes from the analysis of Shubhnikov-de Haas oscillations of the conductivity in the presence of both perpendicular and tilted magnetic fields. A recent experiment [68] on Si-MOSFET has revealed an unusual feature of the electron effective mass (m^*): while m^* exhibits a strong dependence on the electron density (r_s), it does not depend on the degree of spin polarization. Also, the masses of electrons with up and down spins are the same. We have made use of two independent approaches, perturbation theory in the weak-coupling limit and Landau's phenomenological approach, to show that the experimental results are in apparent contradiction with Fermi-liquid theory, which predicts two different and polarization-dependent masses in a partially spin-polarized regime. To explain the experimental observation, we have considered the effective mass of the Coulomb gas in the large-N limit (for Si MOSFET, $N = 4$). We show that the effective mass is renormalized primarily due to a polaronic effect: emission and absorption of high energy plasmons. As plasmons are classical objects, the quantum degeneracy, and hence polarization, does not affect the effective mass to the leading order in $1/N$. Polarization dependence shows up only at the next-to-leading order. We find that for $r_s = 2 - 6$ the change in effective mass between the unpolarized and fully polarized states is within $1 - 3\%$, a result which is consistent with the experiment.

APPENDIX A
SPECIFIC HEAT CONTRIBUTION: COULOMB POTENTIAL

In the following analysis we will reconsider the plasmon-pole and particle-hole contribution to the specific heat from an alternate approach. The thermodynamic potential given in Eq. (3.48) can be rewritten in the following form

$$\frac{\Delta\Omega}{A} = -\frac{T}{2}\sum_{iw_n}\int\frac{d^2k}{(2\pi)^2}\int_0^{e^2}de_o^2\frac{2\pi}{k}\frac{\Pi(k,iw_n)}{1-V(k)\Pi(k,iw_n)}. \tag{A.1}$$

The frequency summation can be converted to frequency integration by using the Eliashberg approach. The contour encloses all the discrete frequencies except $iw_n = 0$, the branch cut and the two poles. The branch cut corresponds to the particle-hole region, for a given value of k it extends from $-w(k)$ to $+w(k)$ (Fig. 3–5). The origin of the branch cut is due to the Π term which satisfies $\Pi(k,\omega+i\delta) \neq \Pi(k,\omega-i\delta)$ for ω's such that $\omega < \omega(k)$, where $\omega(k) = kv_F + k^2/2m$ is the boundary of the particle-hole continuum. The poles correspond to the solution of $\varepsilon_o(k,w) = 0$, hence the solutions are the plasmons for a system of charge e_o, which is beyond the particle-hole region. For an arbitrary value of e_o^2 ($< e^2$) the pole lies between the particle-hole and the plasmon curve. We can express the frequency summation as follows

$$\begin{aligned}\frac{1}{\beta}\sum_{iw_n}\frac{\Pi(k,iw_n)}{1-V\Pi(k,iw_n)} &= \Big[P\int_{-w(k)}^{+w(k)}\frac{d\varepsilon}{2\pi i}n_B(\varepsilon)\frac{\Pi(k,\varepsilon+i\delta)}{1-\frac{2\pi e^2}{k}\Pi(k,\varepsilon+i\delta)} \\ &\quad - P\int_{-w(k)}^{+w(k)}\frac{d\varepsilon}{2\pi i}n_B(\varepsilon)\frac{\Pi(k,\varepsilon-i\delta)}{1-\frac{2\pi e^2}{k}\Pi(k,\varepsilon-i\delta)}\Big] \\ &\quad - \Big[\Big(\frac{1}{e^{-\beta w_{pl}(k)}-1}\Big)\frac{\Pi(k,-w_{pl}(k))}{-\frac{2\pi e^2}{k}\frac{\partial\Pi(k,\varepsilon)}{\partial\varepsilon}}\Big|_{\varepsilon\to -w_{pl}(k)} \\ &\quad + \Big(\frac{1}{e^{\beta w_{pl}(k)}-1}\Big)\frac{\Pi(k,w_{pl}(k))}{-\frac{2\pi e^2}{k}\frac{\partial\Pi(k,\varepsilon)}{\partial\varepsilon}}\Big|_{\varepsilon\to w_{pl}(k)}\Big].\end{aligned} \tag{A.2}$$

The first expression in the summation corresponds to the particle-hole region, where as the second region would correspond to the plasmon-pole region (where $\omega_{pl} = v_F\sqrt{me^2k}$). The above expression can be written in a further simplified form by making use of the

following properties 1). $\Pi^R(k,\varepsilon) = [\Pi^A(k,\varepsilon)]^*$, 2). $\Pi(k,\pm w_{pl}(k)) = 1/V(k)$ and

$$3). \quad \frac{\partial\Pi(k,\varepsilon)}{\partial\varepsilon}|_{\varepsilon\to\omega_{pl}} = -\frac{m}{\pi}\frac{q^2v_F^2}{\omega_{pl}^3}$$

is odd in ω_{pl}. The simplified form is

$$\begin{aligned}\frac{1}{\beta}\sum_{iw_n}\frac{\Pi(k,iw_n)}{1-V\Pi(k,iw_n)} &= P\int_{-w(k)}^{+w(k)}\frac{d\varepsilon}{\pi}n_B(\varepsilon)\mathrm{Im}\frac{\Pi^R(k,\varepsilon)}{1-\frac{2\pi e^2}{k}\Pi^R(k,\varepsilon)} \\ &\quad + \Big[\coth(\frac{\beta w_{pl}(k)}{2})\frac{1}{(\frac{2\pi e^2}{k})^2\frac{\partial\Pi^R(k,\varepsilon)}{\partial\varepsilon}}|_{\varepsilon\to w_{pl}(k)}\Big], \qquad (A.3)\end{aligned}$$

thus,

$$\begin{aligned}\frac{\partial}{\partial T}\frac{1}{\beta}\sum_{iw_n}\frac{\Pi(k,iw_n)}{1-V\Pi(k,iw_n)} &= \frac{\partial}{\partial T}P\int_{-w(k)}^{+w(k)}\frac{d\varepsilon}{\pi}n_B(\varepsilon)\mathrm{Im}\frac{\Pi^R(k,\varepsilon)}{1-\frac{2\pi e^2}{k}\Pi^R(k,\varepsilon)} \\ &\quad + \Big[\frac{\partial}{\partial T}\coth(\frac{\beta w_{pl}(k)}{2})\frac{1}{(\frac{2\pi e^2}{k})^2\frac{\partial\Pi^R(k,\varepsilon)}{\partial\varepsilon}}|_{\varepsilon\to w_{pl}(k)}\Big] \\ &= P\int_{-w(k)}^{+w(k)}\frac{d\varepsilon}{\pi}\frac{\frac{1}{4T^2}}{\sinh^2(\varepsilon/2T)}\mathrm{Im}\frac{\Pi^R(k,\varepsilon)}{1-\frac{2\pi e^2}{k}\Pi^R(k,\varepsilon)} \\ &\quad + \Big[\frac{w_{pl}(k)}{2T^2\sinh^2(w_{pl}(k)/2T)}\frac{1}{(\frac{2\pi e^2}{k})^2\frac{\partial\Pi^R(k,\varepsilon)}{\partial\varepsilon}}|_{\varepsilon\to w_{pl}(k)}\Big].\end{aligned}$$

As before, we will first calculate the contribution from the Plasmon-pole,

$$\frac{\partial\Omega_{pl}/A}{\partial T} = \frac{1}{16\pi mv_F^2T^2}\int_0^{k_o}dk\int_0^{e^2}de_o^2\frac{\omega_{pl}^4}{\sinh^2(\omega_{pl}/2T)e_o^4}, \qquad (A.4)$$

where the k-integration is limited till $k_o = me^2$. At k_o the plasmon-pole enters the particle-hole spectrum and is no longer free. This integral is easily evaluated by making use of the result

$$\int_0^\infty\frac{y^3dy}{\sinh^2(y)} = \frac{3\zeta(3)}{2}, \qquad (A.5)$$

we obtain

$$\begin{aligned}\frac{\partial\Omega_{pl}/A}{\partial T} &= \frac{3\zeta(3)T^2}{2\pi v_F^2} \\ C_{V-pl} &= -T\frac{\partial}{\partial T}\frac{\partial\Omega_{pl}/A}{\partial T} \\ &= -\frac{3\zeta(3)T^2}{\pi v_F^2}. \qquad (A.6)\end{aligned}$$

The remaining contribution is from the particle-hole region,

$$\left.\frac{\partial}{\partial T}\frac{1}{\beta}\sum_{iw_n}\frac{\Pi(k,iw_n)}{1-V\Pi(k,iw_n)}\right|_{PH} = P\int_0^{+w(k)}\frac{d\varepsilon}{\pi}\frac{\varepsilon}{2T^2\sinh^2(\varepsilon/2T)} \times \mathrm{Im}\frac{\Pi^R(k,\varepsilon)}{1-\frac{2\pi e^2}{k}\Pi^R(k,\varepsilon)}, \tag{A.7}$$

where the Im term is odd in ε. Plugging this in Eq. (A.1), we obtain

$$\left.\frac{\frac{\partial\Delta\Omega}{\partial T}}{A}\right|_{PH} = -\int\frac{d^2k}{(2\pi)^2}\int_0^{e^2}de_o^2\frac{2\pi}{k}P\int_0^{+w(k)}\frac{d\varepsilon}{\pi}\frac{\varepsilon}{2T^2\sinh^2(\varepsilon/2T)}\mathrm{Im}\frac{\Pi^R(k,\varepsilon)}{1-\frac{2\pi e^2}{k}\Pi^R(k,\varepsilon)},$$

next performing the e^2 integration we obtain an identical expression as in Eq. (3.21), with the frequency and the momentum integration limited to be on the PH region. The evaluation of this term proceeds exactly as before and we will not pursue it any further.

APPENDIX B
SPIN-DEPENDENT EFFECTIVE MASS

In this Section we will calculate the effective mass of spin-polarized electrons. The first term of Eq. (4.14) is frequency independent, thus it does not contribute to the $\partial\Sigma^{\uparrow\downarrow}/\partial i\tilde{\omega}$ term in the effective mass. We need to consider only the 2^{nd} term of Eq. (4.14) in the self-energy expansion

$$\begin{aligned}\Sigma^{2\uparrow\downarrow}(p,i\tilde{\omega}) &= -\int_{-\infty}^{+\infty}\frac{d\omega}{2\pi}\int_0^{\infty}\frac{kdk}{(2\pi)^2}\frac{V^2(k)\Pi(k,i\omega)}{1-V(k)\Pi(k,i\omega)}\int_0^{2\pi}d\theta G^{\uparrow\downarrow}_{(0)}(p+k,i\omega+i\tilde{\omega}) \\ &= -\int_0^{+\infty}\frac{d\omega}{2\pi}\int_0^{\infty}\frac{kdk}{(2\pi)^2}\frac{V^2(k)\Pi(k)}{1-V(k)\Pi(k)}\int_0^{2\pi}d\theta\Big[G^{\uparrow\downarrow}_{(0)}(p+k,i\omega+i\tilde{\omega})+ \\ &\quad + G^{\uparrow\downarrow}_{(0)}(p+k,-i\omega+i\tilde{\omega})\Big]. \qquad \text{(B.1)}\end{aligned}$$

The angular integration yields

$$\begin{aligned}\int_0^{2\pi}d\theta G^{\uparrow\downarrow}_{(0)}(p+k,-i\omega+i\tilde{\omega}) &= -\frac{2\pi i}{\frac{p^{\uparrow\downarrow}_F k}{m}}\Big[\frac{\Theta(\omega+\tilde{\omega})-\Theta(-\omega-\tilde{\omega})}{\sqrt{1+\frac{m^2(\omega+\tilde{\omega})^2}{(p^{\uparrow\downarrow}_F k)^2}}}\Big], \\ \int_0^{2\pi}d\theta G^{\uparrow\downarrow}_{(0)}(p+k,-i\omega+i\tilde{\omega}) &= -\frac{2\pi i}{\frac{p^{\uparrow\downarrow}_F k}{m}}\Big[\frac{\Theta(-\omega+\tilde{\omega})-\Theta(\omega-\tilde{\omega})}{\sqrt{1+\frac{m^2(-\omega+\tilde{\omega})^2}{(p^{\uparrow\downarrow}_F k)^2}}}\Big]. \qquad \text{(B.2)}\end{aligned}$$

We will differentiate $\Sigma^{\uparrow\downarrow}$ by taking the limit $\tilde{\omega}\to 0^+$. The result remains the same if instead we had taken the limit $\tilde{\omega}\to 0^-$. The Θ functions are defined as follows

$$\begin{aligned}\Theta(x) &= 1; \quad \text{for, } x>0; \\ \Theta(x) &= 0; \quad \text{for, } x<0.\end{aligned}$$

Hence $\Sigma^{2\uparrow\downarrow}$ can be written as

$$\begin{aligned}\Sigma^{2\uparrow\downarrow} &= -\int_0^{\infty}\frac{d\omega}{2\pi}\int_0^{\infty}\frac{kdk}{(2\pi)^2}\bar{V}(k,i\omega)\frac{2\pi i}{(\frac{p^{\downarrow\uparrow}_F k}{m})}\Big[\frac{1}{\sqrt{1+\frac{m^2(\omega-\tilde{\omega})^2}{(p^{\downarrow\uparrow}_F k)^2}}}-\frac{1}{\sqrt{1+\frac{m^2(\omega+\tilde{\omega})^2}{(p^{\downarrow\uparrow}_F k)^2}}}\Big] \\ &\quad + 2\int_0^{\tilde{\omega}}\frac{d\omega}{2\pi}\int_0^{\infty}\frac{kdk}{(2\pi)^2}\bar{V}(k,i\omega)\Big[\frac{2\pi i}{(\frac{p^{\downarrow\uparrow}_F k}{m})\sqrt{1+\frac{m^2(-\omega+\tilde{\omega})^2}{(p^{\downarrow\uparrow}_F k)^2}}}\Big] \\ &= \Sigma^{2\uparrow\downarrow}_{(1)}+\Sigma^{2\uparrow\downarrow}_{(2)}, \qquad \text{(B.3)}\end{aligned}$$

where $\bar{V}(k,i\omega)$ has been used to represent

$$\bar{V}(k,i\omega)=\frac{V^2(k)\Pi(k,i\omega)}{1-V^2(k)\Pi(k,i\omega)}.$$

The contribution from the first term $\Sigma^{2\uparrow\downarrow}_{(1)}$ is:

$$\left.\frac{\partial\Sigma^{2\uparrow\downarrow}_{(1)}}{\partial i\tilde{\omega}}\right|_{\tilde{\omega}=0} = -\int_0^\infty\frac{d\omega}{2\pi}\int_0^\infty\frac{kdk}{(2\pi)^2}\bar{V}(k)(\frac{2\pi m}{p_F^{\uparrow\downarrow}k})\Big[\frac{2(\frac{m}{p_F^{\uparrow\downarrow}k})^2\omega}{(1+\frac{m^2\omega^2}{(p_F^{\uparrow\downarrow}k)^2})^{\frac{3}{2}}}\Big].$$

We will make the following substitution in the above integral $\omega\rightarrow\omega\sqrt{4\omega_k E_F^{\uparrow\downarrow}}$, $k\rightarrow kk_F^{\uparrow\downarrow}$ and $(E_F^{\downarrow}/E_F^{\uparrow})^2=(1-\xi)/(1+\xi)$, where ξ is the polarization (we will assume $\xi\ll 1$). This results in the following equation,

$$\begin{aligned}\left.\frac{\partial\Sigma^{2\uparrow\downarrow}_{(1)}}{\partial i\tilde{\omega}}\right|_{\tilde{\omega}=0} &= -\frac{me^2}{\pi p_F^{\uparrow}}\int_0^\infty d\omega\int_0^\infty\frac{dk}{k}\frac{\omega}{(1+\omega^2)^{\frac{3}{2}}}\\ &\quad\times\Big[\frac{\frac{\omega}{\sqrt{1+\omega^2}}+\frac{\omega}{\sqrt{\frac{1+\xi}{1-\xi}+\omega^2}}-2}{\frac{\sqrt{2}k}{r_s^{\uparrow}}-(\frac{\omega}{\sqrt{1+\omega^2}}+\frac{\omega}{\sqrt{\frac{1+\xi}{1-\xi}+\omega^2}}-2)}\Big].\end{aligned}\tag{B.4}$$

Expanding Eq. (B.4) about δ, where $1+\delta^{\uparrow\downarrow}=(1\mp\xi)/(1\pm\xi)\Rightarrow\delta^{\uparrow\downarrow}\approx\mp 2\xi$, we obtain

$$\begin{aligned}\left.\frac{\partial\Sigma^{2\uparrow\downarrow}_{(1)}}{\partial i\tilde{\omega}}\right|_{\tilde{\omega}=0} &= -\frac{r_s^{\uparrow\downarrow}}{\pi\sqrt{2}}\int_0^\infty d\omega\int_0^\infty\frac{dk}{k}\frac{\omega}{(1+\omega^2)^{\frac{3}{2}}}\Big[\frac{\frac{\omega}{\sqrt{1+\omega^2}}-1}{\frac{k}{\sqrt{2}r_s^{\uparrow}}+1-\frac{\omega}{\sqrt{1+\omega^2}}}\Big]\\ &\quad+\frac{\delta^{\uparrow\downarrow}}{8\pi}\int_0^\infty d\omega\int_0^\infty dk\frac{\frac{\omega^2}{(1+\omega^2)^3}}{(\frac{k}{\sqrt{2}r_s^{\uparrow}}+1-\frac{\omega}{\sqrt{1+\omega^2}})^2}.\end{aligned}\tag{B.5}$$

To prevent ultra-violet singularities, an upper cut off on the k-integral at $k=k_F$ is imposed. Such a cut-off is needed since the form of Π was obtained by considering contributions due to small k-values. Thus we have

$$\begin{aligned}\left.\frac{\partial\Sigma^{2\uparrow\downarrow}_{(1)}}{\partial i\tilde{\omega}}\right|_{\tilde{\omega}=0} &= -\frac{r_s^{\uparrow\downarrow}}{\pi\sqrt{2}}\int_0^\infty d\omega\int_0^1\frac{dk}{k}\frac{\omega}{(1+\omega^2)^{\frac{3}{2}}}\Big[\frac{\frac{\omega}{\sqrt{1+\omega^2}}-1}{\frac{k}{\sqrt{2}r_s^{\uparrow}}+1-\frac{\omega}{\sqrt{1+\omega^2}}}\Big]\\ &\quad+\frac{\delta^{\uparrow\downarrow}}{8\pi}\int_0^\infty d\omega\int_0^1 dk\Big[\frac{\frac{\omega^2}{(1+\omega^2)^3}}{(\frac{k}{\sqrt{2}r_s^{\uparrow}}+1-\frac{\omega}{\sqrt{1+\omega^2}})^2}\Big].\end{aligned}\tag{B.6}$$

The second term of $\Sigma^{2\uparrow\downarrow}$ represented by $\Sigma^{2\uparrow\downarrow}_{(2)}$ gives the following contribution

$$\begin{aligned}\left.\frac{\partial\Sigma^{2\uparrow\downarrow}_{(2)}}{\partial i\tilde{\omega}}\right|_{\tilde{\omega}\to 0} &= 2\frac{\partial}{\partial i\tilde{\omega}}\int_0^{\infty}\frac{d\omega}{2\pi}\int_0^{\infty}\frac{kdk}{(2\pi)^2}\frac{V^2(k)\Pi(k,\omega)}{1-V(k)\Pi(k,\omega)}\frac{2\pi i}{\frac{p_F^{\downarrow}k}{m}\sqrt{1+\frac{m^2(\omega-\tilde{\omega})^2}{(p_F^{\downarrow}k)^2}}} \\ &= -\frac{r_s^{\uparrow\downarrow}}{\pi\sqrt{2}}\Big(\int_0^1\frac{dk}{k}-\int_0^1\frac{dk}{k+\sqrt{2}r_s^{\uparrow\downarrow}}\Big). \end{aligned} \tag{B.7}$$

Adding up $\Sigma^{2\uparrow\downarrow}_{(1)}$ and $\Sigma^{2\uparrow\downarrow}_{(2)}$, the result assumes the following form

$$\begin{aligned}\left.\frac{\partial\Sigma^{\uparrow\downarrow}}{\partial i\tilde{\omega}}\right|_{i\tilde{\omega}\to 0} &= \left.\frac{\partial\Sigma^{2\uparrow\downarrow}}{\partial i\tilde{\omega}}\right|_{i\tilde{\omega}\to 0} = \left.\frac{\partial\Sigma^{2\uparrow\downarrow}_{(1)}}{\partial i\tilde{\omega}}\right|_{i\tilde{\omega}\to 0}+\left.\frac{\partial\Sigma^{2\uparrow\downarrow}_{(2)}}{\partial i\tilde{\omega}}\right|_{i\tilde{\omega}\to 0} \\ &= \frac{r_s^{\uparrow\downarrow}}{\pi\sqrt{2}}\int_0^{\infty}d\omega\int_0^1\frac{dk}{k}\frac{\omega}{(1+\omega^2)^{\frac{3}{2}}}\Big[\frac{1-\frac{\omega}{\sqrt{1+\omega^2}}}{\frac{k}{\sqrt{2}r_s^{\uparrow\downarrow}}+1-\frac{\omega}{\sqrt{1+\omega^2}}}\Big] \\ &+\frac{\delta^{\uparrow\downarrow}}{8\pi}\int_0^{\infty}d\omega\frac{\omega^2}{(1+\omega^2)^3}\frac{1}{\Big[1-\frac{\omega}{\sqrt{1+\omega^2}}\Big]\Big[\frac{1}{\sqrt{2}r_s^{\uparrow\downarrow}}+(1-\frac{\omega}{\sqrt{1+\omega^2}})\Big]} \\ &+\frac{r_s^{\uparrow\downarrow}}{\pi\sqrt{2}}\int_0^1\frac{dk}{k(\frac{k}{\sqrt{2}r_s^{\uparrow\downarrow}}+1)}, \end{aligned} \tag{B.8}$$

simplifying it further and keeping terms of the order of $r_s^{\uparrow\downarrow}$, Eq. (B.8) reduces to,

$$\begin{aligned}\left.\frac{\partial\Sigma^{\uparrow\downarrow}}{\partial i\tilde{\omega}}\right|_{i\tilde{\omega}=0} &= -\frac{r_s^{\uparrow\downarrow}}{\sqrt{2}}\Big[\frac{1}{2}+\frac{1}{\pi}\Big]+\frac{r_s^{\uparrow\downarrow}\delta^{\uparrow\downarrow}}{4\sqrt{2}\pi}\int_0^{\infty}d\omega\frac{\omega^2}{(1+\omega^2)^3}\frac{1}{1-\frac{\omega}{\sqrt{1+\omega^2}}} \\ &+O(r_s^2). \end{aligned} \tag{B.9}$$

Next we will calculate $\partial\Sigma/\partial\xi_p$. Unlike the earlier case, where we needed to perform frequency differentiation on only the $\Sigma^{2\uparrow\downarrow}_{(2)}$, both terms $\Sigma^{1\uparrow\downarrow}$ and $\Sigma^{2\uparrow\downarrow}$, need to be differentiated with respect to ξ_p. The contribution due to the first term is:

$$\Sigma^{1\uparrow\downarrow} = -\int\frac{d^2k}{(2\pi)^2}V(k)\int_{-\infty}^{\infty}d\omega G^{\uparrow\downarrow}_{(0)}(p+k,i\omega+i\tilde{\omega}), \tag{B.10}$$

completing the frequency integral we have

$$\begin{aligned}\Sigma^{1\uparrow\downarrow} &= -\int\frac{d^2k}{(2\pi)^2}V(k)\Theta(p_F^{\uparrow\downarrow}-|p+k|) \\ &= -\frac{\omega_F^{\uparrow\downarrow}r_s^{\uparrow\downarrow}}{\pi\sqrt{2}}\int\frac{d^2k}{k}\Theta(1-(k^2+p^2-2kp\cos\theta)) \\ &= -\frac{2\omega_F^{\uparrow\downarrow}r_s^{\uparrow\downarrow}}{\pi\sqrt{2}}\int_0^{\infty}dk\int_{-1}^{1}\frac{dx}{\sqrt{1-x^2}}\Theta(1-\sqrt{k^2+p^2-2kpx}), \end{aligned} \tag{B.11}$$

notice we have expressed the above integration variables in dimensionless units. The Θ function imposes a restriction on the range of values of x $(= \cos\theta)$ and k. The restriction are as follows

$$1 - \sqrt{k^2 + p^2 - 2kpx} > 0$$

$$\Rightarrow x > (k^2 + p^2 - 1)/2kp,$$

and the restriction on x, $-1 < x < 1$, implies $(k^2 + p^2 - 2kpx)/2kp < 1$

$$\Rightarrow p - 1 < k < p + 1$$

Finally when we take the derivative, $\partial\Sigma^{1\uparrow\downarrow}/\partial\xi_p^{\uparrow\downarrow}$, we will take the limit $p \to 1+$; thus the range of values k can take is

$$p - 1 < k < p + 1,$$

and the range of values x can take is

$$\frac{k^2 + p^2 - 1}{2pk} < x < 1.$$

Since $(k + p)^2 > 1$ the lower limit of x in Eq. (B.11) can be replaced from -1 to $(k^2 + p^2 - 1)/(2pk)$.

Evaluating the x integration, we obtain

$$\begin{aligned}\Sigma^{1\uparrow\downarrow} &= -\frac{2\omega_F^{\uparrow\downarrow} r_s^{\uparrow\downarrow}}{\pi\sqrt{2}} \int_{p-1}^{p+1} dk \int_{\frac{k^2+k^2-1}{2pk}}^{1} \frac{dx}{\sqrt{1-x^2}} \\ &= -\frac{\sqrt{2}\omega_F^{\uparrow\downarrow} r_s^{\uparrow\downarrow}}{\pi} \int_{p-1}^{p+1} dk \frac{k^2 - p^2 + 1}{\sqrt{2pk - (p^2 + k^2 - 1)}\sqrt{2pk + (p^2 + k^2 - 1)}}, \end{aligned} \tag{B.12}$$

substituting $k = t + p$ in Eq. (B.12), we obtain

$$\Sigma^{1\uparrow\downarrow} = -\frac{\sqrt{2}\omega_F^{\uparrow\downarrow} r_s^{\uparrow\downarrow}}{\pi} \int_{-1}^{1} dt \frac{t^2 + 2tp + 1}{\sqrt{1-t^2}\sqrt{(2p+t)^2 - 1}}. \tag{B.13}$$

Next we will differentiate the above term with respect to the momentum, thus we obtain

$$\frac{\partial\Sigma^{1\uparrow\downarrow}}{\partial p}\Big|_{p=1} = \frac{8\omega_F^{\uparrow\downarrow} r_s^{\uparrow\downarrow}}{\pi\sqrt{2}} \int_{-1}^{1} dt \frac{p + t}{\sqrt{1-t^2}[(2p+t)^2 - 1]^{\frac{3}{2}}}\Big|_{p=1}, \tag{B.14}$$

substituting $t = 2u - 1$ in Eq. (B.14), Eq. (B.14) modifies to

$$\frac{\partial \Sigma^{1\uparrow\downarrow}}{\partial p}\Big|_{p=1} = \frac{2\omega_F^{\uparrow\downarrow} r_s^{\uparrow\downarrow}}{\pi\sqrt{2}} \int_0^1 \frac{du}{u(1+u)(1-u^2)^{\frac{1}{2}}} = \frac{2\omega_F^{\uparrow\downarrow} r_s^{\uparrow\downarrow}}{\pi\sqrt{2}} \Big[\log 2 - \int_0^1 \frac{du}{u(1-u^2)^{\frac{1}{2}}} + \int_0^1 \frac{du}{u} \Big]. \tag{B.15}$$

$$\Rightarrow \frac{\partial \Sigma^{1\uparrow\downarrow}}{\partial \xi_p^{\uparrow\downarrow}}\Big|_{\xi_p^{\uparrow\downarrow}\to 0} = \frac{r_s^{\uparrow\downarrow}}{\pi\sqrt{2}} \Big[\log 2 - 1 + \int_0^1 \frac{du}{u} \Big]. \tag{B.16}$$

The infra-red divergence of Eq. (B.16) is cancelled by a similar divergent term originating from the $\partial\Sigma^{2\uparrow\downarrow}/\partial\xi_p^{\uparrow\downarrow}$ term. The contribution from the $\Sigma^{2\uparrow\downarrow}$ term is calculated below. The contribution to $\partial\Sigma^{\uparrow\downarrow}/\partial\xi_{p\uparrow\downarrow}$, due to the second term $\Sigma^{2\uparrow\downarrow}$ is given by

$$\Sigma^{2\uparrow\downarrow} = -\int_0^{+\infty} \frac{d\omega}{2\pi} \int_0^{\infty} \frac{kdk}{(2\pi)^2} \frac{V^2(k)\Pi(k)}{1 - V(k)\Pi(k)} \int_0^{2\pi} d\theta \Big[G_{(0)}^{\uparrow\downarrow}(p+k, i\omega + i\bar{\omega}) + + G_{(0)}^{\uparrow\downarrow}(p+k, -i\omega + i\bar{\omega}) \Big]. \tag{B.17}$$

We will *a priori* set the external frequency $\bar{\omega} = 0$, the angular integration gives

$$I_1^{\uparrow\downarrow} = \int_0^{2\pi} d\theta \Big[G_{(0)}^{\uparrow\downarrow}(p+k, i\omega) + G_{(0)}^{\uparrow\downarrow}(p+k, -i\omega) \Big] = -\frac{2m\pi i}{pk} \frac{1}{\sqrt{1 - \frac{m^2(\omega_k + \xi_p^{\uparrow\downarrow} - i\omega)^2}{(pk)^2}}} + \frac{2m\pi i}{pk} \frac{1}{\sqrt{1 - \frac{m^2(i\omega + \omega_k + \xi_p^{\uparrow\downarrow})^2}{(pk)^2}}}, \tag{B.18}$$

we differentiate the above expression with respect to $\xi_p^{\uparrow\downarrow}$, to obtain

$$\frac{\partial I_1^{\uparrow\downarrow}}{\partial \xi_p^{\uparrow\downarrow}}\Big|_{\xi_p^{\uparrow\downarrow}=0} = -\pi i \Big[-\frac{4\omega_k - 2(\omega_k + \xi_p^{\uparrow\downarrow}) + 2i\omega}{(4\omega_k\omega_p - (\omega_k + \xi_p^{\uparrow\downarrow})^2 + \omega^2 + 2i\omega(\omega_k + \xi_p^{\uparrow\downarrow}))^{\frac{3}{2}}} + \frac{4\omega_k - 2(\omega_k + \xi_p^{\uparrow\downarrow}) - 2i\omega}{(4\omega_k\omega_p - (\omega_k + \xi_p^{\uparrow\downarrow})^2 + \omega^2 - 2i\omega(\omega_k + \xi_p^{\uparrow\downarrow}))^{\frac{3}{2}}} \Big]\Big|_{\xi_p^{\uparrow\downarrow}=0}. \tag{B.19}$$

By linearizing the spectrum (discarding ω_k terms compared to $\omega \sim k v_F$ terms), Eq. (B.19) acquires a simpler expression

$$\frac{\partial I_1^{\uparrow\downarrow}}{\partial \xi_p^{\uparrow\downarrow}}\Big|_{\xi_p^{\uparrow\downarrow}=0} = -\frac{4\pi\omega}{(4\omega_{p_F^{\uparrow\downarrow}}\omega_k + \omega^2)^{\frac{3}{2}}}. \tag{B.20}$$

Using the above relation, we obtain the following form for $\partial\Sigma^{2\uparrow\downarrow}/\partial\xi_p^{\uparrow\downarrow}$

$$\frac{\partial\Sigma^{2\uparrow\downarrow}}{\partial\xi_p^{\uparrow\downarrow}} = \int_0^\infty \frac{d\omega}{2\pi}\int_0^\infty \frac{kdk}{(2\pi)^2}\frac{V^2(k)(\Pi^{\uparrow\downarrow}(k,i\omega)+\Pi^{\downarrow}(k,i\omega))}{1-V(k)(\Pi^{\uparrow\downarrow}(k,i\omega)+\Pi^{\downarrow}(k,i\omega))} \Big[\frac{4\pi\omega}{(4\omega_{p_F^{\uparrow\downarrow}}\omega_k+\omega^2)^{\frac{3}{2}}}\Big]. \tag{B.21}$$

Similar change of variables, as in Eq. (B.12) is made, $w \to w\sqrt{4w_k w_F^{\uparrow\downarrow}}$, $k \to k k_F^{\uparrow\downarrow}$ and $(w_F^{\downarrow}/w_F^{\uparrow})^2 = (1-\xi)/(1+\xi) = 1+\delta$, expanding in the small parameter δ, and keeping terms of the order of r_s we obtain

$$\begin{aligned}\frac{\partial\Sigma^{2\uparrow\downarrow}}{\partial\xi_p^{\uparrow\downarrow}} &= \frac{r_s^{\uparrow\downarrow}}{\pi\sqrt{2}}\Big[-\int_0^1\frac{dk}{k}+\frac{\pi}{2}+1-\log(\sqrt{2}r_s^{\uparrow\downarrow}) \\ &\quad +\sqrt{2}r_s^{\uparrow\downarrow}\int_0^\infty d\omega\frac{\omega}{(1+\omega^2)^{\frac{3}{2}}}\left(1-\frac{\omega}{\sqrt{1+\omega^2}}\right)+\ldots\Big] \\ &\quad -\frac{\delta^{\uparrow\downarrow}r_s^{\uparrow\downarrow}}{4\sqrt{2}\pi}\int_0^\infty d\omega\frac{\frac{\omega^2}{(1+\omega^2)^3}}{\left(1-\frac{\omega}{\sqrt{1+\omega^2}}\right)}\Big[1-\frac{r_s^{\uparrow\downarrow}}{\sqrt{2}}\left(1-\frac{\omega}{\sqrt{1+\omega^2}}\right)+\ldots\Big]\end{aligned} \tag{B.22}$$

The infra-red divergence is eliminated once we add contributions from $\partial\Sigma^{1\uparrow\downarrow}/\partial\xi_p^{\uparrow\downarrow}$ [Eq. (B.16)] and $\partial\Sigma^{2\uparrow\downarrow}/\partial\xi_p^{\uparrow\downarrow}$ [Eq. (B.22)],

$$\begin{aligned}\frac{\partial\Sigma^{\uparrow\downarrow}}{\partial\xi_p^{\uparrow\downarrow}}\Big|_{\xi_p^{\uparrow\downarrow}\to 0} &= \frac{r_s^{\uparrow\downarrow}}{\pi\sqrt{2}}\Big[\frac{\pi}{2}+\log\frac{1}{r_s^{\uparrow\downarrow}}\Big] \\ &\quad -\frac{\delta^{\uparrow\downarrow}r_s^{\uparrow\downarrow}}{4\sqrt{2}\pi}\int_0^\infty d\omega\frac{\frac{\omega^2}{(1+\omega^2)^3}}{\left(1-\frac{\omega}{\sqrt{1+\omega^2}}\right)}\Big[1-\frac{r_s^{\uparrow\downarrow}}{\sqrt{2}}\left(1-\frac{\omega}{\sqrt{1+\omega^2}}\right)+\ldots\Big].\end{aligned} \tag{B.23}$$

Finally, results from Eq. (B.9) and Eq. (B.23) are plugged back into Eq. (4.13) to obtain the effective mass in terms of the interaction strength

$$\frac{m^{*\uparrow\downarrow}}{m} = \frac{1+\frac{r_s^{\uparrow\downarrow}}{\sqrt{2}}(\frac{1}{2}+\frac{1}{\pi})+0.23\frac{r_s^{\uparrow\downarrow}}{\sqrt{2}}\xi}{1+\frac{r_s^{\uparrow\downarrow}}{\pi\sqrt{2}}(\frac{\pi}{2}+\log\frac{1}{r_s^{\uparrow\downarrow}})+0.23\frac{r_s^{\uparrow\downarrow}}{\sqrt{2}}\xi}, \tag{B.24}$$

APPENDIX C
CORRECTIONS TO THE SPIN SUSCEPTIBILITY

In this Section, we will evaluate the corrections to the spin susceptibility due to the contributions from vertex and self-energy insertions.

Vertex function. We will go beyond the Lindhard form of the susceptibility and calculate the corrections to the spin susceptibility from the vertex function (Fig. 4–6(B1)),

$$\begin{aligned}\delta\Pi_1(\vec{q},i\omega) &= -\frac{2}{(2\pi)^6}\int d^2q_1\int_{-\infty}^{\infty}d\omega_1\int d^2p\int_{-\infty}^{\infty}d\varepsilon G_M(\vec{p},i\varepsilon)G_M(\vec{p}-\vec{q_1},i\varepsilon-i\omega_1)\\ &\quad G_M(\vec{p}-\vec{q_1}-\vec{q},i\varepsilon-i\omega_1-i\omega)G_M(\vec{p}-\vec{q},i\varepsilon-i\omega)D(q_1,\omega_1),\end{aligned}\tag{C.1}$$

where $\vec{q}$, ω are the external momentum and frequency transfer respectively. The effective potential is

$$D(q,i\omega)=\frac{V(q)}{1-\Pi(q,\omega)V(q)},$$

where $V(q)=2\pi e^2/q$ is the 2D Coulomb potential and

$$\Pi(q,\omega_1)=-\frac{2n(q^2/2m)}{\omega_1^2+(q^2/2m)^2},$$

is the polarization operator in the limit of large momentum and frequency transfer. The external frequency ω will be set to $\omega=0$, as we are interested in the static and long wave-length form of the spin susceptibility, though we refrain from setting $\vec{q}=0$, and take the long wave-length limit at the very end of calculation. Thus we have,

$$\begin{aligned}\delta\Pi_1(\vec{q}) &= -\frac{2}{(2\pi)^6}\int d^2q_1\int_{-\infty}^{\infty}d\omega_1\int d^2p\int_{-\infty}^{\infty}d\varepsilon G_M(\vec{p},i\varepsilon)G_M(\vec{p}-\vec{q_1},i\varepsilon-i\omega_1)\\ &\quad G_M(\vec{p}-\vec{q_1}-\vec{q},i\varepsilon-i\omega_1)G_M(\vec{p}-\vec{q},i\varepsilon)D(q_1,\omega_1).\end{aligned}\tag{C.2}$$

Integration on the frequency variable ε is performed by closing the contour of integration from above.

We obtain

$$\begin{aligned}
\delta\Pi_1(\vec{q}) &= -\frac{4\pi i}{(2\pi)^6}\int d^2q_1\int_{-\infty}^{\infty}d\omega_1\int d^2pD(\vec{q_1},\omega_1)\\
&\times\Bigg[\frac{\Theta(-\xi_{\vec{p}})}{(-i\xi_{\vec{p}}-\omega_1+i\xi_{\vec{p}-\vec{q_1}})(-i\xi_{\vec{p}}-\omega_1+i\xi_{\vec{p}-\vec{q_1}-\vec{q}})(-i\xi_{\vec{p}}+i\xi_{\vec{p}-\vec{q}})}\\
&+\frac{\Theta(-\xi_{\vec{p}-\vec{q_1}})}{(\omega_1-i\xi_{\vec{p}-\vec{q_1}}+i\xi_{\vec{p}})(i\xi_{\vec{p}-\vec{q}-\vec{q_1}}-i\xi_{\vec{p}-\vec{q_1}})(\omega_1+i\xi_{\vec{p}-\vec{q}}-i\xi_{\vec{p}-\vec{q_1}})}\\
&+\frac{\Theta(-\xi_{\vec{p}-\vec{q_1}-\vec{q}})}{(\omega_1-i\xi_{\vec{p}-\vec{q_1}-\vec{q}}+i\xi_{\vec{p}})(i\xi_{\vec{p}-\vec{q_1}}-i\xi_{\vec{p}-\vec{q_1}-\vec{q}})(\omega_1-i\xi_{\vec{p}-\vec{q}-\vec{q_1}}+i\xi_{\vec{p}-\vec{q}})}\\
&+\frac{\Theta(-\xi_{\vec{p}-\vec{q}})}{(i\xi_{\vec{p}-\vec{q}}-i\xi_{\vec{p}})(\omega_1+i\xi_{\vec{p}-\vec{q}}-i\xi_{\vec{p}-\vec{q_1}})(-\omega_1+i\xi_{\vec{p}-\vec{q}-\vec{q_1}}-i\xi_{\vec{p}-\vec{q}})}\Bigg]. \qquad \text{(C.3)}
\end{aligned}$$

By appropriate choice of variables, the Θ function is made to have the same variable in all the four expressions inside the big bracket,

$$\begin{aligned}
\delta\Pi_1(\vec{q}) &= -\frac{4\pi i}{(2\pi)^6}\int d^2q_1\int d\omega_1\int d^2pD(\vec{q_1},\omega_1)\\
&\times\Bigg[\frac{\Theta(-\xi_{\vec{p}})}{(-i\xi_{\vec{p}}-\omega_1+i\xi_{\vec{p}-\vec{q_1}})(-i\xi_{\vec{p}}-\omega_1+i\xi_{\vec{p}-\vec{q_1}-\vec{q}})(-i\xi_{\vec{p}}+i\xi_{\vec{p}-\vec{q}})}\\
&+\frac{\Theta(-\xi_{-\vec{p}})}{(\omega_1+i\xi_{-\vec{p}+\vec{q_1}}-i\xi_{-\vec{p}})(i\xi_{-\vec{p}-\vec{q}}-i\xi_{-\vec{p}})(\omega_1+i\xi_{-\vec{p}+\vec{q_1}-\vec{q}}-i\xi_{-\vec{p}})}\\
&+\frac{\Theta(-\xi_{-\vec{p}})}{(\omega_1+i\xi_{-\vec{p}+\vec{q_1}+\vec{q}}-i\xi_{-\vec{p}})(i\xi_{-\vec{p}+\vec{q}}-i\xi_{-\vec{p}})(\omega_1-i\xi_{-\vec{p}}+i\xi_{-\vec{p}+\vec{q_1}})}\\
&+\frac{\Theta(-\xi_{-\vec{p}})}{(i\xi_{-\vec{p}}-i\xi_{-\vec{p}+\vec{q}})(\omega_1+i\xi_{-\vec{p}}-i\xi_{-\vec{p}+\vec{q}-\vec{q_1}})(i\xi_{-\vec{p}-\vec{q_1}}-\omega_1-i\xi_{-\vec{p}})}\Bigg]. \qquad \text{(C.4)}
\end{aligned}$$

The above expression can be represented in a compact form, for this purpose we utilize the following property of the integral. The integral remains invariant under the following change of variables $\omega_1\to-\omega_1$, $\vec{q_1}\to-\vec{q_1}$, $\vec{p}\to-\vec{p}$ [where we have utilized the property of Matsubara potential $D(\vec{q_1},\omega_1)=D(|\vec{q_1}|,|\omega_1|)$]. Thus we obtain

$$\begin{aligned}
\delta\Pi_1(\vec{q}) &= -\frac{16\pi i}{(2\pi)^6}\int d^2q_1\int_{-\infty}^{\infty}d\omega_1\int d^2p\Bigg[\frac{\Theta(-\xi_{\vec{p}})D(\vec{q_1},\omega_1)}{(\omega_1+i\xi_{\vec{p}}-i\xi_{\vec{p}-\vec{q_1}})(\omega_1+i\xi_{\vec{p}}-i\xi_{\vec{p}-\vec{q_1}-\vec{q}})}\\
&\times\frac{1}{(-i\xi_{\vec{p}}+i\xi_{\vec{p}-\vec{q}})}\Bigg]. \qquad \text{(C.5)}
\end{aligned}$$

This contribution along with the contribution from the self-energy insertion will be added together in the following analysis, to obtain the final result.

Self-energy insertion. In this Section, we will calculate the corrections to the spin susceptibility from the self-energy insertion to the green's function. As shown in Fig. 4–6B, there are two such diagrams which contribute equally to the corrections. The effective potential as before is $D(q,i\omega) = V(q)/(1-\Pi(q,\omega)V(q))$, where $V(q) = 2\pi e^2/q$ is the 2D Coulomb potential and the polarization operator in the limit of large momentum and frequency transfer is given by

$$\Pi(q,\omega_1) = -\frac{2n(q^2/2m)}{\omega_1^2 + (q^2/2m)^2}.$$

The correction term is

$$\begin{aligned}
\delta\Pi_2(\vec{q},i\omega) &= -\frac{2\times 2}{(2\pi)^6}\int d^2q_1 \int_{-\infty}^{\infty} d\omega_1 \int d^2p \int_{-\infty}^{\infty} d\varepsilon G_M(\vec{p}-\vec{q},i\varepsilon)G_M^2(\vec{p},i\varepsilon) \\
&\quad G_M(\vec{p}-\vec{q}_1,i\varepsilon - i\omega_1)D(q_1,\omega_1) \\
&= -\frac{4}{(2\pi)^6}\int d^2q_1 \int_{-\infty}^{\infty} d\omega_1 \int d^2p \int_{-\infty}^{\infty} d\varepsilon \frac{D(q_1,\omega_1)}{(\varepsilon + i\xi_{\vec{p}-\vec{q}})(\varepsilon + i\xi_{\vec{p}-\vec{q}})^2} \\
&\quad \times \frac{1}{(\varepsilon - \omega_1 + i\xi_{\vec{p}-\vec{q}_1})(\varepsilon - \omega_1 + i\xi_{\vec{p}-\vec{q}_1})}.
\end{aligned} \tag{C.6}$$

As a reminder, the factor of 2 is due to the contributions from two identical bubbles. Continuing further, we will perform the ε integration by closing the contour from the top

$$\begin{aligned}
\delta\Pi_2(\vec{q},i\omega) &= -\frac{8\pi i}{(2\pi)^6}\int d^2q_1 \int_{-\infty}^{\infty} d\omega_1 \int d^2p D(q_1,\omega_1) \\
&\quad \times\Big[\frac{\Theta(-\xi_{\vec{p}-\vec{q}})}{(i\xi_{\vec{p}} - i\xi_{\vec{p}-\vec{q}})^2(-\omega_1 - i\xi_{\vec{p}-\vec{q}} + i\xi_{\vec{p}-\vec{q}_1})} \\
&\quad + \frac{\Theta(-\xi_{\vec{p}-\vec{q}_1})}{(\omega_1 - i\xi_{\vec{p}-\vec{q}_1} + i\xi_{\vec{p}-\vec{q}})(\omega_1 - i\xi_{\vec{p}-\vec{q}_1} - i\xi_{\vec{p}})^2} \\
&\quad - \frac{\Theta(-\xi_{\vec{p}})}{(i\xi_{\vec{p}} - i\xi_{\vec{p}-\vec{q}})^2(-\omega_1 - i\xi_{\vec{p}} + i\xi_{\vec{p}-\vec{q}_1})} \\
&\quad + \frac{\Theta(-\xi_{\vec{p}})}{(-i\xi_{\vec{p}} + i\xi_{\vec{p}-\vec{q}})(-\omega_1 - i\xi_{\vec{p}} + i\xi_{\vec{p}-\vec{q}_1})^2}\Big].
\end{aligned} \tag{C.7}$$

As before, trivial change of variables is made to keep same argument in the Θ function.

$$\begin{aligned}\frac{\delta\Pi_2(\vec{q},i\omega)(2\pi)^6}{8\pi i} &= -\int d^2q_1\int_{-\infty}^{\infty}d\omega_1\int d^2pD(q_1,\omega_1)\Theta(-\xi_{\vec{p}})\\ &\Big[-\frac{1}{(i\xi_{\vec{p}}-i\xi_{\vec{p}-\vec{q}})^2(\omega_1+i\xi_{\vec{p}}-i\xi_{\vec{p}-\vec{q}-\vec{q}_1})}\\ &-\frac{1}{(\omega_1+i\xi_{\vec{p}}-i\xi_{\vec{p}-\vec{q}_1-\vec{q}})(\omega_1+i\xi_{\vec{p}}-i\xi_{\vec{p}-\vec{q}_1})^2}\\ &+\frac{1}{(i\xi_{\vec{p}-\vec{q}}-i\xi_{\vec{p}})^2(\omega_1+i\xi_{\vec{p}}-i\xi_{\vec{p}-\vec{q}_1})}\\ &-\frac{1}{(-i\xi_{\vec{p}}+i\xi_{\vec{p}-\vec{q}})(\omega_1+i\xi_{\vec{p}}-i\xi_{\vec{p}-\vec{q}_1})^2}\Big].\end{aligned}\tag{C.8}$$

Corrections from the vertex and self-energy insertion:. In the analysis below we will make use of the following notation:

$$\begin{aligned}iy &= i\xi_{\vec{p}}-i\xi_{\vec{p}-\vec{q}_1}\\ ix &= i(\varepsilon_q-\frac{\vec{q}.(\vec{p}-\vec{q}_1)}{m})\\ \frac{1}{\omega_1+i\xi_{\vec{p}}-i\xi_{\vec{p}-\vec{q}_1}} &= \frac{1}{\omega_1+iy}\\ \frac{1}{\omega_1+i\xi_{\vec{p}}-i\xi_{\vec{p}-\vec{q}_1-\vec{q}}} &= \frac{1}{\omega_1+iy-ix},\end{aligned}$$

where $1/(\omega_1+i\xi_{\vec{p}}-i\xi_{\vec{p}-\vec{q}_1-\vec{q}})$ will be taylor expanded in the small parameter $ix = i(\varepsilon_q-\frac{\vec{q}.(\vec{p}-\vec{q}_1)}{m})$ (x is small since in the long wavelength limit $q\to 0$). Adding up the contributions from the vertex function and from the self energy insertion we obtain

$$\begin{aligned}\delta\Pi &= \delta\Pi_1+\delta\Pi_2\\ &= -\frac{8\pi i}{(2\pi)^6}\int d^2pd^2q_1d\omega_1\Theta(-\xi_p)D(q_1,\omega_1)\\ &\quad\times\Big[\frac{1}{(\omega_1+iy)^2}\Big(-\frac{i\vec{q}_1.\vec{q}/m}{(i\xi_{\vec{p}-\vec{q}}-i\xi_{\vec{p}})^2}\Big)-\frac{1}{(\omega_1+iy)^3}\Big(\frac{(i\vec{q}_1.\vec{q}/m)^2}{(i\xi_{\vec{p}-\vec{q}}-i\xi_{\vec{p}})^2}\Big)\\ &\quad-\frac{1}{(\omega_1+iy)^4}\Big(\frac{ix(i\vec{q}_1.\vec{q}/m)^2}{(i\xi_{\vec{p}-\vec{q}}-i\xi_{\vec{p}})^2}\Big)+\cdots\Big].\end{aligned}\tag{C.9}$$

Large momentum transfer regions, $q_1\gg p_F$, are the dominant contributors to $\delta\Pi$, we will Taylor expand $1/(\omega_1+i\xi_{\vec{p}}-i\xi_{\vec{p}-\vec{q}_1})$ in the small energy term $\vec{p}.\vec{q}_1/m$ (where $p\approx p_F$) to

obtain

$$\begin{aligned}\delta\Pi &= -\frac{8\pi i}{(2\pi)^6}\int d^2p d^2q_1 d\omega_1 \Theta(-\xi_p) D(q_1,\omega_1) \\ &\Big[-\frac{1}{(\omega_1 - i\varepsilon_{q_1})^2}\frac{i\vec{q_1}.\vec{q}/m}{(i\xi_{\vec{p}-\vec{q}} - i\xi_{\vec{p}})^2} \\ &+\frac{\frac{2i\vec{q_1}.\vec{p}/m}{(\omega_1 - i\varepsilon_{q_1})}}{(\omega_1 - i\varepsilon_{q_1})^2}\frac{i\vec{q_1}.\vec{q}/m}{(i\xi_{\vec{p}-\vec{q}} - i\xi_{\vec{p}})^2} \\ &-\frac{1}{(\omega_1 - i\varepsilon_{q_1})^3}\Big(\frac{(i\vec{q_1}.\vec{q}/m)^2}{(i\xi_{\vec{p}-\vec{q}} - i\xi_{\vec{p}})^2}\Big) \\ &+\frac{\frac{3i\vec{q_1}.\vec{p}/m}{(\omega_1 - i\varepsilon_{q_1})}}{(\omega_1 - i\varepsilon_{q_1})^3}\Big(\frac{(i\vec{q_1}.\vec{q}/m)^2}{(i\xi_{\vec{p}-\vec{q}} - i\xi_{\vec{p}})^2}\Big) + \cdots\Big]. \end{aligned} \tag{C.10}$$

The first term of the above equation is zero since $< \vec{q_1}.\vec{q} >_{\theta_1} = 0$, where θ_1 is the angle between vectors $\vec{q_1}$ and $\vec{q}$. The second term is also zero :

$$\begin{aligned} 2^{nd}\text{term} &= \frac{8\pi i}{(2\pi)^6}\int d^2p d^2q_1 d\omega_1 \Theta(-\xi_p) D(q_1,\omega_1)\Big[\frac{-\frac{2i\vec{q_1}.\vec{p}/m}{(\omega_1 - i\varepsilon_{q_1})}}{(\omega_1 - i\varepsilon_{q_1})^2}\Big(-\frac{i\vec{q_1}.\vec{q}/m}{(i\xi_{\vec{p}-\vec{q}} - i\xi_{\vec{p}})^2}\Big)\Big] \\ &= \frac{8\pi i}{(2\pi)^6}\int d^2p q_1 dq_1 d\omega_1 \Theta(-\xi_p) D(q_1,\omega_1)\Big(\frac{2\pi q_1^2/m^2}{(\omega_1 - i\varepsilon_{q_1})^3}\Big)\Big[\frac{\Theta(-\xi_p)}{i^2(\varepsilon_q - pq/m\cos\theta)} \\ &\quad -\frac{\varepsilon_q\Theta(-\xi_p)}{i^2(\varepsilon_q - pq/m\cos\theta)^2}\Big], \end{aligned}$$

where

$$\int d^2p\Big[\frac{\Theta(-\xi_p)}{i^2(\varepsilon_q - pq/m\cos\theta)} - \frac{\varepsilon_q\Theta(-\xi_p)}{i^2(\varepsilon_q - pq/m\cos\theta)^2}\Big] = 0. \tag{C.11}$$

The last term of Eq. (C.10) is zero as well, since $< (\vec{q_1}.\vec{p})(\vec{q_1}.\vec{q})^2 >_{\theta_i} = 0$. The third term is the leading term which survives,

$$\begin{aligned}\delta\Pi &= \frac{8\pi i}{(2\pi)^6}\int d^2p d^2q_1 d\omega_1 \Theta(-\xi_p) D(q_1,\omega_1)\Big[\frac{1}{(\omega_1 - i\varepsilon_{q_1})^3}\Big(\frac{(i\vec{q_1}.\vec{q}/m)^2}{(i\xi_{\vec{p}-\vec{q}} - i\xi_{\vec{p}})^2}\Big)\Big] \\ &= \frac{m}{\pi}\int\frac{q_1 dq_1}{2\pi}\frac{d\omega_1}{2\pi}D(q_1,\omega_1)\Big[\frac{q_1^2/m}{(i\omega_1 + \varepsilon_{q_1})^3}\Big]. \end{aligned}$$

Hence

$$\begin{aligned}\Pi^* &= \Pi_0 + \delta\Pi \\ &= -\frac{m}{\pi}\Big[1 - \int\frac{q_1 dq_1}{2\pi}\frac{d\omega_1}{2\pi}D(q_1,\omega_1)\Big[\frac{q_1^2/m}{(i\omega_1 + \varepsilon_{q_1})^3}\Big]\Big] \\ &= -\frac{m^*}{\pi}. \end{aligned} \tag{C.12}$$

REFERENCES

[1] E. Wigner, Phys. Rev. **46**, 1002-1011 (1934).

[2] E. Abrahams, P. W. Anderson, D. C. Licciardello, and T. V. Ramakrishnan, Phys. Rev. Lett. **42**, 673-676 (1979).

[3] B. L. Altshuler, A. G. Aronov, and P. A. Lee, Phys. Rev. Lett. **44**, 1288 (1980).

[4] K. v. Klitzing, G. Dorda, and M. Pepper, Phys. Rev. Lett. **45**, 494-497 (1980).

[5] D. C. Tsui, H. L. Stormer, and A. C. Gossard, Phys. Rev. Lett. **48**, 1559-1562 (1982).

[6] R. G. Mani, J. H. Smet, K. von Klitzing, V. Narayanamurti, W. B. Johnson, and V. Umansky, Nature (London) **420**, 646 (2002).

[7] M. A. Zudov, R. R. Du, L. N. Pfeiffer, and K. W. West, Phys. Rev. Lett. **90**, 046807 (2003).

[8] a) P. W. Anderson, Phys. Rev. Lett. **64**. 1839 (1990); b) *ibid.* **65**, 2306 (1990).

[9] L. D. Landau, Zh. Eksp. Teor. Fiz. **30**, 1058 (1956) [Sov. Phys. JETP 3, 920 (1957)]; **32**, 59 (1957) [**5**, 101 (1957)]; **35**, 97 (1958) [**8**, 70 (1959)].

[10] D W. E. Pickett, H. Krakauer, R. E. Cohen and D. J. Singh, Science **255**, 46 (1992).

[11] C. M. Varma, P. B. Littlewood, S. SchmittRink, E. Abrahams, and A. E. Ruckenstein, Phys. Rev. Lett. **63**, 1996 (1989).

[12] J. A. Hertz, Phys. Rev. B **14**, 1165 (1976); A. J. Millis, Phys. Rev. B **48**, 7183 (1993) ; T. Moriya and T. Takimoto, J. Phys. Soc. Jpn. **64**, 960 (1995).

[13] A. V. Chubukov, C. Pepin, and J. Rech, Phys. Rev. Lett. **92**, 147003 (2004).

[14] D. Belitz, T.R. Kirkpatrick, and Thomas Vojta, cond-mat/0403182, http://xxx.lanl.gov/find/cond-mat (2004).

[15] D. Belitz, T. R. Kirkpatrick, and T. Vojta, Phys. Rev. B **55**, 9452 (1997).

[16] A. A. Abrikosov, L. P. Gorkov, and I. E. Dzyaloshinski *Methods of Quantum Field Theory in Statistical Physics* (Dover Publications, New York, 1963).

[17] E. M. Lifshitz and L. P. Pitaevski, *Statistical Physics* (Pergamon Press, 1980).

[18] G. M. Eliashberg, Sov. Phys. JETP **16**, 780 (1963).

[19] S. Doniach and S. Engelsberg, Phys. Rev. Lett. **17**, 750 (1966).

[20] W. F. Brinkman and S. Engelsberg, Phys. Rev. Lett. **17**, 750 (1966).

[21] D. Coffey and K. S. Bedell, Phys. Rev. Lett. **71**, 1043 (1993).

[22] a) A. V. Chubukov and D. L. Maslov, Phys. Rev. B **68**, 155113 (2003); b) *ibid.* **69**, 121102 (2004).

[23] V. M. Galitski and S. Das Sarma, cond-mat/0311559, http://xxx.lanl.gov/find/cond-mat (2003).

[24] M. A. Baranov, M. Yu. Kagan, and M. S. Mar'enko, JETP Lett. **58**, 709 (1993).

[25] D. S. Greywall, Phys. Rev. B **27**, 2747 (1988).

[26] G. R. Stewart, Rev. Mod. Phys. **56**, 755 (1984).

[27] Casey, H. Patel, J. Nyeki, B. P. Cowan, and J. Saunders, Phys. Rev. Lett. **90**, 115301 (2003).

[28] Yu. A. Bychkov, L. P. Gorkov, and I. E. Dzyaloshinskii, Sov. Phys. JETP **23**. 489 (1966).

[29] W. Metzner, C. Castellani and C. D. Castro, Adv. Phys. **47**, 317 (1998).

[30] J. R. Engelbrecht and M. Randeria, Phys. Rev. Lett. **65**, 1032 (1990).

[31] C. Castellani, C. D. Castro, and W. Metzner, Phys. Rev. Lett. **72**, 316 (1994).

[32] H. Fukuyama and M. Ogata, J. Phys. Soc. Jpn. **63**, 3923 (1995).

[33] C. J. Halboth and W. Metzner, Phys. Rev. B **57**, 8873 (1998).

[34] A. V. Chubukov, D. L. Maslov, S. Gangadharaiah and L. I. Glazman, cond-mat/0412283, http://xxx.lanl.gov/find/cond-mat (2004); S. Gangadharaiah, D. L. Maslov, A. V. Chubukov and L. I. Glazman, cond-mat/0501013, http://xxx.lanl.gov/find/cond-mat (2005).

[35] D. J. Thouless, Phys. Rep. **13**, 93 (1974).

[36] L. P. Gor'kov, A. I. Larkin, and D. E. Khmel'nitskii, Zh. Eksp. Teor. Fiz. Pis'ma Red. **30**, 248 (1979) [JETP Lett. **30**, 248 (1979)].

[37] D. J. Thouless, Phys. Rev. Lett. **39**, 1167 (1977) .

[38] B. L. Altshuler, A. G. Aronov, and D. E. Khmel'nitskii, Solid State Commun. **39**, 619 (1981).

[39] B. L. Altshuler, A. G. Aronov, and D. E. Khmel'nitskii, J. Phys. C **15**, 7367 (1982).

[40] G. J. Dolan and D. D. Osheroff, Phys. Rev. Lett. **43**, 721 (1979).

[41] D. J. Bishop, D. C. Tsui, and R. C. Dynes, Phys. Rev. Lett. **44**, 1153 (1980).

[42] M. J. Uren, R. A. Davies, and M. Pepper, J. Phys. C **13**. L985 (1980).

[43] D. J. Bishop, R. C. Dynes, and D. C. Tsui, Phys. Rev. B **26**, 773 (1982).

[44] P. A. Lee, and T. V. Ramakrishnan, Phys. Rev. B **26**, 4009 (1982).

[45] Altshuler and D. E. Khmel'nitskii, A. I. Larkin, and P. A. Lee, Phys. Rev. B **22**, 5142 (1980).

[46] A. M. Finkelstein, Zh. Eksp. Teor. Fiz. **84**, 168 (1983); [Sov. Phys. JETP **57**, 97 (1983)].

[47] A. M. Finkelstein, Pis'ma Zh. Eksp. Teor. Fiz. **37**, 436 (1983).

[48] B. L. Altshuler and A. G. Aronov, Solid State Commun. **46**, 429 (1983).

[49] C. Castellani, C. Di Castro, P. A. Lee, and M. Ma, Phys. Rev. B **30**, 527 (1984).

[50] S. V. Kravchenko, G. V. Kravchenko, J. E. Furneaux, V. M. Pudalov, and M. D'Iorio, Phys. Rev. B **50**, 8039 (1994).

[51] S. V. Kravchenko, W. E. Mason, G. E. Bowker, J. E. Furneaux, V. M. Pudalov, and M. D'Iorio, Phys. Rev. B **51**, 7038 (1995).

[52] P. T. Coleridge, R. L. Williams, Y. Feng, and P. Zawadzki Phys. Rev. B **56**, R12764 (1997).

[53] S. J. Papadakis, E. P. De Poortere, H. C. Manoharan, M. Shayegan and R. Winkler, Science, **283**, 2056 (1999).

[54] Y. Hanein, D. Shahar, J. Yoon, C. C. Li, D. C. Tsui, and H. Shtrikman, Phys. Rev. B **58**, R13338 (1998).

[55] S. J. Papadakis and M. Shayegan, Phys. Rev. B **57**, R15068 (1998).

[56] S. A. Vitkalov, M. P. Sarachik, and T. M. Klapwijk, Phys. Rev. B **65**, 201106 (2002).

[57] O. Prus, M. Reznikov, U. Sivan, and V. Pudalov, Phys. Rev. Lett. **88**, 016801 (2002).

[58] S. Chakravarty, L. Yin, and E. Abrahams, Phys. Rev. B **58**, R559 (1998).

[59] V. Dobrosavljevic, E. Abrahams, E. Miranda, and S. Chakravarty, Phys. Rev. Lett. **79**, 455 (1997).

[60] G. Zala, B. N. Narozhny, and I. L. Aleiner, Phys. Rev. B **64**, 214204 (2001).

[61] A. Punnoose and A. M. Finkelstein, Phys. Rev. Lett. **88**, 016802 (2002).

[62] B. Spivak, Phys. Rev. B **67**, 125205 (2003).

[63] B. Spivak and S. A. Kivelson, Phys. Rev. B **70**, 155114 (2004).

[64] S. A. Vitkalov, K. James, B. N. Narozhny, M. P. Sarachik, and T. M. Klapwijk, Phys. Rev. B **67**, 113310 (2003).

[65] V. M. Pudalov, M. E. Gershenson, H. Kojima, G. Brunthaler, A. Prinz, and G. Bauer, Phys. Rev. Lett. **91**, 126403 (2003).

[66] V. M. Pudalov, M. E. Gershenson, H. Kojima, N. Butch, E. M. Dizhur, G. Brunthaler, A. Prinz, and G. Bauer, Phys. Rev. Lett. **88**, 196404 (2002).

[67] S. V. Kravchenko, A. A. Shashkin, David A. Bloore, and T. M. Klapwijk, Solid State Commun. **116**, 495 (2000).

[68] A. A. Shashkin, M. Rahimi, S. Anissimova, S. V. Kravchenko, V. T. Dolgopolov, and T. M. Klapwijk, Phys. Rev. Lett. **91**, 046403 (2003).

[69] S. Curnoe and P.C.E. Stamp, Phys. Rev. Lett. **80**, 3312 (1998).

[70] G. W. Martin, D. L. Maslov, and M. Yu. Reizer, Phys. Rev. B **68**, 241309 (2003).

[71] J.M. Luttinger, Phys. Rev. **121**, 1251 (1961).

[72] Yu.A. Bychkov and L.P. Gor'kov, Zh. ksp. Teor. Fiz. **41**, 1592 (1961) [Sov. Phys. JETP 14, 1132 (1962)].

[73] K. Miyake and C.M. Varma, Solid State Commun. **85**, 335 (1993).

[74] S.A. Vitkalov, H. Zheng, K.M. Mertes, M.P. Sarachik, and T.M. Klapwijk, Phys. Rev. Lett. **85**, 2164 (2000).

[75] A. A. Shashkin, S. V. Kravchenko, V. T. Dolgopolov, and T. M. Klapwijk, Phys. Rev. Lett. **87**, 086801 (2001).

[76] S. A. Vitkalov, H. Zheng, K. M. Mertes, M. P. Sarachik, and T. M. Klapwijk, Phys. Rev. Lett. **87**, 086401 (2001).

[77] W. F. Brinkman and T. M. Rice, Phys. Rev. B **2**, 4302 (1970).

[78] M. C. Gutzwiller, Phys. Rev. **137**, A1726 (1965) .

[79] V. M. Galitski and V. A. Khodel, cond-mat/0308203, http://xxx.lanl.gov/find/cond-mat (2003).

[80] Andrey V. Chubukov, Victor M. Galitski, and Victor M. Yakovenko, Phys. Rev. Lett. **94**, 046404 (2005).

[81] F. Stern, Phys. Rev. Lett. **18**, 546 (1967).

[82] G. F. Giuliani and J. J. Quinn Phys. Rev. B **26**, 4421 (1982); D. C. Marinescu, J. J. Quinn, and G. F. Giuliani Phys. Rev. B **65**, 045325 (2002).

[83] A. L. Fetter and J. D. Walecka, *Quantum Theory of Many Particle Systems* (McGraw-Hill, New York, 1971).

[84] J. M. Luttinger and J. C. Ward, Phys. Rev. **118**, 1417 (1960).

[85] A. V. Chubukov, D. L. Maslov, S. Gangadharaiah and L. I. Glazman, cond-mat/0502542, http://xxx.lanl.gov/find/cond-mat (2005).

[86] D. Vollhardt, Rev. Mod. Phys. **56**, 99 (1984).

[87] G. Baym and C. Pethick, *Landau Fermi-Liquid Theory* (John Wiley & Sons, Inc., 1991).

[88] A. Meyerovich, J. Low Temp. Phys. **53**, 487 (1983).

[89] Y.-W. Tan, J. Zhu, H. L. Stormer, L. N. Pfeiffer, K. W. Baldwin, and K. W. West, Phys. Rev. Lett. **94**, 016405 (2005).

[90] S. V. Iordanski and A. Kashuba, JETP Lett. **76**, 563 (2002).

[91] Y. P. Shkolnikov, K. Vakili, E. P. De Poortere, and M. Shayegan, Phys. Rev. Lett. **92**, 246804 (2004).

BIOGRAPHICAL SKETCH

Suhas Ganagadharaiah was born on July 14, 1976, in Chintamani, Karnataka State, India. He spent his childhood in the northern Indian city of Kanpur, where he completed high school. After high school, he joined the Physics Department of the Indian Institute of Technology, Kanpur, in 1994, and graduated in 1999 with a Master of Science degree. While pursuing his studies at the Institute he developed a keen interest in theoretical physics.

In fall 1999, he joined the doctoral program of the Physics Department at the University of Florida. Since fall 2000, he has worked in the research group of Professor Dmitrii Maslov and completed the Ph.D. program under his supervision in May 2005.

[68] A. A. Shashkin, M. Rahimi, S. Anissimova, S. V. Kravchenko, V. T. Dolgopolov, and T. M. Klapwijk, Phys. Rev. Lett. **91**, 046403 (2003).

[69] S. Curnoe and P.C.E. Stamp, Phys. Rev. Lett. **80**, 3312 (1998).

[70] G. W. Martin, D. L. Maslov, and M. Yu. Reizer, Phys. Rev. B **68**, 241309 (2003).

[71] J.M. Luttinger, Phys. Rev. **121**, 1251 (1961).

[72] Yu.A. Bychkov and L.P. Gor'kov, Zh. ksp. Teor. Fiz. **41**, 1592 (1961) [Sov. Phys. JETP 14, 1132 (1962)].

[73] K. Miyake and C.M. Varma, Solid State Commun. **85**, 335 (1993).

[74] S.A. Vitkalov, H. Zheng, K.M. Mertes, M.P. Sarachik, and T.M. Klapwijk, Phys. Rev. Lett. **85**, 2164 (2000).

[75] A. A. Shashkin, S. V. Kravchenko, V. T. Dolgopolov, and T. M. Klapwijk, Phys. Rev. Lett. **87**, 086801 (2001).

[76] S. A. Vitkalov, H. Zheng, K. M. Mertes, M. P. Sarachik, and T. M. Klapwijk, Phys. Rev. Lett. **87**, 086401 (2001).

[77] W. F. Brinkman and T. M. Rice, Phys. Rev. B **2**, 4302 (1970).

[78] M. C. Gutzwiller, Phys. Rev. **137**, A1726 (1965) .

[79] V. M. Galitski and V. A. Khodel, cond-mat/0308203, http://xxx.lanl.gov/find/cond-mat (2003).

[80] Andrey V. Chubukov, Victor M. Galitski, and Victor M. Yakovenko, Phys. Rev. Lett. **94**, 046404 (2005).

[81] F. Stern, Phys. Rev. Lett. **18**, 546 (1967).

[82] G. F. Giuliani and J. J. Quinn Phys. Rev. B **26**, 4421 (1982); D. C. Marinescu, J. J. Quinn, and G. F. Giuliani Phys. Rev. B **65**, 045325 (2002).

[83] A. L. Fetter and J. D. Walecka, *Quantum Theory of Many Particle Systems* (McGraw-Hill, New York, 1971).

[84] J. M. Luttinger and J. C. Ward, Phys. Rev. **118**, 1417 (1960).

[85] A. V. Chubukov, D. L. Maslov, S. Gangadharaiah and L. I. Glazman, cond-mat/0502542, http://xxx.lanl.gov/find/cond-mat (2005).

[86] D. Vollhardt, Rev. Mod. Phys. **56**, 99 (1984).

[87] G. Baym and C. Pethick, *Landau Fermi-Liquid Theory* (John Wiley & Sons, Inc., 1991).

[88] A. Meyerovich, J. Low Temp. Phys. **53**, 487 (1983).

[89] Y.-W. Tan, J. Zhu, H. L. Stormer, L. N. Pfeiffer, K. W. Baldwin, and K. W. West, Phys. Rev. Lett. **94**, 016405 (2005).

[90] S. V. Iordanski and A. Kashuba, JETP Lett. **76**, 563 (2002).

[91] Y. P. Shkolnikov, K. Vakili, E. P. De Poortere, and M. Shayegan, Phys. Rev. Lett. **92**, 246804 (2004).

BIOGRAPHICAL SKETCH

Suhas Ganagadharaiah was born on July 14, 1976, in Chintamani, Karnataka State, India. He spent his childhood in the northern Indian city of Kanpur, where he completed high school. After high school, he joined the Physics Department of the Indian Institute of Technology, Kanpur, in 1994, and graduated in 1999 with a Master of Science degree. While pursuing his studies at the Institute he developed a keen interest in theoretical physics.

In fall 1999, he joined the doctoral program of the Physics Department at the University of Florida. Since fall 2000, he has worked in the research group of Professor Dmitrii Maslov and completed the Ph.D. program under his supervision in May 2005.